

Synthesis of single-walled carbon nanotubes using binary (Fe, Co, Ni) alloy nanoparticles prepared in situ by the reduction of oxide solid solutions

E. Flahaut ^a, A. Govindaraj ^{b,c}, A. Peigney ^a, Ch. Laurent ^a, A. Rousset ^a,
C.N.R. Rao ^{b,c,*}

^a Laboratoire de Chimie des Matériaux Inorganiques, ESA CNRS 5070, Université Paul-Sabatier, F-31062 Toulouse Cedex 4, France

^b CSIR Centre of Excellence in Chemistry, Indian Institute of Science, Bangalore 560 012, India

^c Jawaharlal Nehru Centre for Advanced Scientific Research, Jakkur P.O., Bangalore 560 064, India

Received 21 October 1998

Abstract

Passing a H₂–CH₄ mixture over oxide spinels containing two transition elements as in Mg_{0.8}M_yM'_zAl₂O₄ (M, M' = Fe, Co or Ni, y + z = 0.2) at 1070°C produces small alloy nanoparticles which enable the formation of carbon nanotubes. Surface area measurements are found to be useful for assessing the yield and quality of the nanotubes. Good-quality single-walled nanotubes (SWNTs) have been obtained in high yields with the FeCo alloy nanoparticles, as evidenced by transmission electron microscope images and surface area measurements. The diameter of the SWNTs is in the 0.8–5 nm range, and the multiwalled nanotubes, found occasionally, possess very few graphite layers. © 1999 Elsevier Science B.V. All rights reserved.

1. Introduction

Carbon nanotubes are attracting much attention because of their novel mechanical and electronic properties. In order to suitably make use of the nanotubes, it is necessary to have them in uniform size, with a narrow size distribution. Towards this purpose, most workers employ metal particles to catalyse the decomposition of hydrocarbons or carbon monoxide. The metal particles are suggested to play a catalytic role at an atomic level rather than as heterogeneous nucleation sites [1]. Although Ni and

Co nanoparticles appear to be the best amongst monometallic catalysts, nanoparticles of bimetallic alloys formed by these metals give 10–100 times higher yields of single-walled nanotubes (SWNTs) [2,3]. If the particle size of the metals and alloys is large, carbon filaments or fibres rather than the Iijima-type nanotubes are generally obtained [4–8]. Small nanoparticles of transition metals produced by the pyrolysis of organometallics containing Fe, Co and Ni along with hydrocarbons give multiwalled nanotubes (MWNTs), but through a careful manipulation of partial pressures, SWNTs are obtained [9,10]. We have employed reduced spinel oxides containing small quantities of two transition metals (amongst Fe, Co, and Ni) to synthesize nanotubes,

* Corresponding author. E-mail: cnrrao@sscu.iisc.ernet.in

since the method is known to give rise to narrow compositions of small alloy nanoparticles [11].

In the method employed in the present study, high-temperature hydrogen reduction of the oxide spinels of the general composition $Mg_{0.8}M_yM'_zAl_2O_4$ ($M, M' = Fe, Co, Ni$, $y + z = 0.2$ and y or $z = 0.05, 0.10, 0.15$ and 0.20) generates catalytic transition metal alloy nanoparticles required for the formation of the nanotubes by the pyrolysis of methane. Surface area measurements have been employed to quantify the yield and quality of nanotubes. High-quality SWNTs have been obtained particularly with FeCo alloy nanoparticles.

2. Experimental

Spinel oxides of the general formula $Mg_{0.8}M_yM'_zAl_2O_4$ ($M, M' = Fe, Co, Ni$, $y + z = 0.2$ and y or $z = 0.05, 0.10$ and 0.15) were prepared starting with a stoichiometric mixture of the metal nitrates and subjecting the nitrate mixture along with urea to the usual procedure employed in combustion synthesis [12]. The combustion product was attrition-milled in a Nylon vessel in an aqueous medium, passed through a sieve, washed with ethanol

Table 1
Some characteristics of the carbon nanotubes obtained in the present study

Specimen ^a	C_n (wt%)	S_r ($m^2 g^{-1}$)	S_o ($m^2 g^{-1}$)	ΔS ($m^2 g^{-1}$)	$\Delta S/C_n$ ($m^2 g^{-1}$)
Fe	5.81	18.20	10.48	7.72	133
Fe _{0.75} Co _{0.25}	7.10	25.06	10.14	14.92	210
Fe _{0.50} Co _{0.50}	6.99	31.65	11.79	19.86	284
Fe _{0.25} Co _{0.75}	5.61	25.29	10.41	14.88	265
Co	3.77	23.27	10.52	12.75	338
Fe	5.81	18.20	10.48	7.72	133
Fe _{0.75} Ni _{0.25}	5.12	20.01	10.05	9.96	195
Fe _{0.50} Ni _{0.50}	4.07	19.55	10.15	9.40	231
Fe _{0.25} Ni _{0.75}	2.58	15.17	8.75	6.42	249
Ni	1.97	13.54	9.20	4.34	220
Co	3.77	23.27	10.52	12.75	338
Co _{0.75} Ni _{0.25}	2.39	19.14	11.29	7.85	328
Co _{0.50} Ni _{0.50}	1.75	13.22	8.70	4.52	259
Co _{0.25} Ni _{0.75}	2.00	15.67	8.93	6.74	338
Ni	1.97	13.54	9.20	4.34	220

^a Metal content was 6.7 wt% in all the compositions.

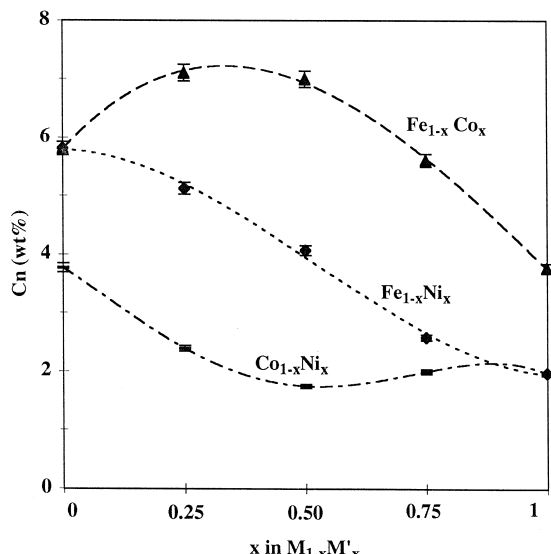


Fig. 1. Variation of the carbon content (C_n) with the composition of the alloy nanoparticle. The dashed lines are guides to the eye.

and calcined at 500°C for 30 min. The oxide product contained essentially the lacunar spinel phase [11,13] of the general formula $D_{1-3\alpha}T_{2+2\alpha}(\cdot)_\alpha O_4$, where D and T stand for divalent and trivalent cations and (\cdot) represents vacancies. A dry mixture of H_2-CH_4 (18 mole% CH_4) was passed over the calcined oxide at 1070°C for 6 min at a flow rate of 250 sccm. This resulted in the reduction of the transition metal ions to the metals in the form of nanoparticles, followed by the formation of carbon nanotubes, the entire process was very facile. We shall designate the various samples by $M_{1-x}M'_x$ ($M, M' = Fe, Co, Ni$) for brevity.

The carbon content, C_n , of the products subjected to the H_2-CH_4 treatment, containing carbon (in the form of nanotubes) along with the metal particles and the oxide, was determined by flash combustion. The values of C_n so obtained are listed in Table 1. The products after H_2-CH_4 treatment were oxidized in air at 900°C for 2 h to eliminate the carbon. The composition of the transition metal alloy clearly affects the conversion of CH_4 to carbon by hydrogen reduction. The values of C_n are plotted against the alloy composition in Fig. 1. $Fe_{0.75}Co_{0.25}$ and $Fe_{0.50}Co_{0.50}$ appear to be most efficient in terms of the carbon yield.

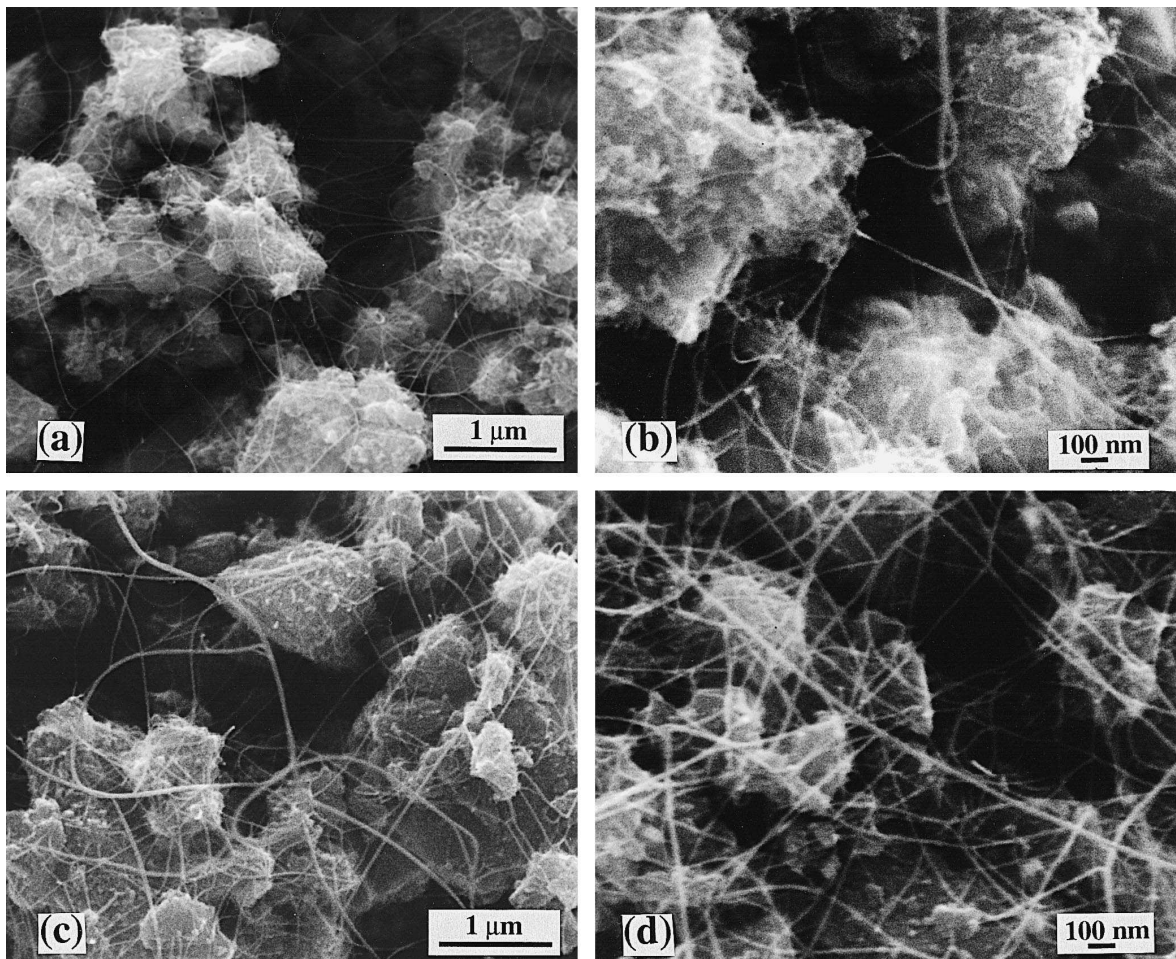


Fig. 2. SEM images of the product obtained by treatment of oxide spinels with the $\text{CH}_4\text{--H}_2$ mixture: (a) and (b) $\text{Fe}_{0.5}\text{Co}_{0.5}$; (c) and (d) $\text{Fe}_{0.5}\text{Ni}_{0.5}$.

BET¹ surface areas of the following materials were measured by N_2 adsorption: reduced product after passing the $\text{H}_2\text{--CH}_4$ mixture and hence containing carbon along with metal particles (S_r) and the material obtained after oxidizing the product of $\text{H}_2\text{--CH}_4$ treatment and hence free of carbon (S_o). The values of the surface areas are listed in Table 1. The products obtained after passing the $\text{H}_2\text{--CH}_4$ mixture over the oxide spinels were examined by X-ray diffraction (XRD), scanning electron microscopy (SEM) as well as transmission electron microscopy (TEM).

3. Results and discussion

The XRD patterns of the products obtained after subjecting the oxide spinels containing the transition metals to treatment with the $\text{H}_2\text{--CH}_4$ mixture at 1070°C showed evidence for the presence of metal or alloy particles (depending on the starting composition) and the oxide spinel, $\text{Mg}_{0.8}\text{Al}_{2.133}(\text{O}_{0.067}\text{O}_4)$ where () represents a vacancy. Thus, the oxide composition containing only Co gave reflections due to $\epsilon\text{-Co}$ whereas those with both Co and Ni gave reflections due to the alloys of the respective compositions. Reflections due to Fe–Ni and Fe–Co alloys were similarly found in the corresponding oxide compositions. With the iron-containing oxide spinel,

¹ Brünauer–Emmett–Teller adsorption isotherm.

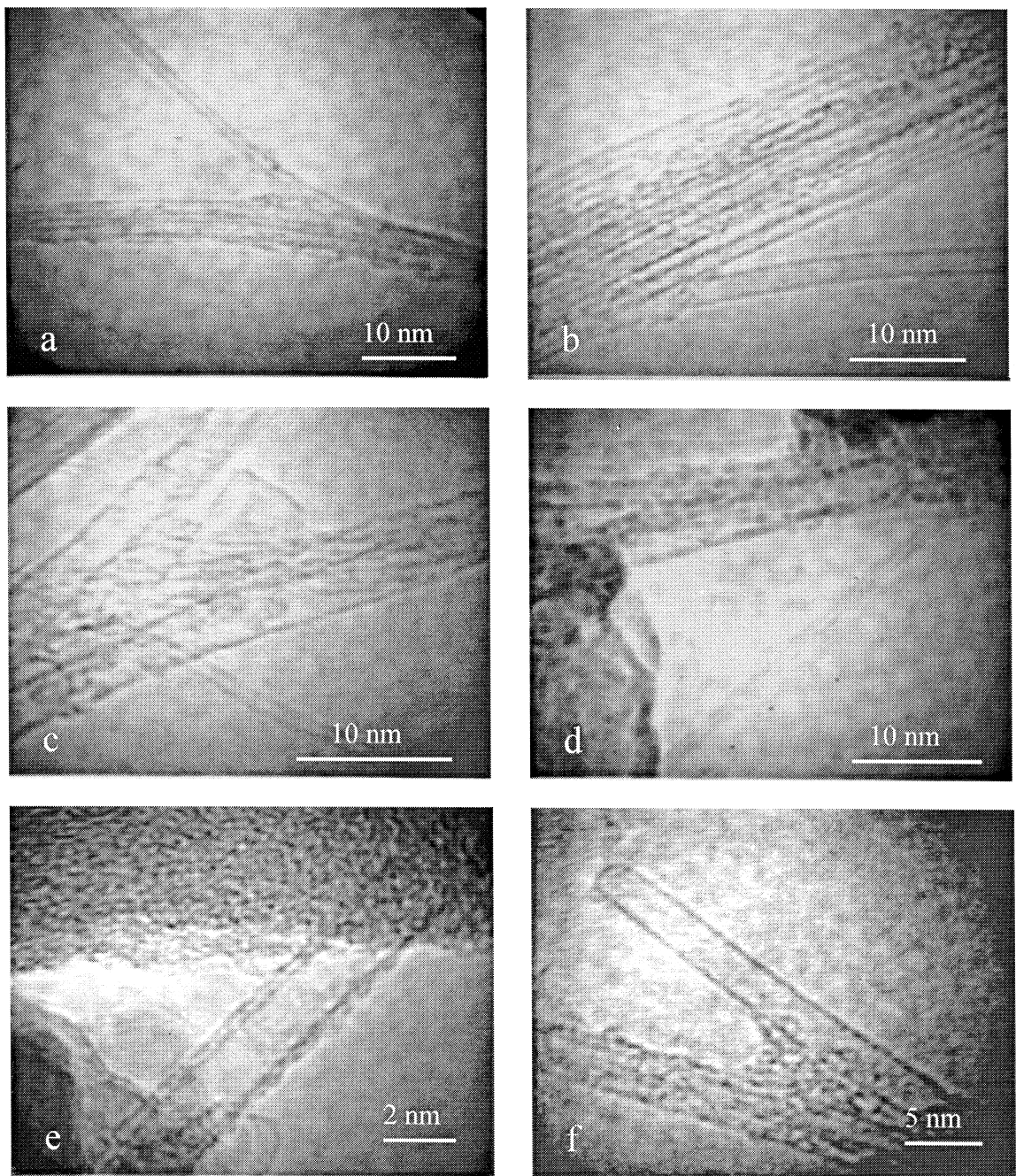


Fig. 3. TEM images of the nanotubes obtained with $\text{Fe}_{0.50}\text{Co}_{0.50}$ nanoparticles: (a) a single-wall nanotube (noted SWNT hereafter) 1.1 nm in diameter emerges from a bundle the diameter of which is ~4 nm; (b) the largest observed bundle, ~14 nm in diameter, with an emerging SWNT, 2 nm in diameter; (c) the thinnest observed SWNT, 0.8 nm in diameter, superimposed with two larger SWNTs; (d) a tight SWNT, 0.85 nm in diameter, with neighbouring larger tubes (between 1.6 and 2.8 nm in diameter); (e) a nanotube with 2 walls (2.1 nm in diameter); (f) a SWNT, 2.5 nm in diameter, with a closed hemisphere tip.

reflections due to Fe_3C were found as well as those due to $\alpha\text{-Fe}$. Clearly, treatment with the $\text{H}_2\text{-CH}_4$ mixture not only reduces the transition metal ions into the metallic state, but also forms binary alloys when two metal ions are present.

The SEM images of the oxide spinels subjected to the $\text{H}_2\text{-CH}_4$ treatment showed the presence of nanotubes in the form of a web-like network of long filaments. In Fig. 2, we show typical SEM images. The images generally reveal the presence of bundles of nanotubes, the bundle diameters varying with the composition of the alloy particles. Thus, with $\text{Fe}_{0.50}\text{Ni}_{0.50}$ and $\text{Co}_{0.50}\text{Ni}_{0.50}$, the bundle diameters are in the 20–50 and 10–20 nm ranges, respectively. Individual filaments are generally much smaller than 5 nm in diameter. The SEM image with $\text{Fe}_{0.50}\text{Co}_{0.50}$ particles shows very few nanotubes mainly because the nanotubes and their bundles are considerably smaller than 10 nm in diameter. The presence of large quantities of single-walled nanotubes in the case of $\text{Fe}_{0.50}\text{Co}_{0.50}$ could, however, be definitively established from the TEM images. SEM fails to reveal such thin nanotubes because of the limitation of the resolution. In Fig. 3, we show typical TEM images revealing the presence of isolated SWNTs as well as bundles of SWNTs. Fig. 3a shows a SWNT 1.1 nm in diameter emerging from a bundle of 4 nm diameter. Amorphous carbon deposits present on the bundle result from the degradation of the nanotubes under electron beam irradiation. Pristine samples accordingly show little of such deposits. The largest bundle observed by us is ~ 14 nm in diameter (Fig. 3b). An emerging SWNT, 2 nm in diameter, can be seen at the bottom of this image. In Fig. 3c, we show the thinnest SWNT (0.8 nm in diameter) observed by us; it is superimposed by two larger SWNTs, the walls of which are irregular because of degradation under the electron beam. A straight SWNT (0.85 nm in diameter) along with larger ones (between 1.6 and 2.8 nm in diameter) are shown in Fig. 3d. A nanotube (2.1 nm in diameter) with two walls is seen in Fig. 3e. It is interesting that most of the isolated nanotubes ($\sim 80\%$) are SWNTs with diameters in the 0.8–5 nm range. Multiwalled nanotubes found occasionally have diameters smaller than 10 nm, and generally possess only two graphite layers. Those with 3, 4 and 5 graphitic sheaths were rarely observed. In Fig. 3f, a SWNT (2.5 nm in diameter)

with a closed hemispheric tip is seen coming out of a thin bundle (3 nm in diameter). Interestingly, no catalyst particle is present at the tube tip.

From the values of the surface areas before and after $\text{H}_2\text{-CH}_4$ treatment (Table 1), we can obtain the contribution to the surface area by the carbon formed by the decomposition of CH_4 [14]. We list the $\Delta S = S_r - S_o$ values in Table 1. We show the variation of ΔS with the composition of the alloy nanoparticles in Fig. 4. The alloys are generally associated with higher ΔS values than either component metal, and the highest values are found with the Fe–Co alloys. The $\Delta S/C_n$ values, corresponding to the surface area per gram of carbon (produced by the decomposition of CH_4) may be taken to represent the quality of the nanotubes, a higher figure denoting a smaller tube diameter as well as a greater nanotube yield. We have listed the $\Delta S/C_n$ values in Table 1 and plotted them against the composition of the metal alloy particles in Fig. 5. A progressive increase in $\Delta S/C_n$ is observed with the Co content in the Fe–Co system, the Fe–Ni system shows such an increase with the Ni content partially. In the case of the Co–Ni system, $\Delta S/C_n$ actually decreases with the Ni content. The $\Delta S/C_n$ values in the alloys are generally in the range 195–338 $\text{m}^2 \text{ g}^{-1}$, the highest

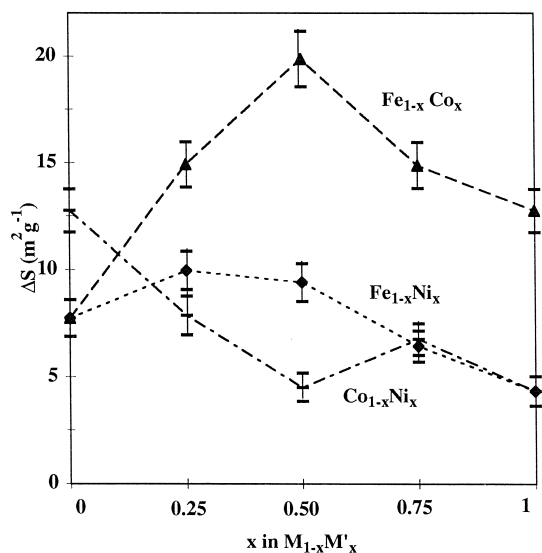


Fig. 4. Variation of the surface area due to the carbon product, ΔS , with the composition of the alloy nanoparticles. The dashed lines are guides to the eye.

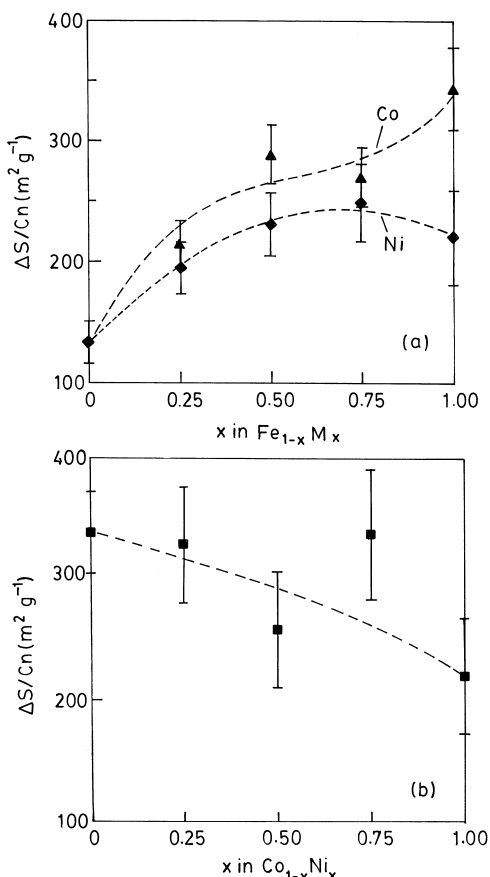


Fig. 5. Surface area per gram of carbon, $\Delta S/C_n$, plotted against the composition of the alloy nanoparticles. The dashed lines are guides to the eye.

value corresponding to that found with cobalt alone. The $\Delta S/C_n$ values found by us indicate that both Fe–Co and Co–Ni alloy particles yield high-quality nanotubes, the presence of Co is probably responsible for the effect. Interestingly, TEM studies also show that the $Fe_{0.5}Co_{0.5}$ alloy gives the highest yield of SWNTs as discussed earlier. The $\Delta S/C_n$ values found by us are close to the recently reported surface area of $268\text{ m}^2\text{ g}^{-1}$ for multi-walled nanotubes [15].

The above results show that transition metal alloy nanoparticles produced by the reduction of oxide spinels are good agents for generating single-walled nanotubes. This is consistent with the earlier observation [11] that reduction of spinels gives relatively small nanoparticles with a narrow size distribution. It

is indeed known that the small size of the nanoparticles is essential to form SWNTs [10,16]. The presence of a metal such as Co appears to prevent the formation of Fe_3C and such carbides. It is likely that the oxide support affords a good distribution of the alloy nanoparticles on its surface. Alloying promotes the decomposition of CH_4 to produce carbon nanotubes, the quality of which depends on the alloy composition. It is noteworthy that the best performance is found with FeCo nanoparticles which give a high yield of SWNTs of good quality, as judged both by electron microscopy and surface area measurements. The successful synthesis of good-quality SWNTs reported here by using FeCo alloy nanoparticles dispersed on oxide spinels is to be compared with the recent report of Kong et al. [17] who obtained SWNTs by chemical vapor deposition of CH_4 over impregnated Fe_2O_3/Al_2O_3 at low loading. These workers could not quantify the yield or quality of the nanotubes.

Acknowledgements

The authors would like to thank Dr. O. Quenard for his help in the preparation of the oxide solid solutions and Mr. L. Datas for his assistance with the TEM observations. The financial support of the Indo-French Centre for the Promotion of Advanced Research (New Delhi) is gratefully acknowledged.

References

- [1] S. Seraphin, D. Zhou, Appl. Phys. Lett. 64 (1994) 2087.
- [2] C.H. Kiang, W.A. Goddard III, Phys. Rev. Lett. 76 (1996) 2515.
- [3] T. Guo, P. Nikolaev, A. Thess, D.T. Colbert, R.E. Smalley, Chem. Phys. Lett. 243 (1995) 49.
- [4] M. Audier, J. Guinot, M. Coulon, L. Bonnetain, Carbon 19 (1981) 99.
- [5] M. Audier, L. Bonnetain, Carbon 23 (1985) 317.
- [6] R.G. Cossen, S. Lee, A. Sacco Jr., Carbon 32 (1994) 1143.
- [7] F.W.A.H. Geurts, R.G. Cossen, A. Sacco Jr., R.R. Biederman, Carbon 32 (1994) 1151.
- [8] S. Herreyre, P. Gadelle, Carbon 33 (1995) 234.
- [9] R. Sen, A. Govindaraj, C.N.R. Rao, Chem. Phys. Lett. 267 (1997) 276.

- [10] B.C. Satishkumar, A. Govindaraj, R. Sen, C.N.R. Rao, *Chem. Phys. Lett.* 293 (1998) 47.
- [11] O. Quenard, E. De Grave, Ch. Laurent, A. Rousset, *J. Mater. Chem.* 7 (1997) 2457.
- [12] K.C. Patil, S.T. Aruna, S. Ekambaram, *Curr. Opin. Solid State Mater. Sci.* 2 (1997) 158.
- [13] O. Quenard, Ch. Laurent, M. Brieu, A. Rousset, *Nanostruct. Mater.* 7 (1996) 497.
- [14] Ch. Laurent, A. Piegney, A. Rousset, *J. Mater. Chem.* 8 (1998) 1263.
- [15] S. Inone, N. Ichikumi, T. Suzuki, T. Uematsu, K. Keneko, *J. Phys. Chem.* 102 (1998) 4689.
- [16] H. Dai, A.G. Rinzler, P. Nikolaev, A. Thess, D.T. Colbert, R.E. Smalley, *Chem. Phys. Lett.* 260 (1996) 471.
- [17] J. Kong, A.M. Casell, H. Dai, *Chem. Phys. Lett.* 292 (1998) 567.

Hierarchical Composites of Single/Double-Walled Carbon Nanotubes Interlinked Flakes from Direct Carbon Deposition on Layered Double Hydroxides

By Meng-Qiang Zhao, Qiang Zhang, Xi-Lai Jia, Jia-Qi Huang,
Ying-Hao Zhang, and Fei Wei*

Three-dimensional hierarchical nanocomposites consisting of one-dimensional carbon nanotubes (CNTs) and two-dimensional lamellar flakes (such as clay, layered double hydroxides) show unexpected properties for unique applications. To achieve a well-designed structure with a specific function, the uniform distribution of CNTs into the used matrix is a key issue. Here, it is shown that a hierarchical composite of single/double-walled CNTs interlinked with two-dimensional flakes can be constructed via *in-situ* CNT growth onto layered double hydroxide (LDH) flakes. Both the wall number and diameter of the CNTs and the composition of the flakes can be easily tuned by changing the proportion of the transition metal in the LDH flakes. Furthermore, a structure with continuously interlinked CNT layers alternating with lamellar flakes is obtained after compression. The hierarchical composite is demonstrated to be an excellent filler for strong polyimide films. This study indicates that LDH is an extraordinary catalyst for the fabrication of hierarchical composites with high-quality single/double-walled CNTs. The as-obtained CNTs/calcined LDHs nanocomposite is a novel structural platform for the design of mechanically robust materials, catalysts, ion-transportation, energy-conversion, and other applications.

1. Introduction

Combining materials with 1D nanowires/nanotubes and 2D lamellar flakes leads to 3D hierarchical nanocomposites with unexpected properties for unique applications.^[1–6] For instance, the combined 3D clay–polymer composites and clay–carbon nanotube (CNT) nanocomposites show extraordinary mechanical and energy-absorbing properties.^[2–6] The key issue for the successful application of nanocomposites lies in the ability to

manipulate the arrangement of the two phases (filler and matrix) into a well-designed structure.^[3,5,7] For example, when the CNTs (filler) are well dispersed as an enhanced network into a polymer (matrix), the mechanical, electrical, and energy-absorbing properties can be significantly improved.^[4,5,8–10] Good dispersion of CNTs in the matrix or other solvents is believed to be a key issue to obtain nanocomposites with extraordinary performance. Thus, surfactants, biomacromolecules, copolymers, DNA, and clays have widely been used for CNT dispersion through shearing or sonication processes.^[11] Ionic liquids have also been selected as a solvent to achieve good dispersion of CNTs.^[12] However, those procedures are usually complicated. Furthermore, the CNTs might be flocculated into CNT bundles or CNT agglomerates because of strong van der Waals interactions during the further mixing and casting procedures. Up to now, the uniform distribution of CNTs into certain matrices with a well-designed structure and certain function has been a challenge.

Recently, it has been shown that CNTs can be directly synthesized on various kinds of matrices to controllably fabricate nanocomposites. Cao et al. grew CNTs on a SiC fiber and the obtained multifunctional brush could be used for several unique tasks such as cleaning nanoparticles from narrow spaces, coating the internal spaces of holes, and functioning as movable electromechanical brush contacts and switches.^[13] Woven SiC fiber/CNT composites via *in-situ* growth showed remarkable improvements in the interlaminar fracture toughness, hardness, delamination resistance, damping, and electrical conductivities.^[6] CNT(Ni)/Al composites with homogeneously dispersed CNTs within the Al powders have been obtained by the *in-situ* growth of CNTs on an Al matrix with low Ni content.^[14] The hardness and tensile strength of the CNT(Ni)/Al matrix composites were 2.0 and 1.8 times higher than those of the same composites obtained by dispersion/mixing methods.^[14] Zhang et al. directly grew CNTs on clays and found that the as-obtained products could be directly filled into a nylon-6 matrix to significantly improve its tensile strength.^[15] These results all indicate that the *in-situ* synthesis of

[*] Prof. F. Wei, Dr. M. Q. Zhao, Dr. Q. Zhang, X. L. Jia, J. Q. Huang, Y. H. Zhang
Beijing Key Laboratory of Green Chemical Reaction Engineering and Technology
Department of Chemical Engineering
Tsinghua University
Beijing 100084 (P.R. China)
E-mail: wf-dce@tsinghua.edu.cn

DOI: 10.1002/adfm.200901522

CNTs on certain matrices achieved very good dispersion^[13–16] and the as-obtained composites generally showed excellent performances. Compared to traditional procedures, in-situ nanocomposite fabrication strategies are quite easy to achieve and cost less. However, in these studies only multiwalled CNTs (MWCNTs) were used for the in-situ fabrication of nanocomposites on certain matrices.^[6,13–16] It should be noted that single/double walled CNTs (S/DWCNTs) have a much more ideal structure in terms of their smaller diameter, larger aspect ratio, and lower defect density.^[17–20] Compared to MWCNTs, S/DWCNTs exhibit better mechanical, thermal, and electrical properties, and can be found in a wide range of applications, such as, in high-performance nanocomposites, high electron mobility components for electronics, and field-emission displays.^[21] If 1D S/DWCNTs can be controllably synthesized on 2D flakes to fabricate a hierarchical composite, novel advanced functional materials with well-dispersed S/DWCNTs could be obtained.

However, the direct growth of S/DWCNTs on the matrices mentioned above (such as SiC fibers, carbon fibers, Al metal, or clays) is not so easy. The reason lies in the difficulty of obtaining a uniform distribution of small catalyst particles (0.5–5 nm) on those matrices at high temperature (750–1300 °C).^[18,22] MgO, Al₂O₃, and SiO₂ have previously been studied as supports for the growth of S/DWCNTs,^[19,20] however, they were found to cause random nanoparticle agglomeration when being used as catalyst supports for S/DWCNT growth.^[19,20,22] Thus, they cannot be used as the 2D material to promote the dispersion of S/DWCNTs. Recently, layered double hydroxides (LDHs), also known as hydrotalcite-like materials, which are a class of 2D nanostructured anionic clays whose structure is based on brucite (Mg(OH)₂)-like layers, can be easily and controllably synthesized on a large scale.^[23,24] Most metals, such as Fe, Co, Ni, Cu, Zn, Mg, Al, Ca, and Li, can be arranged on the atomic level in a lamellar LDH flake with controllable components. This is attributed to the substitution of divalent metal cations by trivalent cations within their hydrotalcite-like layers, which leads the LDH layer to be positively charged and balanced by a wide variety of anions within their interlayer domains. Compared to natural clay, the composition of LDHs is much simpler and can be anticipated, which is very important for their use in actual catalysts, catalyst precursors, or catalyst supports.^[24] After calcination and reduction metal particles can be produced that are uniformly distributed on the flakes and that function as good catalysts for CNT growth. A few reports have described the in-situ growth of CNTs on LDHs.^[25] However, only random MWCNTs with a diameter ranging from 10 to 50 nm and a specified surface area of less than 50 m² g⁻¹ were synthesized in most cases.^[25] Compared to MWCNT growth, high temperatures and small catalyst particles are needed for S/DWCNT growth. Thus

the composition of the LDH flakes and the growth window need to be explored carefully. Moreover, the morphology of the LDHs after growth has rarely been mentioned and the performance of the composites of CNTs and calcined LDH (c-LDH) flakes has seldomly been investigated.

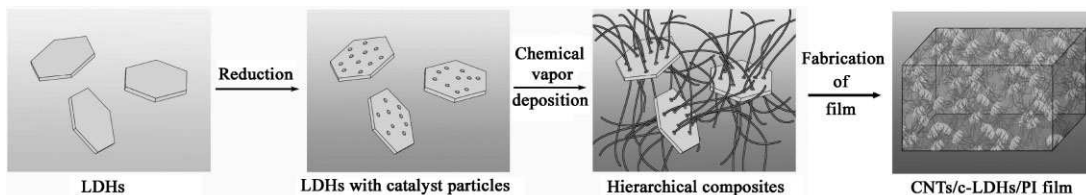
For this report, we used Fe/Mg/Al LDHs, as well as Co/Mg/Al, Ni/Mg/Al, and Co/Fe/Mg/Al LDHs as the catalyst precursor, and we explored the idea of the in-situ fabrication of S/DWCNTs interlinked with lamellar flakes that directly formed a 3D hierarchical nanocomposite. As shown in Scheme 1, the LDHs were used as the 2D lamellar flakes for CNT growth. After calcination and reduction, metal particles with small sizes could be produced. By introducing a carbon source a well-controlled CNT interlinked hierarchical nanocomposite was obtained. After characterization by Raman spectroscopy and transmission electron microscopy (TEM), we found that the CNTs mainly consisted of S/DWCNTs. Moreover, the hierarchical composites could be further pressed into a continuous CNT layer alternating with lamellar c-LDH flakes to form a layered structure. A high-performance CNTs/c-LDHs/polyimide (PI) film was fabricated from the as-grown products to show the extraordinary performance of the hierarchical composite of S/DWCNTs interlinked with c-LDH flakes.

2. Results and Discussion

2.1. Hierarchical Composites of CNTs Interlinked with c-LDH Flakes

A series of Fe/Mg/Al LDH flakes with different iron content were prepared using a co-precipitation reaction, and named as LDH A–E as shown in Table 1. As illustrated in Figure 1a, the as-obtained LDH-C samples show the typical morphology of LDH flakes. One can see clearly that the LDHs are plate-like hexagonal particles with lateral sizes ranging from 1 to 2 μm. A typical powder X-ray diffraction (XRD) pattern for the as-synthesized LDH-C is shown in Figure 1b. The sharp and symmetric features of the diffraction peaks strongly suggest that the produced Fe/Mg/Al LDH flakes were highly crystallized, possessing a 3D order. In addition, all the diffraction peaks could be indexed as a rhombohedral structure with the refined lattice parameters of $a = 0.2994$ nm and $c = 2.2125$ nm. The chemical composition of the prepared LDH A–E samples obtained by elemental analysis is shown in Table 1.

The hierarchical composites A–E were obtained after direct growth of CNTs on LDH A–E by a facile chemical vapor deposition (CVD) process (Table 1). Typical scanning electron microscopy



Scheme 1. Schematic illustration showing the procedure for constructing hierarchical composites of single/double-walled carbon nanotubes interlinked LDHs and the incorporation of CNT/c-LDHs hybrid fillers into a PI matrix to make a CNTs/c-LDHs/PI film.

Table 1. The properties of hierarchical composites of S/DWCNTs interlinked flakes obtained from direct carbon deposition on Fe/Mg/Al layered double hydroxides.

Samples	LDHs	Composition of as-prepared LDHs ($n(\text{Fe})/n(\text{Mg})/n(\text{Al})$)	$\text{SSA}_{\text{CNTs}} [\text{m}^2 \text{ g}^{-1}]$	CNTs content	I_D/I_C
Composite-A	LDH-A	0.05: 1.85: 1	1289.0	15%	0.06
Composite-B	LDH-B	0.10: 1.53: 1	1017.1	30%	0.04
Composite-C	LDH-C	0.20: 1.99: 1	941.6	36%	0.03
Composite-D	LDH-D	0.36: 1.87: 1	770.9	32%	0.04
Composite-E	LDH-E	0.83: 1.61: 1	498.1	25%	0.11

(SEM) images of the composites B and C are shown in Figure 2a and b, respectively. It can be observed that the use of a short growth duration results in the formation of a large amount of CNTs interlinked in the c-LDHs. Powder XRD analysis showed that the hydrotalcite-like structure of the LDHs was lost after the calcination, leaving metal oxides and spinellites as the major elements (Fig. S1). However, the plate-like hexagonal morphology was well preserved and the size was hardly changed after calcination. The fine CNTs intercrossed among the architecture showed a lamellar structure. The CNT content in the as-grown composite C was 36%, indicating that about 0.56 g of CNTs were grown on 1.0 g of c-LDH flakes. Figure 2c shows a typical TEM image of the CNTs in composite C. High-resolution TEM (HRTEM) (Fig. 2d) indicated that the CNTs, which are interlinked among the lamellar particles, mainly consisted of S/DWCNTs.

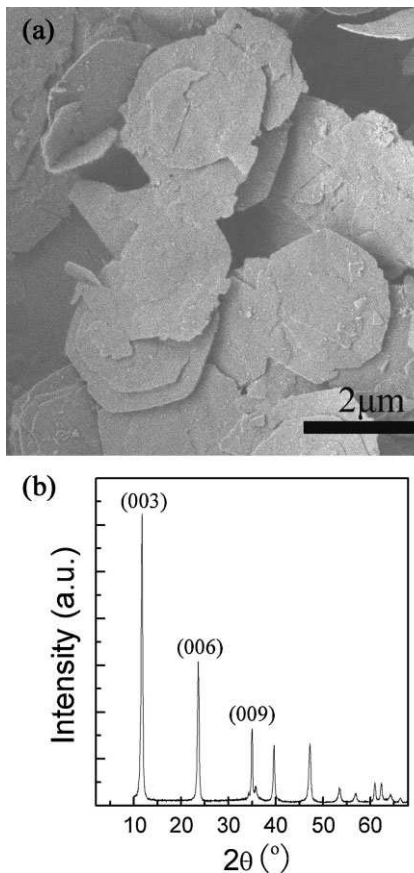


Figure 1. a) SEM image and b) XRD pattern of LDH-C.

They have a small and uniform diameter ranging from 1.5 to 5.0 nm, which is to be discussed further in detail in the following section. Moreover, it can be seen from both the SEM and TEM images that the obtained S/DWCNTs are not strongly entangled. This may be attributed to the orientating function of the c-LDH flakes. It is clear that the roots of the synthesized CNTs are fixed at certain spots of the c-LDH flakes thus preventing aggregation. In this way hierarchical nanocomposites composed of S/DWCNTs interlinked flakes were obtained. The flakes were individually distributed among the entangled S/DWCNTs. This led to a hierarchical structure with the advantage of being able to change the morphology of an ordered material with a layered structure consisting of interlinked S/DWCNT layers alternating with lamellar particles. Moreover, the existence of flakes effectively promoted the homogeneous dispersion of the S/DWCNTs.

A few other reports have described the growth of MWCNTs on Co/Al, Co/Fe/Al, Ni/Mg/Al, and Fe/Zn/Al LDHs.^[25] There were also some reports on carbon nanofibers or MWCNTs grown on natural clay^[15,26] or lava.^[27] However, very few S/DWCNTs were synthesized in these reports. Here, the production of uniform, hierarchical composites of S/DWCNTs interlinked with flakes was

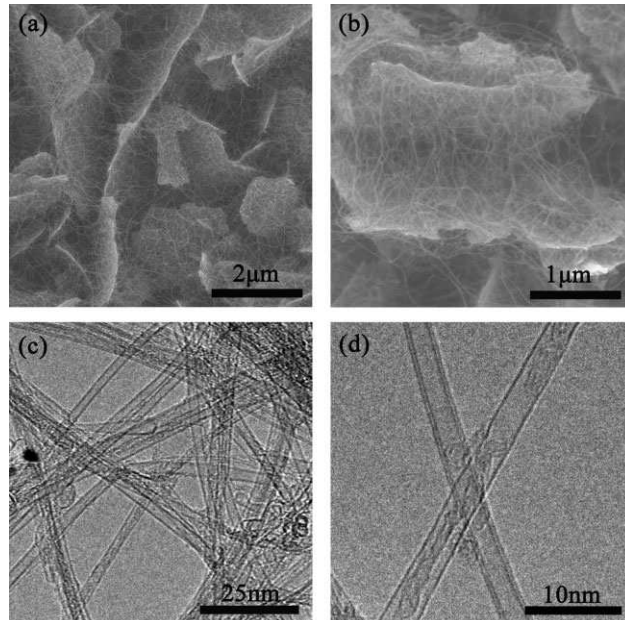


Figure 2. SEM and TEM images of the obtained hierarchical composites from CH_4 over Fe/Mg/Al LDHs at 900°C . a) SEM image of composite B; b) SEM image of composite C; c) TEM image of CNTs in composite C; d) HRTEM image of CNTs in composite C.

realized by an in-situ growth via a facile CVD process. A family of LDH flakes, such as Fe/Mg/Al, Co/Mg/Al, Ni/Mg/Al, and Co/Fe/Mg/Al LDH flakes, was selected as catalyst precursor to synthesize the S/DWCNTs. The metal content (Fe, Co, and/or Ni) in the LDHs ranged from 0.2 to 15%. Furthermore, high temperatures (900 °C) were used to form small catalyst particles (0.5–5 nm) for SWCNT and/or DWCNT growth without the need for a H₂ reduction step. Both the catalyst composition and the growth parameter selection were important for the S/DWCNT growth. All LDH flakes (Co/Mg/Al, Ni/Mg/Al, and Co/Fe/Mg/Al) were demonstrated to be effective catalysts for the construction of hierarchical composites as is shown in the Supporting information (Figs. S2–S4). For example, with Fe/Mg/Al LDHs serving as the catalyst, about 40% of single-walled and 60% of double-walled CNTs were obtained when the Fe content was 3.0 wt % and a mean surface area of 942 m² g⁻¹ was found. The intensity ratio of the Raman D-band over the G-band (I_D/I_G) was just 0.03, which was obviously lower than that of CNTs grown on Fe/Mg/O,^[28] Fe/Mo/Mg/O,^[17] or Fe/Mo/Al/O^[20] catalysts. These indicated that the as grown CNTs were of a high quality containing few defects. A novel general strategy using

LDH flakes serving as a catalyst for the growth of high-quality S/DWCNTs was thus realized.

2.2. Tuning of the Diameter and Wall Number Distribution of CNTs in the Hierarchical Nanocomposites

Apart from the interesting structures obtained above, it should be noted that not only the composition of the c-LDHs, but also the structure of the CNTs in the hierarchical composites can be adjusted. Here we discuss the facile strategy to modulate the wall number, diameter, and content of the CNTs in the hierarchical composites by simply changing the iron proportion in the LDH flakes.

A series of Fe/Mg/Al LDH with different Fe content were used for S/DWCNT growth (Table 1), and similar hierarchical composites were obtained, see before. The TEM and HRTEM images for the CNTs in composites A, C, and E are presented in Figure 3a to f. The distributions of the wall number and the outer

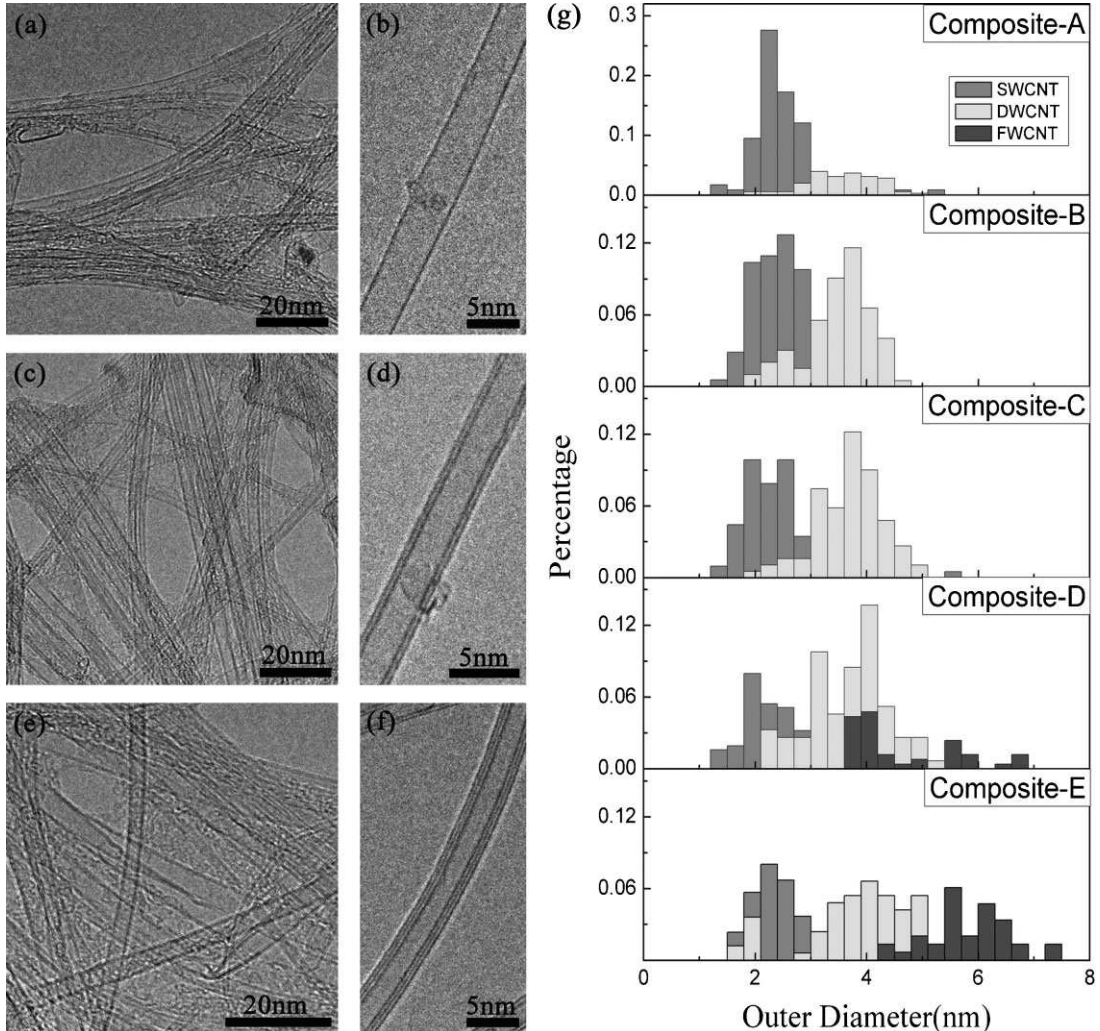


Figure 3. TEM and HRTEM images of CNTs in a,b) composite A; c,d) composite C; e,f) composite E. g) Distribution of the outer diameter for obtained S/D/FWCNTs in composites A–E.

diameter of the CNTs were obtained by measuring around 200 individual CNTs in the HRTEM images, as shown in Figure 3g. For composite A, only SWCNTs and DWCNTs were found, and the amount of SWCNTs could be up to about 77% according to the statistical results. The specific surface area (SSA) of CNTs in composite A was around $1289.0\text{ m}^2\text{ g}^{-1}$ (Table 1). This is close to the theoretical value of individual SWCNTs ($1315\text{ m}^2\text{ g}^{-1}$), and it is higher than that of DWCNTs ($700\text{--}850\text{ m}^2\text{ g}^{-1}$), MWCNTs ($200\text{--}600\text{ m}^2\text{ g}^{-1}$), and SWCNT bundles ($100\text{--}700\text{ m}^2\text{ g}^{-1}$).^[29] This indicates that Fe/Mg/Al LDH flakes with a low iron content show a good selectivity for SWCNT growth, whereby the SWCNTs were also well dispersed. The CNT content in composite A was about 15%. With increasing iron content, more DWCNTs and MWCNTs were found (composites B–E (Fig. 3g)), while the SSA of the CNTs showed an obvious decreasing trend (Table 1). The CNT contents in composites B and C increased to 30% and 36%, indicating that more carbon was deposited on the catalysts. However, the SSA of the CNTs decreased to $1017.1\text{ m}^2\text{ g}^{-1}$ and $941.6\text{ m}^2\text{ g}^{-1}$, respectively. The statistical proportion of SWCNTs in composites B and C is shown to be 52% and 43%, respectively (Fig. 3g). With further increasing Fe content in the LDH flakes, the SSA of the CNTs further decreased (Table 1), and more and more MWCNTs were found in the as-grown products (Fig. 3g). It should be noted that the wall numbers of these observed MWCNTs were not higher than 5, the reason for which we call them few-walled CNTs (FWCNTs).^[30] For composite D, the proportions of DWCNTs and FWCNTs were shown to be 56% and 17%, respectively, whereas those for composite E were statistically calculated to be 43% and 24%, respectively. The CNT content in composites C and D decreased a little (Table 1), which can be attributed to a catalyst deactivation caused by the formation of catalyst particles with larger sizes. An obvious characteristic of the outer-diameter distributions of the CNTs can be seen in Figure 3g. The outer diameter of the CNTs has a distinct dividing line for all samples. The distribution of the outer diameter of the SWCNTs was mainly concentrated on 1.5 to 3.0 nm, while for DWCNTs, it mostly ranged from 3.0 to 5.0 nm. For FWCNTs, outer diameters above 5.0 nm were commonly seen.

The diameter of the CNTs depended heavily on the diameter distribution of the catalyst particles at the growth temperature.^[31] In the LDH flakes, the iron ion is inserted into the hydrotalcite-like layers by isomorphous substitution of Mg^{2+} .^[23] Thus, they are distributed uniformly in the layers at an atomic level. After calcination and reduction, the Fe^{3+} will be reduced into Fe nanoparticles. As shown in Figure 4a, there are large amount of catalyst particles with a size smaller than 5 nm distributed on the flakes. During the CVD process, the carbon source will decompose at the surface of these nanoparticles and the dominating surface diffusion of the carbon atoms on the catalyst particles results in the formation of SWCNTs.^[32] With increasing size of the catalyst particles, both surface and bulk diffusion, which correspond to the formation of the outer and inner layer of DWCNTs, respectively, take place on a single catalyst particle.^[33] Thus, SWCNTs are more inclined to form (Fig. 4b) on particles that are smaller than 3 nm, and DWCNTs usually grow on particles in the size range of 3–5 nm (Fig. 4c). While for particles larger than 5 nm, the formation of FWCNTs and carbon-sphere-encapsulated particles lead to catalyst deactivation (Fig. 4d). The results in Figure 3g can therefore easily be explained by the fact that with

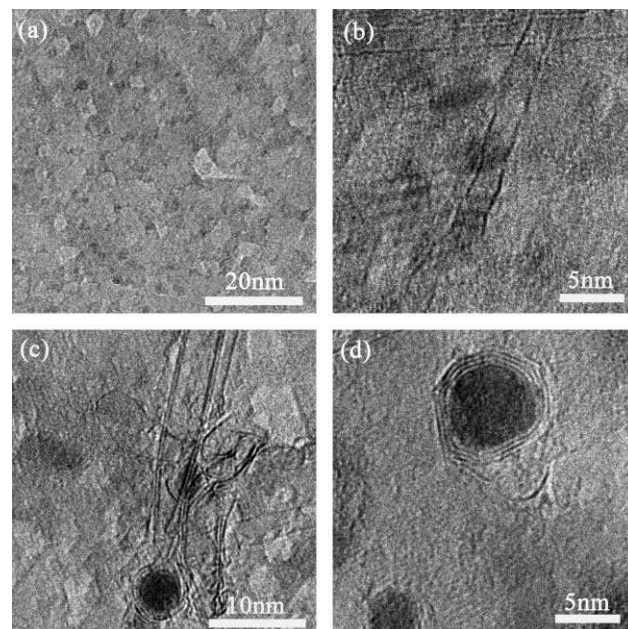


Figure 4. a) Catalyst particles on LDH-C after calcination and reduction. b) SWCNT grown from a catalyst particle smaller than 3 nm on LDH-A. c) DWCNT grown from a catalyst particle with a size of 4 nm on LDH-C. d) Carbon spheres encapsulated catalyst particles with a size of 7 nm on LDH-E.

increasing iron content the catalyst particles grow larger during the reduction course.

2.3. Compressing of CNTs Interlinked in Hierarchical Composites into Alternating CNTs/c-LDHs

We have found that the constitution of the hierarchical composites can be easily modulated by changing the composition of the LDHs. Furthermore, from the SEM images demonstrated in Figure 2, the CNTs are in a low-density, well-dispersed state, and the CNTs interlinked with c-LDH flakes show abundant pores. As shown in Figure 5, the synthesized CNTs occupy the interspaces between the lamellar c-LDH particles, leading to the reduction of the pore volume of pores between 230 and 3000 nm in diameter. However, the volume of pores ranging from 5 to 230 nm increased significantly, indicating that CNTs have a certain possibility to broaden the pores among c-LDH flakes and thus promote the dispersion of c-LDH flakes. Because of the good electrical conductivity and abundant mesopores and macropores, hierarchical composites of S/DWCNTs interlinked flakes can potentially be used for applications in supercapacitors and Li-ion batteries.^[34] Furthermore, the hierarchical composites can easily be densified by simple compression. As shown in Figure 6, when the as-prepared hierarchical composite is compressed in a die at a pressure of 100 MPa, a block of densified CNTs/c-LDHs can be obtained. The compressed block shows a uniform pore-size distribution ranging from 5 to 12 nm (Fig. 6b), which can be attributed to the interspaces between lamellar particles or between the CNTs. The density of the block was measured to be $1.8\text{ cm}^3\text{ g}^{-1}$,

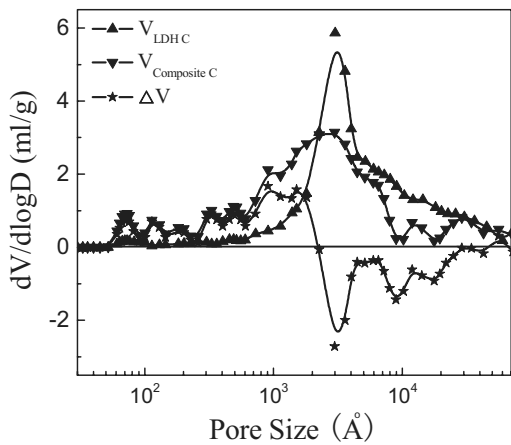


Figure 5. Pore-size distributions for prepared LDH-C and the obtained hierarchical sample of composite C.

which is 85 times higher than that before the compression. The volume fraction of the CNTs in the block is estimated to be around 60%. The schematic illustration for the structure of the block is shown in the inserted picture. It can be seen from the SEM image of the cross section of the block cleaved with a razor that the block shows a clearly layered structure, as shown in Figure 6c. Aligned S/DWCNTs with high density were formed following the line of cleaving on the cross section of the block because of the pliability, toughness, and easy-combing properties of the CNTs interlinked with c-LDH flakes. From the bird's-eye view of the compressed block, as shown in Figure 6d, it can be seen that the

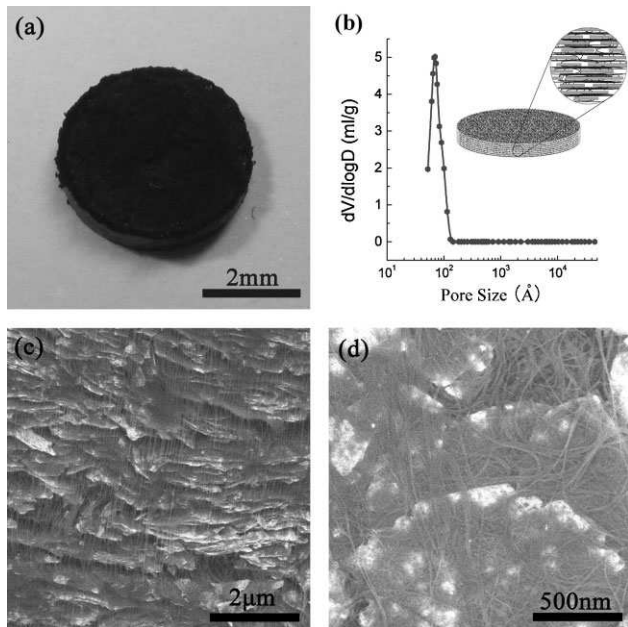


Figure 6. a) A block of the CNTs/c-LDHs nanocomposites after compression at a pressure of 100 MPa. b) Pore-size distribution of the compressed composite C, the inset shows a schematic illustration of the structure of the block. c) SEM image of the cross section and d) a bird's eye view of the block.

layered structure consists of interlinked CNT layers alternating with lamellar c-LDH particles. Thus a great ordered material with layered structure composed of interlinked S/DWCNT layers alternating with lamellar particles was obtained after the hierarchical composite was compressed at high pressure. Thousands of layers of CNTs and c-LDH flakes were assembled into an alternating structure that will have great potential in high-performance composites, energy storage and -conversion, sensors, and other applications.^[3,35]

2.4. Fabrication of Strong CNTs/c-LDHs/PI Films

The CNTs/c-LDHs hierarchical composite discussed above is expected to be an ideal filler for high-performance polymers because of the homogenous dispersion of both CNTs and LDH flakes. In order to demonstrate the enhancement effect of the prepared filler, we have fabricated CNTs/c-LDHs/polyimide (PI) films via an in-situ polymerization method using composite C. The reasons for using PI for this is that PI is a polymer with good transparency, toughness, and light weight, and it is under consideration for applications in advanced spacecraft, in indium tin oxide (ITO) soleplates for liquid crystal displays, in solar cell soleplates, and in optical waveguides for communication purposes.^[36] Increasing the mechanical properties of PI is an important issue to realize those applications. Here, the as-obtained stress-strain curves are shown in Figure 7a, and the tensile properties of neat PI and CNTs/c-LDHs/PI film are summarized in Table 2. It can be seen that the incorporation of only 0.40 wt % of composite C significantly improves the mechanical properties of PI. The elastic modulus of PI is improved from 651.3 to 770.9 MPa, and the tensile strength is improved from 78.1 to 109.1 MPa. The elongation-at-break of the composite film increases significantly from 26.6% to 59.6%, indicating that PI becomes more robust after the incorporation of the CNTs/c-LDHs hybrid filler. The energy absorbed^[10] during the tensile testing is improved by 220% (Table 2). These results indicate that the mechanical properties of the CNTs/c-LDHs/PI film are substantially superior to those of neat PI.

It is very interesting to compare the mechanical properties of the CNTs/c-LDHs/PI film with those of CNTs/PI films with various loading levels of purified CNT filler. Yu et al. reported that the incorporation of 0.30 wt % SWCNTs into PI leads to an increase of the tensile strength by only 5% and an increase of the Young's modulus by 18%.^[9] Zhang et al. prepared composites containing functionalized CNTs and PI, and the measurement of the mechanical properties showed that the addition of 1.0 wt % MWCNTs in the PI matrix caused a small increase of 6.7% in the tensile strength and an increase of 29.8% in the Young's modulus.^[37] Here, the elastic modulus of PI is improved by about 20%, and the tensile strength is improved by about 40%. The enhancement of the mechanical properties upon incorporation of 0.40 wt % CNTs/c-LDHs filler is thus even higher than that in the case of using neat CNTs alone. The high performance of the composite is obviously related to the homogeneous dispersion of both the 1D CNTs and the 2D c-LDH flakes. Figure 7b shows a high-resolution SEM image of the fractured surface of a CNTs/c-LDHs/PI film after tensile testing. It clearly

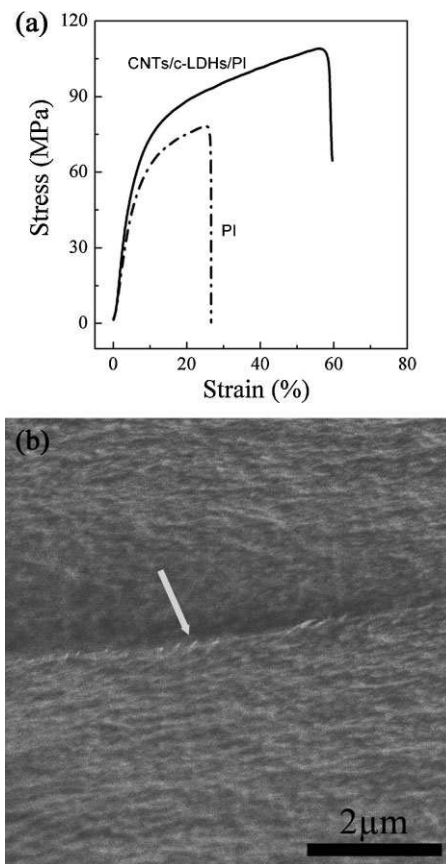


Figure 7. a) Stress–strain curves of a neat PI and a composite CNTs/c-LDHs/PI film containing 0.40 wt % CNTs/c-LDHs hybrid filler. b) SEM image of the typical morphology of the failure surface of a CNTs/c-LDHs/PI film.

shows that the CNTs/c-LDHs hierarchical composite has a close interfacial connection with the PI matrix, which is indicated by the white arrow. The jagged line is the c-LDH flake and the small bright dots are the ends of the ruptured CNTs on the fractured surface. The observation that most CNTs were broken upon failure rather than just pulled out of the matrix is clear evidence of the strong interfacial adhesion between the CNTs/c-LDHs filler and the PI matrix. This is responsible for the significant reinforcement of the mechanical properties of the prepared film. Moreover, because of the uniform distribution of S/DWCNTs in the c-LDHs, the composite can also be used for the self-organization of ordered structures to improve the electrical and thermal conductivities of various polymers. The CNTs/c-LDHs composite is a good platform for wide applications of CNTs in catalysis, ion-transportation, and energy-conversion areas.

Table 2. Tensile properties of neat PI and its composite CNTs/c-LDHs/PI containing 0.40 wt % CNTs/c-LDHs hybrid filler.

Samples	Tensile modulus [MPa]	Tensile strength [MPa]	Elongation-at-break [%]	Energy absorbed [kJ kg ⁻¹]
Neat PI film	651.3	78.1	26.6	19.1
CNTs/c-LDHs/PI films	770.9	109.1	59.6	60.9

3. Conclusions

Hierarchical composites of S/DWCNTs interlinked with flakes were constructed via direct carbon deposition on LDH flakes. The lamellar structure of the LDHs was preserved; moreover, they were individually distributed among the entangled S/DWCNTs. The synthesized CNTs showed large SSA values, little defects, and were obtained in high yield. The combination of the 1D CNTs and the 2D c-LDH flakes promoted CNT dispersion. The diameter and wall number of the CNTs could easily be tuned by changing the proportion of iron in the LDHs. A lower iron content favored the growth of SWCNTs because of the formation of large amounts of catalyst particles smaller than 3 nm. While for higher iron content, catalyst particles with a size ranging from 3 to 5 nm were more likely to be formed and the growth of DWCNTs was favored. A structure composed of interlinked CNT layers alternating with lamellar flakes could be obtained after the compression of the hierarchical composites. The mechanical properties of CNTs/c-LDHs/PI films were demonstrated to have been significantly improved compared to neat PI. This work provides a novel structural platform towards the design of mechanically robust materials; it also provides novel materials for catalytical, ion-transportation, energy-conversion, and other applications.

4. Experimental

Preparation of LDH Flakes: The Fe/Mg/Al LDH flakes were prepared using a co-precipitation reaction. Mg(NO₃)₂ · 6H₂O, Al(NO₃)₃ · 9H₂O, and urea were dissolved in 250.0 mL of deionized water with [Mg²⁺] + [Al³⁺] = 0.15 mol L⁻¹, n(Mg)/n(Al) = 2:1, [urea] = 3.0 mol L⁻¹. Fe(NO₃)₃ · 9H₂O was then dissolved in the solution, the molar ratios of Fe to Al were controlled at 0.05, 0.1, 0.2, 0.4, and 0.8, respectively. The prepared solution was heated to 100 °C under continuous magnetic stirring for 12 h in a flask (equipped with a reflux condenser) of 500.0 mL under ambient atmosphere. Then, the obtained suspension was kept at 95 °C for another 12 h without stirring. After filtering, washing, and freeze-drying, the final products were ground to brown-yellow powders with different color depths. The LDH flakes obtained were named as LDH A–E. The other LDH flakes were prepared through the same process. The composition of these LDH flakes was fixed as n(Co)/n(Mg)/n(Al) = 0.4:2:1, n(Ni)/n(Mg)/n(Al) = 0.4:2:1 and n(Co)/n(Fe)/n(Mg)/n(Al) = 0.2:0.2:2:1.

Construction of Hierarchical Composites of CNTs Interlinked Lamellar Flakes: The preparation of hierarchical composites of CNTs interlinked lamellar flakes was carried out using a catalytic chemical vapor deposition (CVD) process. About 10 mg of the LDH catalyst was sprayed uniformly into a quartz boat, which was then placed at the center of a horizontal quartz tube inserted into a furnace at atmospheric pressure. Then the furnace was heated under flowing Ar (600 mL min⁻¹). On reaching 900 °C, the flow rate of Ar was turned down to 100 mL min⁻¹ and maintained as such for 10 min. CH₄ (500 mL min⁻¹) was then introduced into the reactor for 5 min after which H₂ (50 mL min⁻¹) was also added. The growth was maintained for 30 min at 900 °C before the furnace was cooled to room temperature under Ar flow. The as-obtained powders were named as composite A to E, corresponding to their starting LDH A to E.

Fabrication of CNTs/c-LDHs/PI Films: Composite C was used as the reinforcement filler, and the synthesis procedure for a typical well-dispersed CNTs/c-LDHs/PI film was as follows: composite C (0.025 g) and 4,4'-diaminodiphenyl ether (3.006 g, 98%) were first dispersed in dimethyl acetamide (65 mL) in an ultrasonic bath for 3 h at room temperature in N₂ atmosphere to yield a uniform suspension. Then, pyromellitic dianhydride (3.341 g, >98.5%) was dissolved in the suspension under strong stirring in an ice-water bath for 1 h under N₂ protection. The obtained suspension was then put into vacuum for 2 h to get rid of the bubbles existing in the suspension. After that, the suspension was poured onto glass slides, and a film-coating device was used to coat films with a thickness of around 60 µm. These glass slides with coated films were dried at 50 °C for 12 h to remove the solvent. The dried films were then placed at the center of a horizontal quartz tube inserted into a furnace at atmospheric pressure and under Ar protection. The furnace was operated following a fixed temperature program for in-situ polymerization of PI. It was heated from room temperature to 100 °C over a period of 60 min and was then maintained at this temperature for another 60 min. After this, the furnace was further heated to 200 °C over 100 min, and kept there for 60 min. Then the temperature was raised to 300 °C over another 100 min and the furnace was again kept at that temperature for 60 min. Finally, the furnace was cooled down to room temperature under an Ar atmosphere, and the obtained PI/LDH-CNT nanocomposite films were peeled off from the glass slides for tensile testing. The neat PI films were prepared in a similar way without the incorporation of composite C.

Characterization: The samples were characterized using a JSM 7401F (JEOL Ltd., Tokyo, Japan) scanning electron microscope operated at 5.0 kV and a JEM 2010 (JEOL Ltd., Tokyo, Japan) transmission electron microscope operated at 120.0 kV. Energy-dispersive spectroscopy (EDS) analysis was performed using a JSM-7401F apparatus with the analytical software INCA, and the accelerating voltage applied was 15.0 kV. XRD patterns were recorded on a Rigaku D/max-RB diffractometer at 40.0 kV and 120 mA using Cu K α radiation. Raman spectra were obtained under He–Ne laser excitation at 514 and 633 nm using a Renishaw RM2000 spectrometer. The carbon content was obtained by thermogravimetric analysis under heating at 10 °C min⁻¹ using Q500. The pore-size distribution of the samples was measured by an ex-situ Hg penetration method. The BET specific surface area of all samples was measured by N₂ adsorption at liquid-N₂ temperature using a Micromeritics Flow Sorb II 2300. The tensile tests were operated on an electronic universal testing machine WDW 3020 at a stretching rate of 5.0 mm min⁻¹.

Acknowledgements

The authors thank Prof. Dang-Sheng Su from the Fritz Haber Institute of the Max Planck Society, Germany, for instructive discussions. The work was supported by the Natural Scientific Foundation of China (No. 20736004, No. 20736007, No. 2007AA03Z346) and the China National Program (No. 2006CB0N0702). Supporting Information is available online from Wiley InterScience or from the author.

Received: August 13, 2009

Published online: January 19, 2010

- [1] a) P. B. Messersmith, E. P. Giannelis, *Chem. Mater.* **1994**, *6*, 1719.
b) S. S. Ray, M. Okamoto, *Prog. Polym. Sci.* **2003**, *28*, 1539.
- [2] a) E. P. Giannelis, *Adv. Mater.* **1996**, *8*, 29. b) D. F. Schmidt, F. Clement, E. P. Giannelis, *Adv. Funct. Mater.* **2006**, *16*, 417.
- [3] a) Q. Zhang, M. Q. Zhao, Y. Liu, A. Y. Cao, W. Z. Qian, Y. F. Lu, F. Wei, *Adv. Mater.* **2009**, *21*, 2876. b) L. Y. Jiang, C. M. Leu, K. H. Wei, *Adv. Mater.* **2002**, *14*, 426.
- [4] a) P. Dubois, M. Alexandre, *Adv. Eng. Mater.* **2006**, *8*, 147. b) M. Okamoto, T. Fujigaya, N. Nakashima, *Adv. Funct. Mater.* **2008**, *18*, 1776.
- [5] L. Liu, J. C. Grunlan, *Adv. Funct. Mater.* **2007**, *17*, 2343.

- [6] V. P. Veedu, A. Y. Cao, X. S. Li, K. G. Ma, C. Soldano, S. Kar, P. M. Ajayan, M. N. Ghasemi-Nejhad, *Nat. Mater.* **2006**, *5*, 457.
- [7] Y. J. Xu, G. Weinberg, X. Liu, O. Timpe, R. Schlogl, D. S. Su, *Adv. Funct. Mater.* **2008**, *18*, 3613.
- [8] a) E. Frackowiak, K. Metenier, V. Bertagna, F. Beguin, *Appl. Phys. Lett.* **2000**, *77*, 2421. b) E. J. Stochi, D. C. Working, C. Park, P. T. Lillehei, J. H. Rouse, C. C. Topping, A. R. Bhattacharya, S. Kumar, *Compos. Part B-Eng.* **2004**, *35*, 439. c) J. N. Coleman, U. Khan, W. J. Blau, Y. K. Gun'ko, *Carbon* **2006**, *44*, 1624. d) H. Y. Ma, L. F. Tong, Z. B. Xu, Z. P. Fang, *Adv. Funct. Mater.* **2008**, *18*, 414.
- [9] A. P. Yu, H. Hui, E. Belyarova, M. E. Itkis, J. Gao, B. Zhao, R. C. Haddon, *Compos. Sci. Technol.* **2006**, *66*, 1190.
- [10] A. B. Dalton, S. Collins, E. Muñoz, J. M. Razal, V. H. Ebron, J. P. Ferraris, J. N. Coleman, B. G. Kim, R. H. Baughman, *Nature* **2003**, *423*, 703.
- [11] a) X. Y. Gong, J. Liu, S. Baskaran, R. D. Voise, J. S. Young, *Chem. Mater.* **2000**, *12*, 1049. b) T. Chatterjee, K. Yurekli, V. G. Hadjiev, R. Krishnamoorti, *Adv. Funct. Mater.* **2005**, *15*, 1832. c) J. Li, P. C. Ma, W. S. Chow, C. K. To, B. Z. Tang, J. K. Kim, *Adv. Funct. Mater.* **2007**, *17*, 3207. d) J. Y. Shin, T. Premkumar, K. E. Geckeler, *Chem. Eur. J.* **2008**, *14*, 6044. e) B. Krause, G. Petzold, S. Pegel, P. Potschke, *Carbon* **2009**, *47*, 602.
- [12] J. Y. Wang, H. B. Chu, Y. Li, *ACS Nano* **2008**, *2*, 2540.
- [13] A. Y. Cao, V. P. Veedu, X. S. Li, Z. L. Yao, M. N. Ghasemi-Nejhad, P. M. Ajayan, *Nat. Mater.* **2005**, *4*, 540.
- [14] C. N. He, N. Q. Zhao, C. S. Shi, X. W. Du, J. J. Li, H. P. Li, Q. R. Cui, *Adv. Mater.* **2007**, *19*, 1128.
- [15] W. D. Zhang, I. Y. Phang, T. X. Liu, *Adv. Mater.* **2006**, *18*, 73.
- [16] a) N. Yamamoto, A. J. Hart, E. J. Garcia, S. S. Wicks, H. M. Duong, A. H. Slocum, B. L. Wardle, *Carbon* **2009**, *47*, 551. b) J. O. Zhao, L. Liu, Q. G. Guo, J. L. Shi, G. T. Zhai, J. R. Song, Z. J. Liu, *Carbon* **2008**, *46*, 380.
- [17] a) A. M. Cassell, J. A. Raymakers, J. Kong, H. J. Dai, *J. Phys. Chem. B* **1999**, *103*, 6484. b) B. C. Liu, S. C. Lyu, S. I. Jung, H. K. Kang, C. W. Yang, J. W. Park, C. Y. Park, C. J. Lee, *Chem. Phys. Lett.* **2004**, *383*, 104. c) Q. Zhang, H. Yu, Y. Liu, W. Z. Qian, Y. Wang, G. H. Luo, F. Wei, *Nano* **2008**, *3*, 45.
- [18] P. Nikolaev, M. J. Bronikowski, R. K. Bradley, F. Rohrmund, D. T. Colbert, K. A. Smith, R. E. Smalley, *Chem. Phys. Lett.* **1999**, *313*, 91.
- [19] a) D. Ciuparu, Y. Chen, S. Lim, G. L. Haller, L. Pfefferle, *J. Phys. Chem. B* **2004**, *108*, 503. b) Y. Li, X. B. Zhang, L. H. Shen, J. H. Luo, X. Y. Tao, F. Liu, G. L. Xu, Y. W. Wang, H. J. Geise, G. Van Tendeloo, *Chem. Phys. Lett.* **2004**, *398*, 276. c) H. Ago, S. Imamura, T. Okazaki, T. Saito, M. Yumura, M. Tsuji, *J. Phys. Chem. B* **2005**, *109*, 10, 035.
- [20] Q. Zhang, W. Z. Qian, Q. Wen, Y. Liu, D. H. Wang, F. Wei, *Carbon* **2007**, *45*, 1645.
- [21] a) R. H. Baughman, A. A. Zakhidov, W. A. de Heer, *Science* **2002**, *297*, 787.
b) S. Banerjee, T. Hemraj-Benny, S. S. Wong, *Adv. Mater.* **2005**, *17*, 17.
- [22] a) H. M. Cheng, F. Li, G. Su, H. Y. Pan, L. L. He, X. Sun, M. S. Dresselhaus, *Appl. Phys. Lett.* **1998**, *72*, 3282. b) F. Wei, Q. Zhang, W. Z. Qian, H. Yu, Y. Wang, G. H. Luo, G. H. Xu, D. Z. Wang, *Powder Technol.* **2008**, *183*, 10.
- [23] D. G. Evans, D. A. Xue, *Chem. Commun.* **2006**, 485.
- [24] a) D. P. Debecker, E. M. Gaigneaux, G. Busca, *Chem. Eur. J.* **2009**, *15*, 3920.
b) Z. Lue, X. Duan, Chin, J. Catal., *Catal.* **2008**, *29*, 839. c) F. Z. Zhang, X. Xiang, F. Li, X. Duan, *Catal. Surv. Asia* **2008**, *12*, 253.
- [25] a) F. Li, Q. Tan, D. G. Evans, X. Duan, *Catal. Lett.* **2005**, *99*, 151. b) Y. Zhao, Q. Z. Jiao, C. H. Li, J. Liang, *Carbon* **2007**, *45*, 2159. c) H. I. Hima, X. Xiang, L. Zhang, F. Li, *J. Mater. Chem.* **2008**, *18*, 1245. d) H. I. Hima, X. Xiang, L. Zhang, F. Li, D. G. Evans, *Chin. J. Inorg. Chem.* **2008**, *24*, 886. e) R. Benito, M. Herrero, F. M. Labajos, V. Rives, C. Royo, N. Latorre, A. Monzon, *Chem. Eng. J.* **2009**, *149*, 455. f) X. Xiang, L. Zhang, H. I. Hima, F. Li, D. G. Evans, *Appl. Clay Sci.* **2009**, *42*, 405.
- [26] a) A. Garcia, M. H. Bocanegra-Bernal, C. Dominguez, A. Aguilar-Elguezabal, *Appl. Clay Sci.* **2009**, *45*, 95. b) H. P. Li, N. Q. Zhao, Y. Liu, C. Y. Liang, C. S. Shi, X. W. Du, J. J. Li, *Compos. Part A-Appl. Sci. Manuf.* **2008**, *39*, 1128. c) A. Rinaldi, J. Zhang, J. Mizera, F. Girsidis, N. Wang, S. B. A. Hamid, R. Schlogl, D. S. Su, *Chem. Commun.* **2008**, 6528.

- d) D. Gournis, M. A. Karakassides, T. Bakas, N. Boukos, D. Petridis, *Carbon* **2002**, *40*, 2641. e) A. Bakandritsos, A. Simopoulos, D. Petridis, *Chem. Mater.* **2005**, *17*, 3468. f) Q. Zhang, M. Q. Zhao, J. Q. Huang, Y. Liu, Y. Wang, W. Z. Qian, F. Wei, *Carbon* **2009**, *47*, 2600. g) F. C. C. Moura, R. M. Lago, *Appl. Catal. B-Environ.* **2009**, *90*, 436.
- [27] a) D. S. Su, *ChemSusChem* **2009**, *2*, 1009. b) D. S. Su, X. W. Chen, *Angew. Chem. Int. Ed.* **2007**, *46*, 1823. c) D. S. Su, X. W. Chen, X. Liu, J. J. Delgado, R. Schlogl, A. Gajovic, *Adv. Mater.* **2008**, *20*, 3597.
- [28] Y. Liu, W. Z. Qian, Q. Zhang, G. Q. Ning, G. H. Luo, Y. Wang, D. Z. Wang, F. Wei, *Chem. Eng. Technol.* **2009**, *32*, 73.
- [29] A. Peigney, C. Laurent, E. Flahaut, R. R. Bacsa, A. Rousset, *Carbon* **2001**, *39*, 507.
- [30] a) C. Qian, H. Qi, J. Liu, *J. Phys. Chem. C* **2007**, *111*, 131. b) P. Landois, A. Peigney, C. Laurent, L. Frin, L. Datas, E. Flahaut, *Carbon* **2009**, *47*, 789.
- [31] a) Y. M. Li, W. Kim, Y. G. Zhang, M. Rolandi, D. W. Wang, H. J. Dai, *J. Phys. Chem. B* **2001**, *105*, 11424. b) E. F. Kukovitsky, S. G. L'Vov, N. A. Sainov, V. A. Shustov, L. A. Chernozatonskii, *Chem. Phys. Lett.* **2002**, *355*, 497. c) Y. Chen, D. Ciuparu, S. Y. Lim, Y. H. Yang, G. L. Haller, L. Pfefferle, *J. Catal.* **2004**, *225*, 453. d) S. Chakrabarti, H. Kume, L. J. Pan, T. Nagasaka, Y. Nakayama, *J. Phys. Chem. C* **2007**, *111*, 1929. e) T. Inoue, I. Gunjishima, A. Okamoto, *Carbon* **2007**, *45*, 2164. f) Q. F. Liu, W. C. Ren, Z. G. Chen, D. W. Wang, B. L. Liu, B. Yu, F. Li, H. T. Cong, H. M. Cheng, *ACS Nano* **2008**, *2*, 1722.
- [32] a) H. Ago, K. Nakamura, N. Uehara, M. Tsuji, *J. Phys. Chem. B* **2004**, *108*, 18908. b) R. Seidel, G. S. Duesberg, E. Unger, A. P. Graham, M. Liebau, F. Kreupl, *J. Phys. Chem. B* **2004**, *108*, 1888. c) J. Y. Raty, F. Gygi, G. Galli, *Phys. Rev. Lett.* **2005**, *95*, 096103.
- [33] a) R. T. K. Baker, *Carbon* **1989**, *27*, 315. b) F. Ding, A. Rosen, K. Bolton, *Carbon* **2005**, *43*, 2215. c) S. Hofmann, G. Csanyi, A. C. Ferrari, M. C. Payne, J. Robertson, *Phys. Rev. Lett.* **2005**, *95*, 036101. d) R. F. Wood, S. Pannala, J. C. Wells, A. A. Puretzky, D. B. Geohegan, *Phys. Rev. B* **2007**, *75*, 235446.
- [34] a) E. Frackowiak, F. Beguin, *Carbon* **2002**, *40*, 1775. b) E. Frackowiak, *Phys. Chem. Chem. Phys.* **2007**, *9*, 1774.
- [35] a) P. T. Hammond, *Adv. Mater.* **2004**, *16*, 1271. b) X. Zhang, H. Chen, H. Y. Zhang, *Chem. Commun.* **2007**, 1395.
- [36] M. X. Ding, *Prog. Polym. Sci.* **2007**, *32*, 623.
- [37] Q. H. Zhang, J. Li, X. Zhao, D. J. Chen, *Polym. Int.* **2009**, *58*, 557.

Selective Chemical Vapor Deposition Synthesis of Double-Wall Carbon Nanotubes on Mesoporous Silica

Palanisamy Ramesh,[†] Toshiya Okazaki,[‡] Risa Taniguchi,[‡] Junichi Kimura,[‡] Toshiki Sugai,[‡] Kenichi Sato,^{†,§} Yuji Ozeki,^{†,§} and Hisanori Shinohara^{*,†,‡}

CREST, Japan Science and Technology Agency, c/o Department of Chemistry, Nagoya University, Nagoya 464-8602, Japan, Department of Chemistry and Institute for Advanced Research, Nagoya University, Nagoya 464-8602, Japan, and Chemical Research Laboratories, Toray Industries, Inc., Nagoya 455-8502, Japan

Received: July 31, 2004; In Final Form: October 26, 2004

Double-wall carbon nanotubes (DWNTs) have been selectively synthesized over Fe/Co loaded mesoporous silica by catalytic chemical vapor deposition of alcohol. Several silica materials with desired pore diameter and morphology have been investigated for the DWNT growth. The diameter distribution and selectivity of the DWNT are found to depend on the reaction temperature, pore size, and thermal stability of the support material. A high-yield synthesis of DWNTs has been achieved at 900 °C over high-temperature stable mesoporous silica. The outer diameter of DWNTs is found to be in the range of 1.5–5.4 nm with a “d” spacing of 0.38 ± 0.02 nm between inner and outer layers, which is much larger than those of multiwall carbon nanotubes.

Introduction

Intriguing electronic, mechanical, and structural properties of carbon nanotubes have stimulated burgeoning research in the nanometer scale.^{1,2} Synthesis, characterization, and applications of the carbon nanotubes have received much attention over the past decade.^{1–7} Various methods such as laser vaporization, DC arc discharge, and chemical vapor deposition (CVD) have been developed for their synthesis.^{1–7} The advent of CVD of carbon-containing molecules such as simple hydrocarbons and alcohols over nanometer-sized metal particles supported on zeolite, alumina, silica, or magnesia has established the possibilities of large-scale synthesis of carbon nanotubes at low temperatures.^{3–7}

Apart from the large-scale production, aligned bundles and patterned formation of nanotubes over a substrate are the advantages of the CVD syntheses compared to other methods.³ Conventionally multiwall carbon nanotubes (MWNTs) have been produced in large scale by CVD methods.⁴ Significant progress has been accomplished in the CVD synthesis of single-wall carbon nanotubes (SWNTs) in recent years and has led to a better understanding of the mechanism of the nanotube growth on the supported metal particles.^{5–7} Various support materials and metal catalysts have been evaluated for the synthesis of SWNTs, and it is well-established that nanometer-sized metal particles are necessary for the growth of SWNTs.^{5–7}

Particular attention has been paid in recent years on the selective synthesis and characterization of DWNTs.^{8–23} They are regarded as the intermediate structure between SWNTs and MWNTs. Their structural stability as in MWNTs and low-threshold voltages as in SWNTs for the field emission property lead to DWNTs being a promising material for long-term field

emitter under lower applied potentials.⁸ The structural properties such as interlayer interactions and mechanical strength are interesting, and DWNTs also exhibit interesting ambipolar transport characteristics compared to SWNTs.⁹ Evidently, there is an increasing demand for the selective growth of DWNTs.

Several reports have already appeared on the synthesis of DWNTs.^{10–23} However, the selective synthesis of DWNTs over other types of nanotube is proven to be crucial for their applications in electronics and other fields. The temperature of the reaction, metal catalyst composition, and the addition of hydrogen or sulfur have dramatically altered the selectivity of DWNTs.^{10–15} It is important to understand and control these parameters in order to achieve a large-scale selective growth of DWNTs.

Among the various parameters found to affect the DWNT growth in the CVD synthesis, the nature of the support material has been studied in less detail. Iijima and co-workers have reported the production of a mixture of DWNTs and SWNTs by the decomposition of methane on mesoporous silica, whereas the zeolite support material is reported to yield only SWNTs.¹⁴ MgO is also used as a support material for DWNT growth.^{12,16,17} Ren and co-workers have reported that high surface area, mesoporous Nantek MgO with mesopores of 3 nm selectively produces DWNTs, whereas nonporous Nanomyte MgO produces large-diameter tubes.¹⁶ The selectivity of DWNTs observed in the above-mentioned case is due to the mesopores and high surface area of MgO. Flahaut and co-workers have reported that the preparation conditions of MgO have drastically affected the selectivity of DWNT over MWNTs.¹² We have previously reported the selective growth of DWNTs on thermally stable zeolite TS-1 using acetylene as the carbon source.¹⁵ The other zeolite materials such as HSZ-320NAA and HSZ-390HUA are found to be not suitable for the production of DWNTs at the same reaction conditions. These observations prompted us to further study the role of supporting material for the selective growth of DWNTs. Possible control on the

* Corresponding author. Telephone: 81-(0)52-789-2482. Fax: 81-(0)52-789-1169. E-mail: noris@cc.nagoya-u.ac.jp.

[†] CREST, Nagoya University.

[‡] Department of Chemistry and Institute for Advanced Research, Nagoya University.

[§] Toray Industries, Inc.

selectivity of DWNT can be achieved if the properties of the support materials are controlled.

Here we aim to understand the role of silica support materials in the production of DWNTs using alcohol as the carbon source. The possibilities of synthesis of silica with desired pore diameters, wall thickness, and morphology are added advantages compared to conventional zeolite materials.^{24–27} Mesoporous silica has already been used as support material for the production of carbon nanotubes by several research groups.^{14,28–30} Maruyama and co-workers have reported the production of SWNTs using alcohol as the carbon source on mesoporous silica prepared by sol–gel method.²⁹ MCM-41 type siliceous materials have been recently introduced by Haller and co-workers for the growth of SWNTs.³⁰

We have employed surfactant-directed sol–gel and hydrothermal syntheses^{24–27} for the preparation of mesoporous silica and studied the effect of their physical and chemical properties on the selective growth of DWNTs in detail. The carbon nanotubes prepared using these silica materials as the catalyst support have been characterized by high-resolution transmission electron microscopy (HRTEM) and Raman spectroscopy.

Experimental Section

Tetraethyl orthosilicate (TEOS), fumed silica, tetramethylammonium hydroxide ((TMA)OH), cetyltrimethylammonium bromide (CTAB), and iron acetate are obtained from Aldrich (St. Louis, MO, USA), and cetylpyridinium chloride (CPC) is a product of Sigma (St. Louis, MO, USA). Cobalt acetate has been obtained from Wako Chemicals (Osaka, Japan). Mesoporous silica has been prepared by sol–gel method using a procedure similar to that reported earlier.²⁴ TEOS, CPC, HCl, water, ethanol, and heptane are mixed in a molar ratio of 5:1:0.027:15:67:33, respectively. This mixture is refluxed for an hour, and then the solvents ethanol and heptane are removed by a rotary evaporator at 60 °C for 10 min. The viscous liquid is then dried in the oven overnight and crushed into powder. This material is calcined for 10 h at 550 °C and designated as SG-1.

Mesoporous silica samples have been prepared by sol–gel and hydrothermal methods using CTAB as the structure-directing agent according to previous reports.^{25–27} Hydrolysis of the silicate is carried out by mixing TEOS with ethanol, HCl, and water in a molar ratio of 1:3:5e⁻⁵:1, respectively. This mixture is refluxed for an hour and then ethanol solution of CTAB is added to it with excess water and HCl. The final molar ratio of TEOS:ethanol:HCl:water:CTAB is maintained as 1:20:4e⁻³:5:0.1, respectively. This mixture is stirred for 48 h at room temperature. The viscous liquid is spread out on a Petri dish and dried in air for 2–3 days. The silica plates obtained by this treatment are crushed into powder, calcined at 550 °C for 8 h and denoted as SG-2.

Hydrothermal synthesis of mesoporous silica has been carried out by using the following procedure.^{26,27} 3.64 g of CTAB and 1.45 g of (TMA)OH are dissolved in 28.8 mL of water at 35 °C, and 2.4 g of fumed silica is added to it and stirred further for an hour. The final molar ratio of SiO₂:CTAB:TMAOH:H₂O is maintained as 1:0.25:0.2:40, respectively. This gel is aged for 20 h and transferred to an autoclave and heated at 150 °C for 48 or 96 h. After the reaction the silica is filtered, washed, dried, and calcined at 550 °C for 8 h. These materials will be referred to as MCM41 and MCM41–96, respectively. The secondary synthesis of mesoporous silica is carried out by using a procedure similar to that above with MCM41 as the silica source instead of fumed silica, and the reaction time is 140 h.

The calcined secondary silica material is designated as 2MCM41–140.

Carbon nanotube synthesis is carried out on a Fe/Co loaded silica sample. Iron acetate and cobalt acetate were dissolved in methanol and loaded into silica using a wet impregnation method as reported previously for zeolite materials from our laboratory.¹⁵ The final weight of the metal is 2.5% each over the weight of silica. The catalyst material is kept on a quartz boat and placed inside a quartz tube in the furnace. The catalyst is activated at 300 °C using 500 mL/min argon flow for 30 min, and then the temperature is raised to 800–900 °C. Ethanol vapor is introduced into the furnace along with 500 mL/min argon flow for 30 min at desired reaction temperatures, and the quartz tube is evacuated continuously during the reaction. The pressure of the quartz tube is maintained between 10 and 40 Torr during the reaction. The as-grown carbon nanotubes are cooled to room temperature in argon atmosphere.

Nitrogen adsorption measurement for the surface area and pore size analysis of the silica materials has been carried out using an automatic vapor adsorption measurement system BELSORP 18. Powder X-ray diffraction (XRD) patterns of the SG-1 and SG-2 have been obtained from the thin films. Powder material has been used for XRD analysis in the case of MCM41 type materials. XRD patterns have been obtained by using 1.54 Å Cu Kα radiation with a 2θ step size of 0.01 (Rigaku RINT2100PC). Ammonia temperature programmed desorption (NH₃-TPD) has been carried out using a TPD-MS:ANELVA AGS-7000 from room temperature to 800 °C with 60 mL/min He gas flow. The total amount of ammonia desorbed has been calculated using the peak area from room temperature to 500 °C. All these silica material characterizations have been carried out using only silica without the metal ions loaded onto them.

Carbon nanotubes are grown over 2.5% Fe/Co loaded silica materials, and details of the preparation are described in the following section. Scanning electron micrographs (SEM) of the nanotubes are obtained from JEOL JSM-6340F operating at 1.7 kV. A small quantity of the as-grown nanotubes is dispersed in ethanol and deposited over a carbon-coated copper grid for TEM analyses. HRTEM images have been obtained using a JEOL JEM-2010F transmission electron microscope operating at 120 kV. Micro-Raman spectroscopic measurements have been carried out using Horiba Jobin Yvon HR-800 with 633 nm He–Ne laser as the excitation source.

Results and Discussion

Surface Area and XRD Measurements of Silica Materials. The silica materials prepared in the present study have been characterized using BET surface area analysis and XRD. Figure 1A shows the nitrogen BET adsorption and desorption isotherms of the silica materials prepared using CPC or CTAB as the structure-directing agent. Sol–gel-derived SG-1 shows an adsorption in the partial pressure range of 0.08–0.22. The adsorption is not well-developed, indicating that this material is microporous and has no long-range order. SG-2 shows an adsorption at the partial pressure range of 0.18–0.31 and also has no long-range order. The adsorption isotherm shows that this material is mesoporous. In contrast, the silica materials prepared by the hydrothermal method show well-developed adsorption isotherms due to the pore-filling effect, indicating that they are mesoporous and possess long-range ordering.²⁶ MCM41, MCM41–96, and 2MCM41–140 show an adsorption in the partial pressure ranges of 0.39–0.47, 0.41–0.47, and 0.46–0.53, respectively.

The porosity and ordering of the pore channels depend on the preparation conditions. The difference observed in the

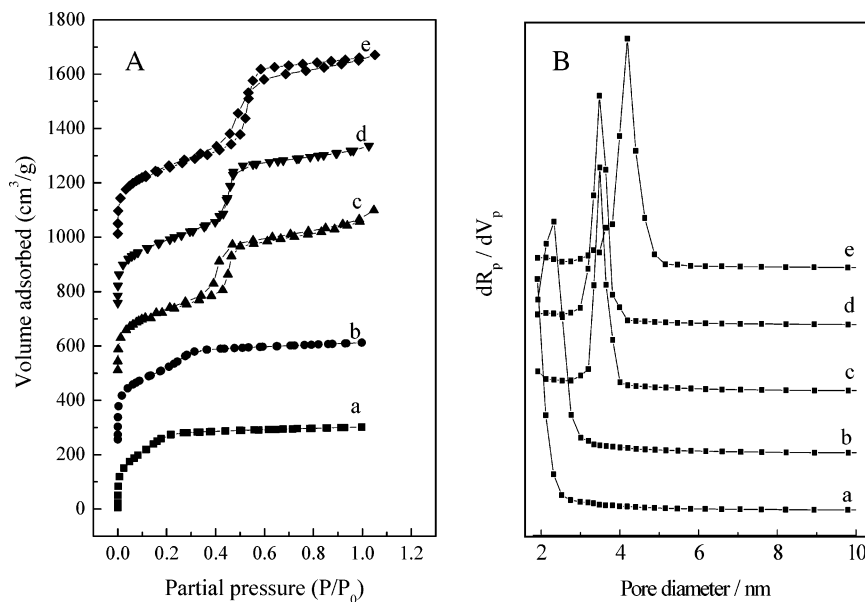


Figure 1. (A) Nitrogen adsorption and desorption isotherms and (B) plot of pore size distribution of the silica materials: (a) SG-1, (b) SG-2, (c) MCM41, (d) MCM41-96, and (e) 2MCM41-140. Each adsorption isotherm is offset by 250 in the y axis for clarity.

TABLE 1: Pore Diameter, Pore Volume, Surface Area, and *d*-Spacing of Silica Materials and DWNT Yields Obtained on These Silica Materials at Different Temperatures

silica samples	pore diam (nm)	pore vol (cm³/g)	surface area (m²/g)	<i>d</i> -spacing (nm)	DWNT yield at 850 °C	DWNT yield at 900 °C
fumed silica	nil	nil	255	nil	NA ^a	NA
SG-1	<2	0.212	935	3.04	20%	5%
SG-2	2.32	0.384	963	3.35	50%	30%
MCM41	3.48	0.865	829	4.21	10%	30%
MCM41-96	3.48	0.904	833	4.40	60%	80%
2MCM41-140	4.18	1.008	903	4.64	40%	50%

^a NA = not available.

adsorption isotherms of silicas is due to the difference in the preparation conditions since the sol-gel method involves an acid catalysis as opposed to the hydrothermal method that involves a base catalysis. Figure 1B shows the pore size measurements of the silica samples. It reveals that the SG-1 is not mesoporous, as already observed from the adsorption isotherm. The other four silica materials prepared by using CTAB as the structure-directing agent are mesoporous in nature.

Table 1 shows the pore diameter, pore volume, and specific surface area of these silica materials. The pore size of silica can be increased from 2.32 to 3.48 and to 4.18 nm when prepared by hydrothermal methods. It is observed that the secondary synthesis leads to a large pore size of 4.18 nm. The increase observed in the pore size may be due to the dissolution of silica during the secondary synthesis of MCM41. The pore volume is found to depend on the pore size of the silica materials. These porous silica materials have a typical surface area of 800–950 m²/g and the surface areas of all these materials are higher than those of nonporous fumed silica. The surface areas observed for sol-gel and hydrothermal materials are comparable, but the pore volume is found to be higher in the case of hydrothermal MCM41 type materials. The fact that an increase in the pore volume is seen with different preparation conditions as the function of pore size and sol-gel derived silica materials offers lower pore volume for adsorption.

XRD analysis shows that the sol-gel-derived silica thin film materials show weak crystallinity as confirmed by their broad diffraction peaks (Figure 2). This is consistent with the BET results that these materials have no long-range ordering. Hydrothermal methods yield crystalline material as seen from

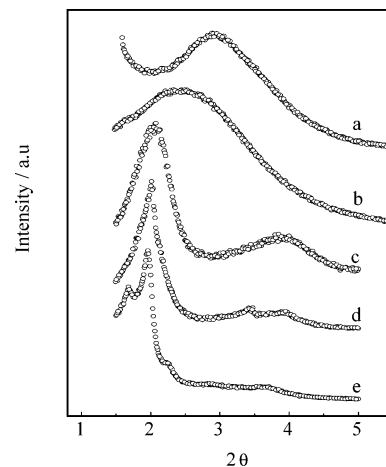


Figure 2. Powder XRD patterns of silica materials: (a) SG-1, (b) SG-2, (c) MCM41, (d) MCM41-96, and (e) 2MCM41-140.

Figure 2. These materials show (100) reflection and weak higher order peaks. A longer reaction time of 96 h and secondary synthesis are reported to result in high silica condensation and thick pore walls.²⁶ It can be seen that there is a moderate increase in the *d*-spacing as the pore size increased (Table 1).

SEM and HRTEM Characterization of Carbon Nanotubes. Figure 3 shows SEM pictures of the as-grown nanotubes at 850 and 900 °C using the silica materials with different morphology as the catalyst support. The morphology of silica support influences the carbon nanotube growth as well as their alignment. Sol-gel-derived SG-1 and SG-2 show a platelike morphology, and the particle size is generally of the order of a

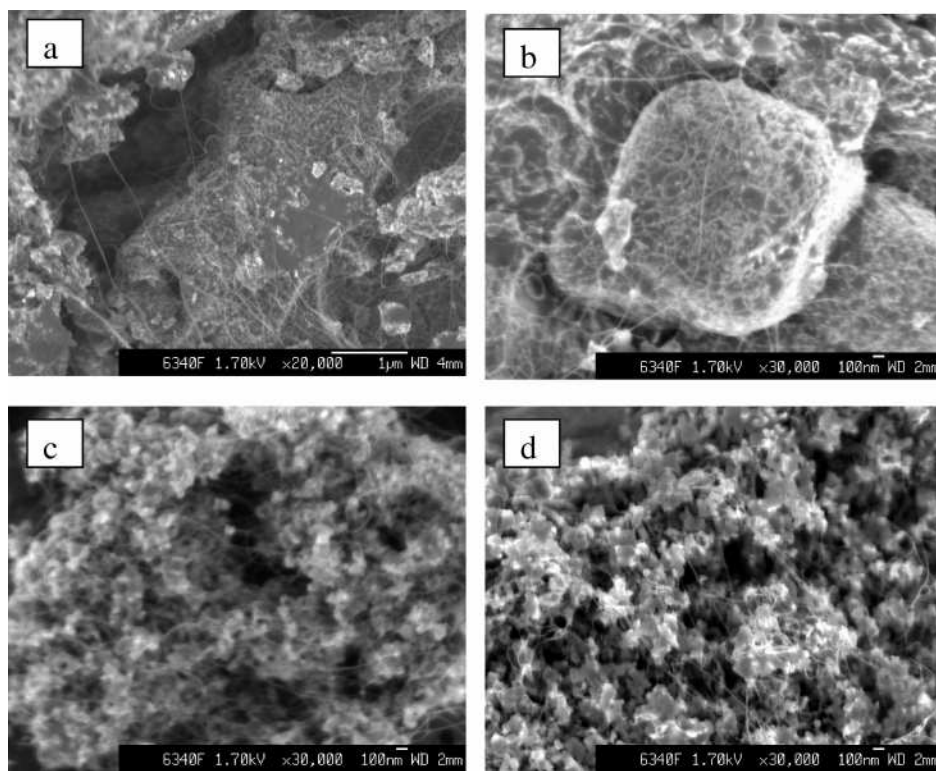


Figure 3. SEM pictures of as-grown nanotubes on silica material with different morphology: (a) SG-1, (b) 2MCM41-140, and (c) MCM41-96 at 850 °C and (d) MCM41-96 at 900 °C.

few micrometers, whereas the MCM-41 type materials synthesized by using the hydrothermal method have spherical particle-like morphology. The MCM41 synthesized for 48 h showed spherical-shape particles of 100 nm aggregated as a large particle.

When the reaction time increased to 96 h, the particles tend to grow as elongated spheres. The secondary synthesis for 140 h leads to larger particles of the order of micrometers with flat surface platelike morphology. Parts a and b of Figure 3 show the nanotubes grown at 850 °C on SG-1 and 2MCM41-140 with a flat platelike morphology. It is observed that most of the carbon nanotubes tend to adhere to the silica surface when the morphology of the support material is large and flat.^{28,29} The orientation of the nanotubes is found to be random over the substrate. The morphology of SG-2 is also similar to SG-1, and hence the nanotubes grown on this support also adhere to the silica surface (not shown). Increased amount of amorphous carbon and carbon fibers of 100 nm are observed in the case of SG-2 at all preparation temperatures. Parts c and d of Figure 3 show the SEM images of the nanotubes synthesized over MCM41-96 at 850 and 900 °C, respectively. If the silica support particles are spherical and smaller, then the nanotubes tend to suspend between such particles as observed from Figure 3c,d. The bundles of the nanotubes are 10–20 nm in diameter and cover the silica support uniformly. The carbon nanotubes grown on MCM41 also show a morphology similar to that of the nanotubes grown on MCM41-96.

HRTEM analysis of the as-grown nanotubes on MCM41 type materials shows that they are mainly composed of SWNTs and DWNTs. Figure 4 shows the individual and bundles of DWNT grown on MCM41 type silica supports at 850 and 900 °C. Very small amounts of amorphous carbon and carbon-coated metal particles are observed in TEM analysis. The outer diameter of the DWNTs grown on these supports varies from 1.45 to 5.4 nm, and the interlayer distance is observed to be 0.38 ± 0.02 nm. The interlayer distance observed in the case of DWNTs is

larger when compared with MWNTs. The higher curvature involved in the DWNTs leads to the uncorrelated graphene layers, and, as a result, a larger interlayer distance between inner and outer tube is observed.^{15,22} We have quantitatively analyzed the DWNT yield using TEM.

The reaction temperature of 800 °C produces about 90% of SWNTs and a very small quantity of DWNTs over the silica materials prepared in the present study. The amount of DWNTs increases as the reaction temperature is increased. Table 1 shows the yields of DWNTs grown at 850 and 900 °C on various silica supports compared to other types of nanotubes (i.e., SWNTs and MWNTs) as observed by TEM. In the case of MCM41 type materials an increase in the temperature from 800 to 900 °C increases the DWNT yield. This clearly indicates that the temperature of the reaction is controlling the DWNT yield. Previous reports from the present laboratory and other reports also confirm the temperature effect on the DWNT yield.^{6,14,15}

In the case of sol–gel silica materials, the DWNT yield was found to decrease at 900 °C and more MWNTs are produced. This may be due to the collapse of the porous structure of sol–gel-derived silica at 900 °C.³¹ When the porous structure is lost, the metal particles can grow larger and lead to the growth of MWNTs. The thermal stability of the support material is important for the high-temperature and high-yield synthesis of DWNTs. The MCM-41 type materials are more stable and yield more DWNT at 900 °C. The relative purity of carbon nanotubes produced using MCM41 and MCM41-96 as the support material is better when compared with the nanotubes produced using other silica support materials. The nanotubes produced using other support material have been coated by amorphous carbon, carbon fibers, and graphite sheets as impurities.

Another parameter that controls the DWNT yield is the pore size of the support materials. We infer that an increase in diameter of the pore leads to large-diameter SWNTs and DWNTs as opposed to zeolite.⁷ Earlier reports on the DWNT preparation indicate that higher temperature and larger diameter

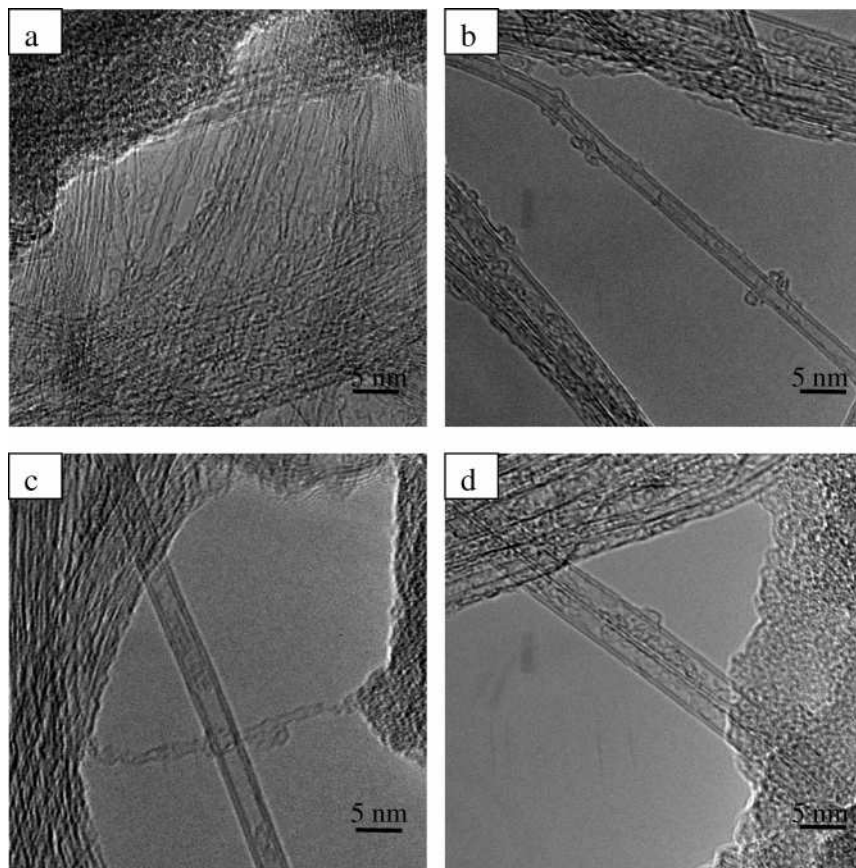


Figure 4. HRTEM images of bundles and isolated DWNT grown on silica materials: (a) MCM41–96 at 850 °C and (b) MCM41–96, (c) MCM41, and (e) 2MCM41–140 at 900 °C.

outer tubes are important for the growth of DWNTs.^{13,15} The present study confirms that the high temperature of 850–900 °C and tubes of outer diameters of more than 2 nm are necessary for the DWNTs growth. The yield of DWNTs is observed to be less if the pore size of the silica support material is in the microporous region (<2 nm) and when the pore size is increased to 2.32 nm the DWNTs yield is increased up to 50%. This observation indicates that mesoporous materials can efficiently produce DWNTs with respect to SWNTs. This observation is in agreement with the previous report on the DWNTs synthesized using mesoporous silica and MgO as catalyst support.^{14,16}

It should be noted that the DWNTs yield is not linearly increased with the pore diameter. The pore diameter of MCM41 is 3.48 nm, but the yield of DWNTs is not as high as that produced on SG-2 with a pore diameter of 2.32 nm at 850 °C. The TEM analysis of as-grown nanotubes over MCM41–96 with a pore diameter similar to that of MCM41 shows that the yield of DWNTs is as high as 60 and 80% at 850 and 900 °C, respectively. The larger pore size material 2MCM41–140 also does not give as high a yield of DWNTs as that of MCM41–96. The physical parameters such as surface area, pore diameter, and *d*-spacing of MCM41 and MCM41–96 are similar to each other, as seen from Table 1. We consider that the origin of the selectivity is due to the difference in the chemical properties of the materials. Apart from the surface area and pore size the chemical properties of the support material can control the DWNT yield.

We have performed NH₃-TPD studies on MCM41 and MCM41–96 to find out the difference in the acidity and possible role of the support material in the DWNT growth. The desorption of ammonia is observed at 300 °C in case of MCM41 type materials, and it has weak acid character compared to

zeolite materials.³² The ammonia desorption is observed above 400 °C in the case of zeolite materials, indicating that the interaction of ammonia with the acidic sites is much stronger. It can be noticed that weak acidic silica support materials can produce more DWNTs compared to zeolite materials.^{7,14} The total amount of ammonia desorbed from MCM41 and MCM41–96 is observed to be 0.49 and 0.33 mL/g, respectively. It is reported that MCM41 has a less condensed silica network, and the longer reaction time of 96 h leads more condensed silica.²⁶ This indicates that MCM41 possesses more acid sites originating from the uncondensed Si–OH functional groups compared to that of MCM41–96. This difference in acidity is responsible for the production of high yield of DWNT in the present study.

The increase in the pore size of the support material is expected to affect the diameter distribution of nanotubes apart from the yield of DWNTs. It is observed that most of the SWNTs and DWNTs produced at 900 °C on MCM41 type materials has a diameter corresponding to the pore size. Figure 5 shows the large DWNTs and the outer diameter distribution of DWNTs produced over MCM41–96 at 900 °C. The distribution of outer diameter of DWNTs is found to be 1.45–5.4 nm. The TEM analysis indicates that DWNTs larger than the pore size of the support material are produced only in small quantities. A partially formed third or fourth graphitic layer is occasionally observed over these larger DWNTs. These observations suggest that some metal particle has grown larger than that of the pore size of the support material, leading to larger DWNTs. The DWNTs grown on MCM41 and 2MCM41–140 are observed to be 2–4 and 2–5.4 nm in outer diameter, respectively. In the case of MCM41 and 2MCM41–140, SWNTs with diameter more than 2 nm are frequently observed, whereas most of the SWNTs observed in the case of MCM41–

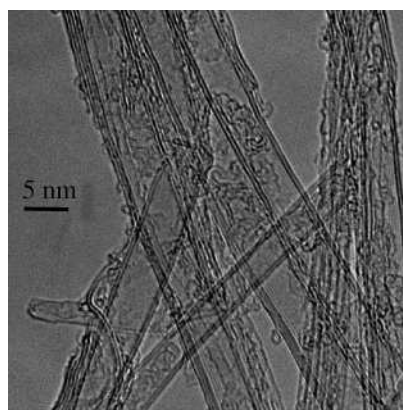


Figure 5. HRTEM image of large DWNTs and diameter distribution of DWNTs observed in nanotubes produced on MCM41–96 at 900 °C.

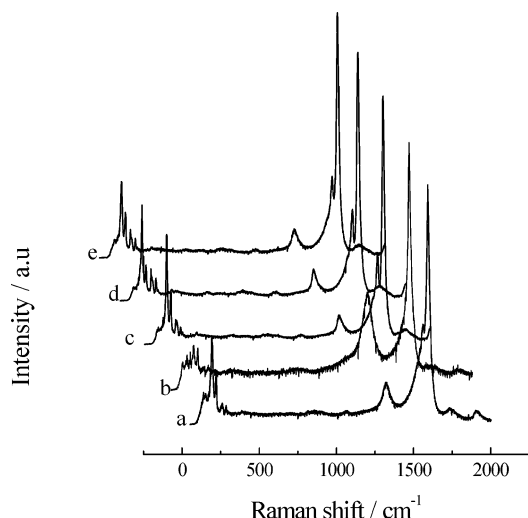


Figure 6. Raman spectra of as-grown nanotubes at 850 °C on different silica materials: (a) SG-1, (b) SG-2, (c) MCM41, (d) MCM41–96, and (e) 2MCM41–140.

96 are less than 2 nm in diameter and DWNTs with outer diameters less than 2 nm are also observed. This indicates that production of the large diameter outer tubes alone does not lead to a high yield of DWNT even at high temperatures. We believe that the strong influence of support material in the reduction of metal ions or alcohol over the metal leads to more DWNTs. This is supported by the observation that MCM41–96 efficiently grows DWNTs compared to others.

Raman Spectroscopic Characterization Carbon Nanotubes. Raman spectroscopy has widely been used to analyze the purity and diameter distribution of carbon nanotubes. Raman spectroscopic studies show that the as-grown carbon nanotubes produced between 800 and 900 °C are mainly SWNTs or DWNTs. Figure 6 shows the Raman spectra of as-grown nanotubes at 850 °C using different silica materials as the catalyst support. The Raman spectra of as-grown nanotubes show bands at 1310 and 1590 cm⁻¹ corresponding to D and G bands, respectively, and radial breathing modes (RBM) between 100 and 400 cm⁻¹. The G band is the tangential mode arising from the E_{2g} mode of the graphene sheet. The origin of the D band is related to the presence of defects in the nanotubes, the presence of MWNTs, and graphitic impurities. The ratio of G/D is usually considered an indicator of the purity of the nanotubes. A high G/D indicates that the sidewalls of nanotubes are less defective and MWNTs and graphitic impurities are absent.

Table 2 shows the average G/D ratios observed from Raman spectra of nanotubes produced at different temperatures using

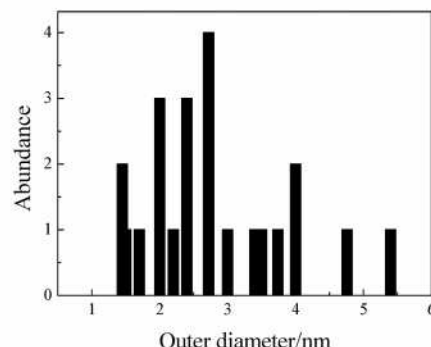


TABLE 2: Average G/D Ratios Observed from Raman Spectra of the As-Grown Nanotubes at 800, 850, and 900 °C on Various Silica Support Materials

silica samples	800 °C	850 °C	900 °C
SG-1	5.9	8.3	1.03
SG-2	3.8	1.85	0.98
MCM41	14.3	10	8.3
MCM41–96	14.3	11.5	8
2MCM41–140	7.7	7.7	10

silica materials as the catalyst support. The intensity of the D band is found to increase with the reaction temperature. In general, SG-1 and SG-2 show low G/D ratios as compared with MCM41 materials. Mesoporous SG-2 shows a strong D band at 850 °C, whereas microporous SG-1 shows a weak D band at the same temperature as that shown in Figure 6. At all reaction temperatures amorphous carbon and carbon fiber are seen in the case of SG-2 in the SEM and TEM analyses, which is also confirmed by the Raman spectra with poor G/D ratios. However, SG-1 is not stable at 900 °C and produces more MWNTs and graphitic sheets as observed by TEM. The Raman spectrum also confirms this observation as the intensity of the D band is increased. As already mentioned, SG-1 and SG-2 are not stable at high temperatures and hence the formation of graphitic sheets as well as MWNTs is favored. It is found from Raman analysis that MCM-41 materials show relatively high G/D ratio. In the case of MCM41 materials, only small quantities of graphite-coated particles and partially formed third and fourth layers over the large DWNTs are observed from TEM analysis. These observations confirm that MCM41 materials are stable up to 900 °C.

The effect of reaction temperature on the shape of the G band and RBM mode is shown in Figure 7. Broadening of the G band is observed as the reaction temperature increased. This indicates that the larger diameter tubes with metallic property are produced. This observation is further supported by the appearance of RBM peaks at the low-frequency region. In the case of MCM41–96, SWNTs and DWNTs are produced at 800 and 900 °C, respectively. This is clearly seen from the appearance of nanotubes having diameters of more than 1.5 nm at 900 °C. The diameter of the nanotubes is estimated via $\omega = 248/d$,^{13,15} where d is the diameter of the nanotube and ω is the Raman shift in cm⁻¹. RBM analysis on the as-grown nanotubes on the silica support material indicates that the diameter distribution shifted to larger values as the reaction temperature increased. In the present study the nanotubes of more than 2 nm show very weak RBM peaks, and hence they are not observed by Raman spectroscopy. However, the nanotubes with diameters of 1.45–2 nm are assigned to be either the inner tube

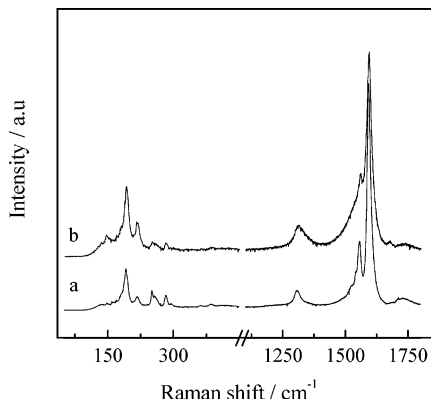


Figure 7. Raman spectra of as-grown SWNTs and DWNTs on MCM41-96 at (a) 800 and (b) 900 °C, respectively.

of a larger DWNT, the outer tube of thin a DWNT, or to SWNTs. The nanotubes observed with diameters less than 1.3 nm are mainly SWNTs, as the TEM studies do not show DWNTs with outer wall diameter of less than 1.45 nm.

We have examined the effect of different alcohols as carbon source in the selectivity of DWNTs. Methanol produces SWNTs with a larger diameter at lower reaction temperature compared with ethanol.⁷ Similar reaction conditions on MCM41-96 using methanol as the carbon source at 750 °C yield only larger diameter SWNTs as observed from Raman spectrum and TEM analysis. This indicates that the larger diameter SWNTs can be produced at low temperatures, whereas DWNTs are not produced at the same temperatures. This further confirms the earlier observations that large diameter tubes alone do not promote the growth of DWNTs.

Conclusions

A selective growth of DWNTs has been achieved on mesoporous silica materials. Higher reaction temperatures such as 850–900 °C and mesopores are found to be important for the present DWNTs growth. Mesoporous silica materials prepared by the hydrothermal method are found to be suitable for the DWNTs growth as compared with the silica prepared by sol–gel methods. High-temperature stable, weak acidic silica is found to be a better support material for the selective DWNTs growth.

Acknowledgment. We thank Professors S. Iijima and S. Bandow (Meijo University) for their help on the TEM observations. We also thank Dr. E. Nishibori (Nagoya University) for XRD analyses. We acknowledge the financial support by the JST CREST project on Novel Carbon Nanotube Materials and the Grants-in-Aid Scientific Research B (No. 16350071) of MEXT, Japan.

Supporting Information Available: Diameter distribution of nanotubes (red-SWNTs and green-DWNTs) produced on (A) MCM41 and (B) MCM41-96 at 900 °C. This material is available free of charge via the Internet at <http://pubs.acs.org>.

References and Notes

- (1) Saito, R.; Dresselhaus, G.; Dresselhaus, M. S. *Physical Properties of Carbon Nanotubes*; Imperial College Press: London, 1998. Baughman, R. H.; Zakhidov, A. A.; de Heer, W. A. *Science* **2002**, 297, 787.
- (2) Iijima, S. *Nature* **1991**, 354, 56.
- (3) Li, W. Z.; Xie, S. S.; Qian, L. X.; Chang, B. H.; Zou, B. S.; Zhou, W. Y.; Zhao, R. A.; Wang, G. *Science* **1996**, 274, 1701. Pan, Z. W.; Xie, S. S.; Chang, B. H.; Wang, C. Y.; Lu, L.; Liu, W.; Zhou, W. Y.; Li, W. Z.; Qian, L. X. *Nature* **1998**, 394, 631. Murakami, Y.; Chiashi, S.; Miyauchi, M.; Hu, M.; Ogura, M.; Okubo, T.; Maruyama, S. *Chem. Phys. Lett.* **2004**, 385, 298.
- (4) Mukhopadhyay, K.; Koshio, A.; Sugai, T.; Tanaka, N.; Shinohara, H.; Konya, Z.; Nagy, J. B. *Chem. Phys. Lett.* **1999**, 303, 117.
- (5) Flahaut, E.; Peigney, A.; Laurent, Ch.; Rousset, A. *J. Mater. Chem.* **2000**, 10, 249. Kong, J.; Cassell, A. M.; Dai, H. *Chem. Phys. Lett.* **1998**, 292, 567. Colomer, J.-F.; Stephan, C.; Lefrant, S.; Tendeloo, G. V.; Willem, I.; Konya, Z.; Fonseca, A.; Laurent, Ch.; Nagy, J. B. *Chem. Phys. Lett.* **2000**, 317, 83. Kitayanan, B.; Alvarez, W. E.; Harwell, J. H.; Resasco, D. E. *Chem. Phys. Lett.* **2000**, 317, 497. Cassell, A. M.; Raymakers, J. A.; Kong, J.; Dai, H. *J. Phys. Chem. B* **1999**, 103, 6484.
- (6) Hafner, J. H.; Bronikowski, M. J.; Azamian, B. R.; Nikolaev, P.; Rinzler, A. G.; Colbert, D. T.; Smith, K. A.; Smalley, R. E. *Chem. Phys. Lett.* **1998**, 296, 195.
- (7) Maruyama, S.; Kojima, R.; Miyauchi, Y.; Chiashi, S.; Kohno, M. *Chem. Phys. Lett.* **2002**, 360, 229.
- (8) Kurachi, H.; Uemura, S.; Yotani, J.; Nagasako, T.; Yamada, H.; Ezaki, T.; Maesoba, T.; Loufty, R.; Moravsky, A.; Nakagawa, T.; Katagiri, S.; Saito, Y. *Proceedings of the 21st International Display Research Conference/8th International Display Workshops*; Society for Information Display: San Jose, CA, 2001; p 1237.
- (9) Shimada, T.; Sugai, T.; Ohno, Y.; Kishimoto, S.; Mizutani, T.; Yoshida, H.; Okazaki, T.; Shinohara, H. *Appl. Phys. Lett.* **2004**, 84, 2412.
- (10) Saito, Y.; Nakahira, T.; Uemura, S. *J. Phys. Chem. B* **2003**, 107, 931.
- (11) Ci, L.; Rao, Z.; Zhou, Z.; Tang, D.; Yan, X.; Liang, Y.; Liu, D.; Yuan, H.; Zhou, W.; Wang, G.; Liu, W.; Xie, S. *Chem. Phys. Lett.* **2002**, 359, 63.
- (12) Flahaut, E.; Peigney, A.; Bacsa, W. S.; Bacsa, R. R.; Laurent, C. *J. Mater. Chem.* **2004**, 14, 646. Flahaut, E.; Bacsa, R.; Peigney, A.; Laurent, C. *Chem. Commun.* **2003**, 1442.
- (13) Sugai, T.; Yoshida, H.; Shimada, T.; Okazaki, T.; Shinohara, H.; Bandow, S. *Nano Lett.* **2003**, 3, 769.
- (14) Zhu, J.; Yudasaka, M.; Iijima, S. *Chem. Phys. Lett.* **2003**, 380, 496.
- (15) Hiraoka, T.; Kawakubo, T.; Kimura, J.; Taniguchi, R.; Okamoto, A.; Okazaki, T.; Sugai, T.; Ozeki, Y.; Yoshikawa, M.; Shinohara, H. *Chem. Phys. Lett.* **2003**, 382, 679.
- (16) Li, W. Z.; Wen, J. G.; Sennett, M.; Ren, Z. F. *Chem. Phys. Lett.* **2003**, 368, 299.
- (17) Lyu, S. C.; Liu, B. C.; Lee, S. H.; Park, C. Y.; Kang, H. K.; Yang, C. W.; Lee, C. J. *J. Phys. Chem. B* **2004**, 108, 2192.
- (18) Huang, H.; Kajiura, H.; Tsutsui, S.; Murakami, Y.; Ata, M. *J. Phys. Chem. B* **2003**, 107, 8794.
- (19) Peigney, A.; Coquay, P.; Flahaut, E.; Vandenberghe, R. E.; Grave, E. D.; Laurent, C. *J. Phys. Chem. B* **2001**, 105, 9699.
- (20) Liu, B. C.; Lyu, S. C.; Lee, T. J.; Choi, S. K.; Eum, S. J.; Yang, C. W.; Park, C. Y.; Lee, C. J. *Chem. Phys. Lett.* **2003**, 373, 475. Lyu, S. C.; Liu, B. C.; Lee, C. J.; Kang, H. K.; Yang, C. W.; Park, C. Y. *Chem. Mater.* **2003**, 15, 3951. Lyu, S. C.; Lee, T. J.; Yang, C. W.; Lee, C. J. *Chem. Commun.* **2003**, 1404.
- (21) Wei, J.; Ci, L.; Jiang, B.; Li, Y.; Zhang, X.; Zhu, H.; Xu, C.; Wu, D. *J. Mater. Chem.* **2003**, 13, 1340. Wei, J.; Jiang, B.; Zhang, X.; Zhu, H.; Wu, D. *Chem. Phys. Lett.* **2003**, 376, 753.
- (22) Saito, R.; Matsuo, R.; Kimura, T.; Dresselhaus, G.; Dresselhaus, M. S. *Chem. Phys. Lett.* **2001**, 348, 187.
- (23) Bandow, S.; Takizawa, M.; Hirahara, K.; Yudasaka, M.; Iijima, S. *Chem. Phys. Lett.* **2001**, 337, 48.
- (24) Ryoo, R.; Ko, C. H.; Cho, S. J.; Kim, J. M. *J. Phys. Chem. B* **1997**, 101, 10610.
- (25) Gross, D.; Balkenende, A. R.; Albouy, P. A.; Lavergne, M.; Mazerolle, L.; Babonneau, F. *J. Mater. Chem.* **2000**, 10, 2085.
- (26) Mokaya, R. *J. Phys. Chem. B* **1999**, 103, 10204.
- (27) Mokaya, R. *Chem. Commun.* **2001**, 933.
- (28) Zheng, F.; Liang, L.; Gao, Y.; Sukamoto, J. H.; Aardahl, C. L. *Nano Lett.* **2002**, 2, 729.
- (29) Murakami, Y.; Yamakita, S.; Okubo, T.; Maruyama, S. *Chem. Phys. Lett.* **2003**, 375, 393.
- (30) Lim, S.; Ciuparu, D.; Pak, C.; Dobek, F.; Chen, Y.; Harding, D.; Pfefferle, L.; Haller, G. *J. Phys. Chem. B* **2003**, 107, 11048. Ciuparu, D.; Chen, Y.; Lim, S.; Haller, G.; Pfefferle, L. *J. Phys. Chem. B* **2004**, 108, 503.
- (31) Gu, G.; Ong, P. P.; Chu, C. *J. Phys. Chem. Solids* **1999**, 60, 943. Matsumoto, A.; Sasaki, T.; Nishimura, N.; Tsutsumi, K. *Colloid. Surf. A* **2002**, 203, 185.
- (32) Zhang, Z.; Han, Y.; Xiao, F.-S.; Qiu, S.; Zhu, L.; Wang, R.; Yu, Y.; Zhang, Z.; Zou, B.; Wang, Y.; Sun, H.; Zhao, D.; Wei, Y. *J. Am. Chem. Soc.* **2001**, 123, 5014.

Review

Catalytic CVD Synthesis of Carbon Nanotubes: Towards High Yield and Low Temperature Growth

Arnaud Magrez ^{1,2,*}, Jin Won Seo ³, Rita Smajda ¹, Marijana Mionić ¹ and László Forró ¹

1 Laboratory of Complex Mater Physics, Ecole Polytechnique Fédérale de Lausanne, 1015 Lausanne, Switzerland; E-Mails: rita.smajda@epfl.ch (R.S.); marijana.mionic@epfl.ch (M.M.); laszlo.forro@epfl.ch (L.F.)

2 Center for Research on Electronically Advanced Materials, Ecole Polytechnique Fédérale de Lausanne, 1015 Lausanne, Switzerland

3 Department Metallurgy and Materials Engineering, Katholieke Universiteit Leuven, 3001 Heverlee, Belgium; E-Mail: maria.seo@mtm.kuleuven.be

* Author to whom correspondence should be addressed; E-Mail: arnaud.magrez@epfl.ch; Tel.: +41-21-693-7656; Fax: +41-21-693-4470.

Received: 12 October 2010 / Accepted: 25 October 2010 / Published: 1 November 2010

Abstract: The catalytic chemical vapor deposition (CCVD) is currently the most flexible and economically attractive method for the growth of carbon nanotubes. Although its principle is simple, the precisely controlled growth of carbon nanotubes remains very complex because many different parameters influence the growth process. In this article, we review our recent results obtained on the synthesis of carbon nanotubes via CCVD. We discuss the role of the catalyst and the catalyst support. Our recent results obtained from the water assisted growth and the equimolar C_2H_2 - CO_2 reaction are also discussed. Both procedures lead to significantly enhanced carbon nanotube growth. In particular, the latter allows growing carbon nanotubes on diverse substrate materials at low temperatures.

Keywords: carbon nanotubes; catalytic chemical vapor deposition; catalyst; catalyst support

1. Introduction

The catalytic chemical vapor deposition (CCVD) is currently the most viable process for the synthesis of carbon nanotubes. Many research groups have successfully attempted to accurately control the physical form of the carbon nanotubes produced [1–6, and references therein]. In particular, the influence of numerous growth parameters on the resulting nanotubes characteristics, such as diameter, length, number of graphene layers, defect density etc., has been studied [7,8]. At present, several basic aspects of the growth mechanisms have been established [9–14, and references therein]: the catalytic decomposition of the carbon precursor molecules on the surface of the supported metal catalyst is followed by diffusion of the carbon atoms produced either on the surface or in the metal particles. The growth temperature, as well as the particle size, determines the limit of carbon solubility in the metal particle. Super-saturation of the metal results in solid carbon precipitation and the subsequent formation of the nanotubes structure. Two different growth mechanisms can occur depending on the catalyst-support interaction. The tip-growth, where the catalyst is lifted off the support while carbon nanotube grows, takes place when the metal-support interaction is weak. In contrast, the root growth process occurs when the metal-support contact is preserved and the catalyst particles remain on the support during the carbon nanotube growth.

Of specific interest has been the carbon nanotubes production efficiency at lower temperatures in order to enable direct integration of carbon nanotubes into devices [15–18]. In particular, catalyst modification by pre-growth chemical activation [17–19] and/or prevention of catalyst poisoning, for instance by introduction of an etching agent which prevents the encapsulation by amorphous carbon precipitation, have been studied [20,21]. Recent outstanding results have demonstrated that the presence of a small and controlled amount of oxygen containing species, in addition to the carbon source, dramatically improves the yield of the reaction [20,21]. The effect observed is not dependent on the carbon source or on the processing method. It is assumed that the presence of H₂O and CO₂ during the growth etches amorphous carbon effectively away and prevents catalyst particle encapsulation by amorphous carbon [22]. Very recently, it was discovered that other additives (e.g., a sulfur-containing compound, thiophene) improved the density of carbon nanotubes indicating that the nucleation and growth of carbon nanotubes can be influenced by novel chemical reactions [23].

The growth of carbon nanotubes still remains complex. In this paper, we review our studies on the synthesis of carbon nanotubes via the CCVD process. We first examine the influence of the catalyst, as well as the influence of the support material. Subsequently, the effect of adding water or CO₂ to the process gas mixture is discussed with respect to the carbon nanotube growth efficiency. Our results demonstrate the “special” case of CaCO₃ which releases CO₂ by its thermal decomposition and actively influences the growth of carbon nanotubes. The interaction between C₂H₂ and CO₂ significantly promotes the carbon nanotube growth and even allows the growth of carbon nanotubes in thermodynamically and/or kinetically unfavorable conditions. We also produced carbon nanotubes using the water-assisted process and compared the bending modulus of the carbon nanotubes obtained from the water-assisted growth and of those produced from the equimolar C₂H₂-CO₂ reaction. The latter provides the possibility to significantly decrease the growth temperature, as well as to obtain carbon nanotubes growth on various substrate materials.

2. Results and Discussion

Most of the growth studies we have performed so far used catalyst particles supported by powder substrates. Due to the higher surface area, powder support leads to higher catalyst efficiency and higher carbon nanotubes yield. Therefore, we rely on the results obtained from powdered support materials in order to discuss the yield and growth efficiency. However, the results are also valid for the carbon nanotubes growth on flat substrates. As we recently demonstrated [24], vertically aligned growth of carbon nanotubes can be obtained on Si with a buffer layer, as well as powder supports pressed to a pellet. As our results demonstrate, the choice of the catalyst and that of the support strongly influence the carbon nanotubes growth. Nevertheless, involving additional species, such as water and CO₂, into the reaction gas can significantly enhance the catalytic activity.

2.1. Catalyst

Generally, nano-sized transition metal particles, e.g., nickel, iron, cobalt, molybdenum and copper, have been successfully used in CCVD either in oxide or metallic forms or as mixtures [7,8]. A very large amount of papers report on the growth of carbon nanotubes, using different compositions, size, preparation methods and crystallographic orientation. A general overview of the different catalysts can be found in the review papers [7–9]. The most important property of the metal particles with regard to carbon nanotube formation is their ability to catalytically decompose gaseous carbon-containing molecules. The solubility of carbon in catalyst particles is size-dependent. As Moisala et al. [7] highlighted in their review, the solubility of carbon in iron and nickel significantly increases for metal particles with a diameter of less than approximately 10 nm. Seidel et al. investigated the difference of the carbon nanotubes growth behaviors for Fe, Co, and Ni catalysts [16]. They observed that the order of the lowest growth temperatures agrees with the order of the bulk melting points of the three transition metals (Ni, 1,450 °C; Co, 1,490 °C; Fe, 1,540 °C). For binary compounds, e.g., cobalt–molybdenum [25], iron–molybdenum [26] and iron–cobalt [27,28], the yield of carbon nanotubes has been observed to increase significantly. However, the precise catalyst composition has a great influence on the final product. We have investigated Fe_{1-x}Co_x and Fe_{1-x}Ni_x alloys for the growth of carbon nanotubes [28,29].

2.1.1. Catalyst composition

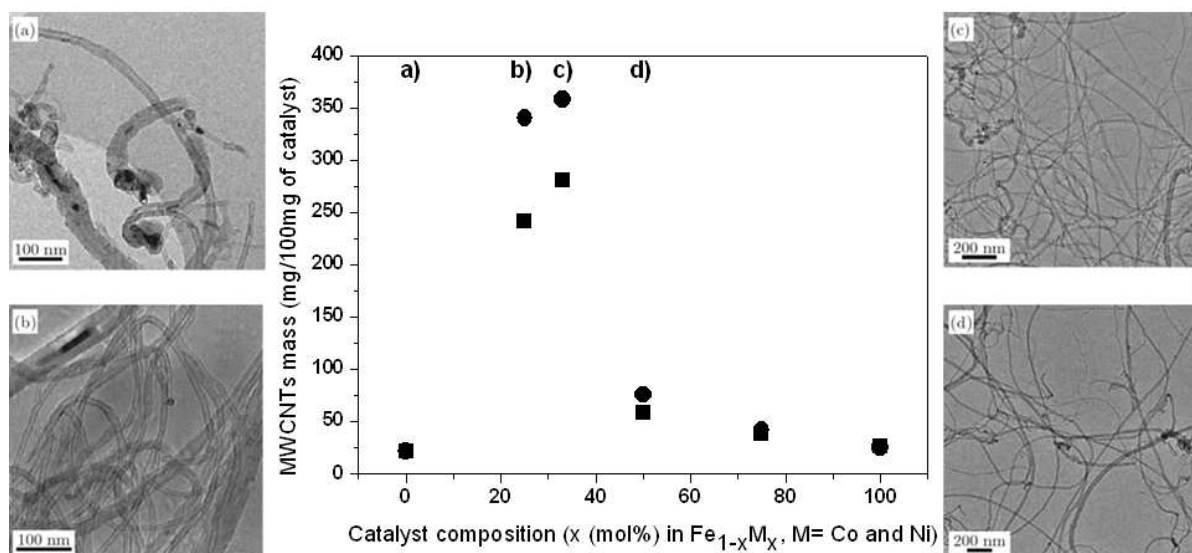
Fe_{1-x}Co_x alloys are among the most efficient catalysts for the synthesis of multi-walled carbon nanotubes [27,28]. The resulting yield, as well as the nanotubes characteristics, strongly depend on the parameter x. The highest yield, the narrowest diameter distribution, and the least defect density in the nanotubes graphitic structure, are obtained at x = 33 mol% [28]. As highlighted in Figure 1, the catalyst efficiency increases almost 100 times by changing x from 0 to 25 mol% for growth temperature at 700 °C. For x = 33 mol%, the increase is even slightly higher but exceeding 33 mol% results in a sudden drop to a catalyst efficiency comparable to that of the monometallic Fe catalyst (x = mol 0%). Increasing x even more does not change the yield significantly and keeps the efficiency similarly low. Thus, the metallic alloy Fe₂Co is the most active catalyst in the Fe_{1-x}Co_x compound with

a catalytic activity for carbon nanotubes growth more than 100 times higher than that of monometallic catalysts Fe and Co [28].

The catalyst efficiency also determines the carbon nanotube diameter, as well as the amount of catalyst particles present in the product. As can be seen in the transmission electron microscopy (TEM) images in Figure 1, carbon nanotubes reveal high diameter distribution with diameters ranging from 10 nm to 50 nm when the composition strongly deviates from $x = 33$ mol%. Moreover, many catalyst particles can be found as embedded particles. In contrast, for $x = 33$ mol% carbon nanotubes with diameter of 15 ± 2 nm are observed without any presence of enclosed catalyst particles. In order to determine the precise structure and the composition of the catalyst, x-ray powder diffraction (XRPD) was performed on supported catalysts under various conditions: After annealing at the carbon nanotubes growth temperature under (i) pure N₂ and (ii) N₂ mixed with acetylene (same conditions as for the carbon nanotubes growth) [28]. According to these measurements, a single-phase catalyst forms at $x = 33$ mol% after 10 min of annealing under N₂. This is identified as the spinel phase Fe₂CoO₄. A deviation from this optimum composition leads to the formation of Fe₂Co₃ and CoO phases for $x < 33$ mol% and $x > 33$ mol%, respectively. Additional annealing under N₂ mixed with C₂H₂ reduces the oxide. Pure Fe₂Co is obtained for $x = 33$ mol% whereas Fe₃C and Co are formed for pure Fe and Co catalysts, respectively. In an intermediate composition, two phases are found, namely Fe₂Co and Fe₃C or Co depending on the Fe- or Co-rich composition. Their fraction is determined by the precise composition. The TEM micrographs shown in Figure 1 clearly demonstrate that any deviation from the $x = 33$ mol% composition results in the presence of the secondary phase Fe₃C or Co, which leads to high density of enclosed particles in carbon nanotubes and significantly reduces the resulting carbon nanotubes yield.

Similarly, we have studied the Fe_{1-x}Ni_x alloys family. Again a spinel phase is formed for $x = 33$ mol%, namely Fe₂NiO₄. The corresponding Fe₂Ni catalyst is more active than pure Ni and pure Fe. The mass of carbon nanotubes produced over Fe₂Ni is more than 10 times higher than over pure Fe or Ni catalyst [29]. As can be seen in Figure 1, the resulting carbon nanotube mass obtained from 100 mg catalyst is even higher for Fe_{1-x}Ni_x at 25 and 33%. Our preliminary results indicate that the multi-walled carbon nanotubes obtained from Fe₂Ni are more defective than those obtained from Fe₂Co indicating that the growth condition still needs to be optimized. Nevertheless, the recent result reported by Chiang and Sankaran [31] indicate that the chirality distribution of as-grown carbon nanotubes can be altered by varying the composition of Fe_{1-x}Ni_x nanocatalysts. By precisely tuning the nanocatalyst composition at constant size they observed a link between the composition-dependent crystal structure of the nanocatalysts and the resulting nanotube chirality.

Figure 1. Effective mass of the obtained multi-walled carbon nanotubes after purification as a function of the catalyst composition $\text{Fe}_{1-x}\text{M}_x$ with $\text{M} = \text{Co}$ (■) and Ni (●). The TEM images show representative carbon nanotubes obtained for (a) $x = 0$ mol%, (b) $x = 25$ mol%, (c) $x = 33$ mol% and (d) $x = 50$ mol% $\text{Fe}_{1-x}\text{Co}_x$ catalyst.



2.1.2. Catalyst drying process

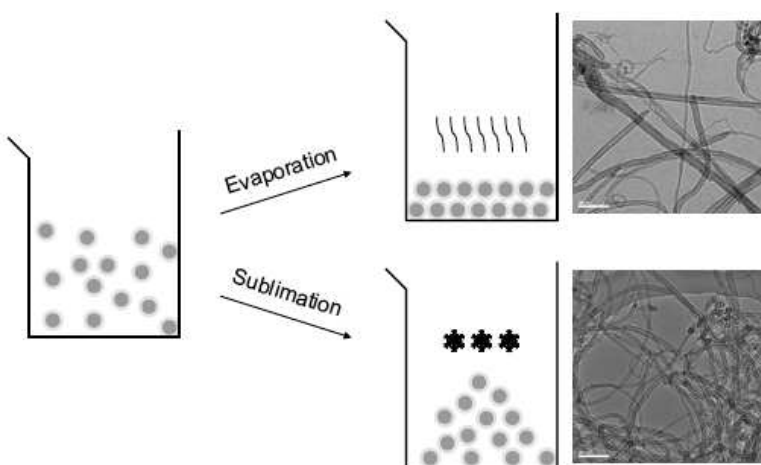
The drying process of the catalyst prior to the carbon nanotubes production is an important step. When catalysts are dried by heating, large agglomerates of catalysts are formed which cannot be broken into small particles by additional mechanical grinding. Consequently, when the catalyst is introduced into the reactor, only the outer surface of the large agglomerates is exposed to the reaction gas. Therefore, the catalyst efficiency is strongly limited. In addition, the multi-walled carbon nanotubes produced are of very poor quality with a broad diameter distribution. The catalyst efficiency can be quantified as the mass of purified multi-walled carbon nanotubes produced, divided by the mass of supported catalyst introduced. Typically, catalysts dried by heating lead to a catalyst efficiency of around 1.2. To be precise, 120 mg of multi-walled carbon nanotubes are produced from 100 mg of catalyst supported by CaCO_3 . Thus, during the synthesis, 18% of acetylene is converted into multi-walled carbon nanotubes.

As we recently reported, freeze drying of the catalyst is a favorable alternative approach which avoids agglomeration of the supported catalyst particles during the sublimation of water [30]. To be precise, the prepared catalyst suspension is frozen by dropping into liquid nitrogen. Once collected, it is subsequently placed in a freeze drying chamber, where sublimation occurs by raising the temperature while keeping the vapor pressure below 5 mbar.

Using the freeze drying method, it was possible to increase the acetylene conversion for carbon nanotubes growth to 85% (using Fe_2Co catalysts loaded on CaCO_3 particles as support). This corresponds to a catalyst efficiency of 5.6, which means 560 mg of multi-walled carbon nanotubes are produced from 100 mg of supported catalyst. Thus, freeze drying is more than four times more efficient than heating. The produced multi-walled carbon nanotubes exhibit a mean diameter of about 11 nm with a diameter distribution of about ± 6 nm. Consequently, the catalyst efficiency dramatically

increases and high quality multi-walled carbon nanotubes are produced with a narrow diameter distribution (see the TEM image in Figure 2).

Figure 2. Schematic drawing illustrating the freeze drying, compared to the hot drying, process. Agglomeration of the supported catalyst particles is avoided when freeze dried. TEM micrographs show representative carbon nanotubes produced from these two drying processes (scale bar is 100 nm).



2.2. Support

Various support materials have been tested for the CCVD synthesis of carbon nanotubes. Most commonly, Al_2O_3 and SiO_2 have been used [7,8]. MgO has been reported to be appropriate for the growth of single-walled carbon nanotubes. A general prerequisite for a support material is thermal and chemical stability under the synthesis conditions. Consequently, direct growth on Si [32] or a metal substrate [33,34] has been difficult because of the diffusion of the catalyst material into the support and formation of silicides or alloys upon heating to the carbon nanotube growth temperature. Additional properties of importance for efficient carbon nanotube growth have been the surface area and porosity. Chemical and/or physical interaction may take place between the support and the catalyst material. Physical interactions (e.g., van der Waals and electrostatic forces, together with obstruction of catalyst particle movement on the support surface due to surface roughness) can reduce the thermally driven diffusion and sintering of metal particles on the support surface. This leads to stabilization of the catalyst particle size distribution. The chemical interactions between the catalyst particles and the support surface can lead to limited particle growth due to decreased particle mobility. By *in situ* photoelectron spectroscopy it has been demonstrated that the catalyst–substrate interaction during the CCVD process determines the chemical oxidation state of the catalyst, which affects the carbon nanotube characteristics [35,36]. Al_2O_3 has been generally observed to be a superior support compared to SiO_2 , TiN or TiO_2 [36,37]. The stronger chemical interaction between Al_2O_3 and the metal catalyst has been appointed to the oxidation process occurring at the catalyst– Al_2O_3 interface.

Support materials such as $\text{Al}(\text{OH})_3$ and CaCO_3 also have shown to positively influence the carbon nanotube growth process by their decomposition [28,38,39]. We have systematically studied the carbon nanotube synthesis using CaCO_3 and other alkaline earth carbonates.

2.2.1. Alkaline earth carbonates

CaCO_3 is one of the most efficient supports used for the synthesis of multi-walled carbon nanotubes [38,40,41]. In our previous paper, we demonstrated that Fe_2Co supported by CaCO_3 results in an efficient selective formation of carbon nanotubes [28,42]. The carbonate is also favorable because of its simple removal allowing a simple one-step purification of carbon nanotubes without any perceivable damage of the carbon nanotube structure. Both metallic particles and catalyst support can be dissolved in diluted mineral acids (e.g., HNO_3 , HCl) [40]. Nevertheless, one of the most exceptional characteristics of CaCO_3 is its decomposition. The CaCO_3 stability is ruled by a dynamic equilibrium of the decomposition reaction $\text{CaCO}_3 \leftrightarrow \text{CaO} + \text{CO}_2$ in the temperature range of 600 to 800 °C. Consequently, CO_2 is available as free gas or bound to the support as CaCO_3 in a ratio that depends on the temperature. In a first approximation, the partial pressure of CO_2 and the average decomposition rate of the carbonate can be deduced from thermogravimetric analysis (TGA) of CaCO_3 [28,43].

In Figure 3, the maximum carbon nanotubes yield obtained from Fe_2Co supported by CaCO_3 is shown as a function of the decomposition rate of CaCO_3 . In the temperature range between 640 and 680 °C about 5% of CaCO_3 decomposes. The highest yield was obtained in this range: About 350 mg of multi-walled carbon nanotubes are produced from 100 mg of $\text{Fe}_2\text{Co}/\text{CaCO}_3$ catalyst in about 30 minutes. This corresponds to a conversion of about 54% of acetylene. By means of a quadrupolar mass spectrometer (QMS), the precise $\text{CO}_2(\text{g})/\text{C}_2\text{H}_2$ ratio at 660 °C was measured to 1:100 and was found to be stable over the entire period of the carbon nanotubes growth. A small variation in the decomposition rate of CaCO_3 , which is controlled by the variation of the growth temperature, can decrease the yield dramatically. For instance, an increase of 40 °C can lead to a 40% reduction of the maximum yield indicating how strongly the CO_2 content influences the reaction.

We also examined other alkaline earth carbonates as supports [28]. Carbon nanotubes are obtained in all samples but the yield strongly varies. The highest yield is obtained with CaCO_3 , which has the decomposition temperature closest to the carbon nanotube growth temperature. For MgCO_3 , the decomposition temperature (300 °C) is significantly lower than the carbon nanotube growth temperature. Therefore, the support fully transforms into MgO , already before the carbon nanotubes growth, and CO_2 cannot contribute to the growth process. For SrCO_3 and BaCO_3 , the decomposition temperature is substantially higher, 970 °C and 1,320 °C, respectively. Hence, CO_2 groups maintain in the carbonate and do not react with acetylene.

CaCO_3 is an excellent support, not only for the production of high-yield multi-walled carbon nanotubes, but also for that of single-walled CNTs [44]. We applied a combustion method in order to produce well dispersed catalysts, with reduced size and with a control of the diameter. The combustion technique is typically used for the production of highly dispersed powder-like materials and exploits an exothermic, very rapid redox-type chemical reaction [45,46]. However, acetylene was found to be a too rich carbon source and extremely difficult to control. By reducing the acetylene flow, only double-walled carbon nanotubes could be obtained. By exposure to ethylene and methane, high density of single-walled carbon nanotubes with a diameter distribution of 1.1 ± 0.3 nm was produced [44].

2.2.2. Size of support particles

For an efficient carbon nanotubes synthesis, also the particle size of the support plays a role. As demonstrated in our previous work [30], calcite powders with very low specific surface area ($S_{BET} < 1 \text{ m}^2/\text{g}$) can mechanically be grinded in order to reduce the particle size and to increase the specific surface area. The resulting average particle size was 50 nm with a diameter distribution of about ± 25 nm. The specific surface area was about $5.6 \text{ m}^2/\text{g}$ as derived from granulometry powder characterization with Malvern Mastersizer S spectrometer. We compared this powder with a second one (from Calofort U), which had a specific surface area of $4.6 \text{ m}^2/\text{g}$ and particle size of about 100 nm with a broad diameter distribution of ± 60 nm.

At first, catalyst particles are produced from Fe_2Co nanoparticles using the second type of CaCO_3 particles with a larger particle size and slightly lower surface area, applying the free drying mentioned in Section 2.1.2. About 44% of acetylene was converted into the formation of multi-walled carbon nanotubes. This corresponds to a catalyst efficiency of 2.9. When fine ground CaCO_3 particles from the first type are employed, the conversion increases to about 85%, which corresponds to a catalyst efficiency of 5.6 (560 mg of multi-walled carbon nanotubes are produced from 100 mg of supported catalyst). This result clearly illustrates that the acetylene conversion into carbon nanotubes formation can be controlled by the support particle size.

The support particle size does not only impact the carbon nanotubes production yield but also the diameter distribution of the resulting carbon nanotubes. The mean diameter of the multi-walled carbon nanotubes obtained from the second type of CaCO_3 particles is about 14 ± 4 nm, whereas the multi-walled carbon nanotubes synthesized from the fine ground CaCO_3 exhibit a smaller average diameter of 11 ± 6 nm. The effect of the support particle size can be explained by the triple point junction area, where nanotubes growth stems. It corresponds to the location where the reaction between CO_2 (originating from the CaCO_3 support) and C_2H_2 is catalyzed by Fe_2Co particles [43]. When catalyst is deposited on materials with a large surface area, Fe_2CO is distributed over a large surface and the co-precipitation process yields small particles. Small particles have larger relative interface to the support with respect to their volume. Hence, the relative interface area (being the active area for the chemical reaction) is larger for small particles and consequently the catalyst efficiency is enhanced, leading to larger quantity of carbon nanotubes being produced.

2.3. CCVD Process

CCVD is a simple and economic technique for synthesizing carbon nanotubes at low temperature (300–1,200 °C) and ambient pressure. It is versatile and can utilize a variety of carbon sources in any state (solid, liquid, or gas); enables the use of various substrates; and allows carbon nanotube growth in a variety of forms, such as powder and films. Therefore this technique is ideally suited for producing arrays of individual, or a mat of aligned carbon nanotubes, as well as for a desired architecture of a nanotube device. Commonly used gaseous carbon sources have been methane, acetylene and carbon monoxide. In the case of liquid carbon sources, an alcohol, such as methanol and ethanol, is heated in a flask and purged with an inert gas in order to carry the vapor into the reaction furnace. Alcohol-assisted growth has yielded single-walled carbon nanotubes at a relatively low minimum temperature of about 550 °C [15]. The most recent breakthroughs in the CCVD synthesis of

carbon nanotubes represent the water-assisted growth [20] and the equimolar CO₂-C₂H₂ reaction [43].

2.3.1. Water assisted growth

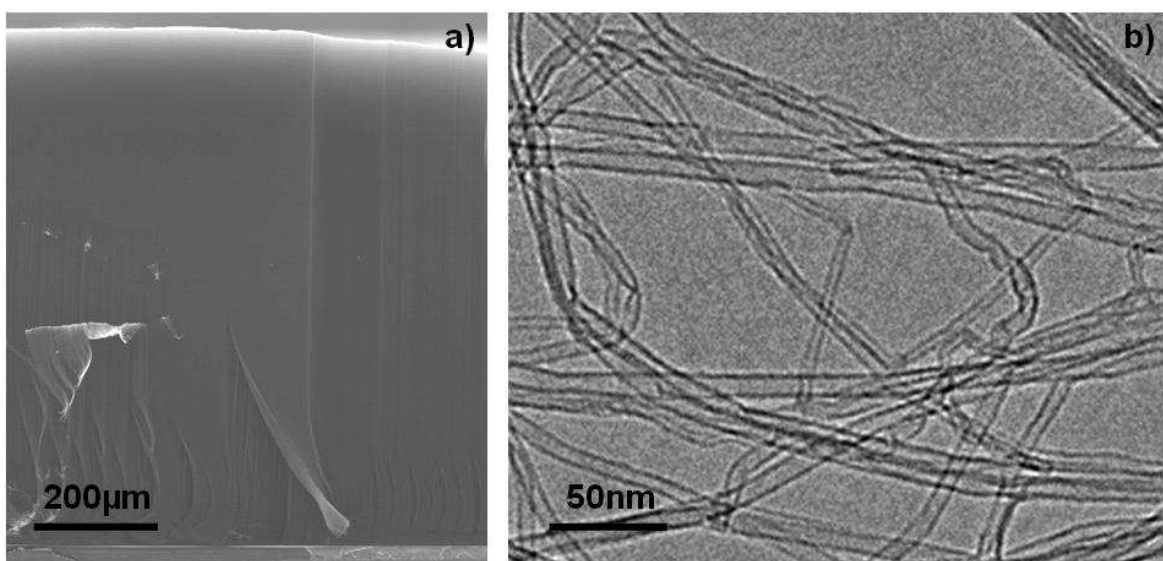
Pioneered by Hata et al. [20], the so-called “super growth CVD process” based on the introduction of traces of water has been considered as one of the most efficient growths resulting in dramatically enhanced carbon nanotubes growth. Water is believed to extend the catalyst lifetime by etching the amorphous carbon deposit on the surface of the catalyst. In the optimum growth conditions, more than 85% of the catalyst nanoparticles are active [47]. The growth kinetics is also strongly extended so that millimeter high carpets of vertically aligned carbon nanotubes can be grown in a few minutes [22]. By optimizing the growth conditions, 1 cm high dense mat of carbon nanotubes forest was demonstrated very recently [48].

We have produced carbon nanotube forests in growth conditions [49] slightly different to those applied in [20,22,47,50]. In particular, gas phase composition in the reactor is enriched with ethylene and water while keeping other growth parameters similar to the ones reported in [20,22,47,50]. The obtained forest height is about 950 μm produced in 30 min, comparable to the previous reported results. TEM studies of the as-grown carbon nanotubes reveal that the grown carbon nanotubes have a narrow diameter distribution. Single-walled, as well as multi-walled, carbon nanotubes with small number of walls (2–5 walls) are found. The average outer diameter is about 7–8 nm. Carbon nanotubes are clean and free of amorphous carbon as well as catalytic particles indicating that high purity carbon nanotubes are produced by the water assisted CCVD process (Figure 3). In particular, the absence of amorphous carbonaceous materials suggests the cleansing role of water during the carbon nanotubes growth. By precisely varying the gas phase composition during the CCVD process, we obtain carbon nanotube forests with different heights. As illustrated in Figure 4, the maximum height is obtained by introducing 800 ppm of water. This corresponds to a H₂O/C₂H₄ ratio of about 1/1000, which is in agreement with the results obtained by the group of Hata [22]. A slight deviation from this value dramatically decreases the forest height indicating that the ethylene/water ratio is one of the most critical parameters to control in order to exploit the advantages of the water assisted CCVD process. Moreover, scanning electron microscopy (SEM) micrographs of forests produced with different water content (see Figure 4) demonstrate that also the carbon nanotubes alignment strongly depends on the H₂O/C₂H₄ ratio.

The best alignment is not found in the forest with the highest height, but in that produced with the highest water content of 1,200 ppm. The alignment in carbon nanotube forest is caused by the strong van der Waals interaction between individual tubes. When carbon nanotubes density is low, van der Waals interaction is low and carbon nanotubes grow randomly and curved so that the carpet height does not reflect the real carbon nanotubes length (Figure 4a). When the water content is raised, alignment improves, because raising the H₂O/C₂H₄ ratio increases the number of active catalytic particles and consequently the density of the forest. However, diffusion of feedstock gas to catalyst particles becomes more and more difficult with the increasing density, as well as with the dense forest thickness. The growth finally stops because of the obstruction of the gas flow. As can be seen in Figure 4b, for the water content of 800 ppm, the highest forest thickness is obtained although the alignment is rather poor. This means that the poor alignment provides space for ethylene to

continuously penetrate down to the catalytic particles. When water content is raised more, all catalytic particles are activated, and a very dense mat of almost perfectly aligned carbon nanotubes is produced. However, ethylene penetration through the carpet is reduced and therefore carpet height is significantly reduced (Figure 4c). Yasuda et al. [48] demonstrated very recently that this limitation could be circumvented by controlling the gas flow direction. Using a gas shower system, providing direct delivery of gases from the top of the forest, they achieved higher carbon nanotubes forests growth stability, uniformity, reproducibility, carbon efficiency (32%), and catalyst lifetime. With this improved growth, they could synthesize a 1 cm tall forest with 1cm x 1cm size and demonstrated the scalability of water-assisted CCVD to A4-size.

Figure 3. (a) Cross-sectional SEM image of a carbon nanotubes forest with a height of about 1mm grown by the water assisted CCVD growth process. (b) Representative TEM image of the carbon nanotubes produced at 750 °C. Carbon nanotubes are clean, free of amorphous carbon and catalytic particles.



Mechanical bending modulus measurements of individual carbon nanotubes indicate that very high quality carbon nanotubes are produced by the water assisted CCVD process. The obtained bending modulus is significantly higher compared to the values measured from the carbon nanotubes produced by the conventional CCVD process [51]. The values (390–631 GPa) are close to the ones obtained from the best CCVD grown carbon nanotubes [52]. Hence, the advantage of the presence of water is twofold: (i) its weak oxidizing effect prevents amorphous carbon deposition and (ii) it does not produce extended damages in the graphitic structure of the carbon nanotubes, even when water concentration as high as 1,200 ppm is used.

Figure 4. The height of the resulting carbon nanotubes forests strongly varies with the ppm of water introduced into the reactor. The SEM micrographs obtained at (a) 500 ppm, (b) 800 ppm and (c) 1,200 ppm, illustrate that the carbon nanotubes alignment, as well as their density, significantly changes with the amount of added water. Whereas the thickest carpet is produced at 800 ppm, the best alignment is obtained at 1,200 ppm. Dashed lines guide the eyes. Scale bars are 2 μ m.

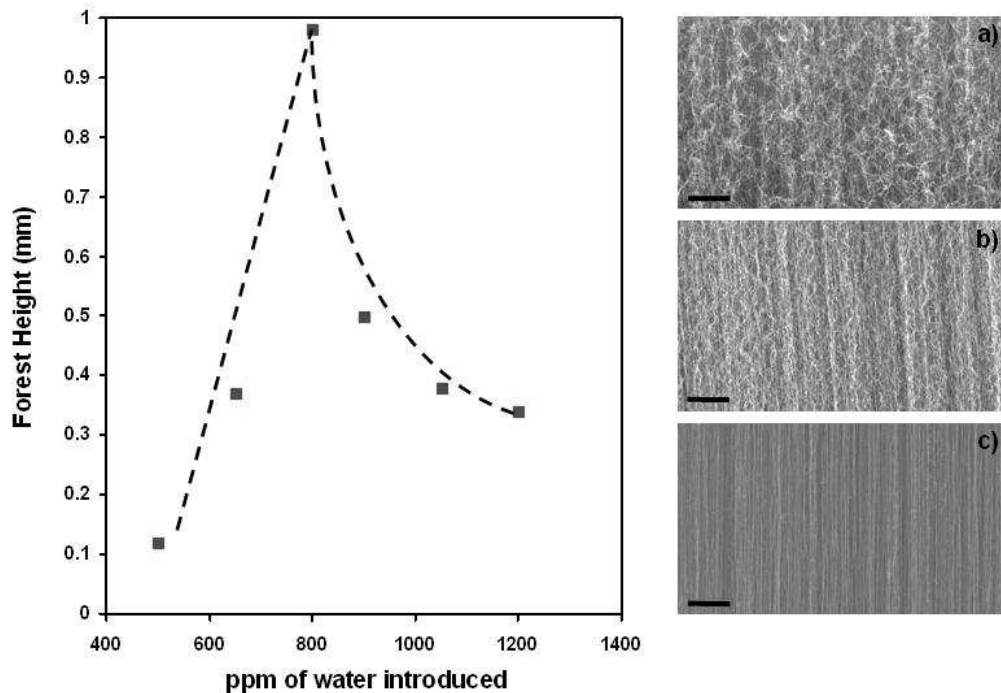


Figure 5. (a) Representative atomic force microscopy (AFM) image of a nanotube suspended over the hole of an alumina membrane for the individual mechanical bending modulus measurements. (b) Representative deformation profile of a suspended carbon nanotube and (c) deflection vs. loading force derived from the deformation profile. The slope is proportional to the bending modulus of the carbon nanotubes.

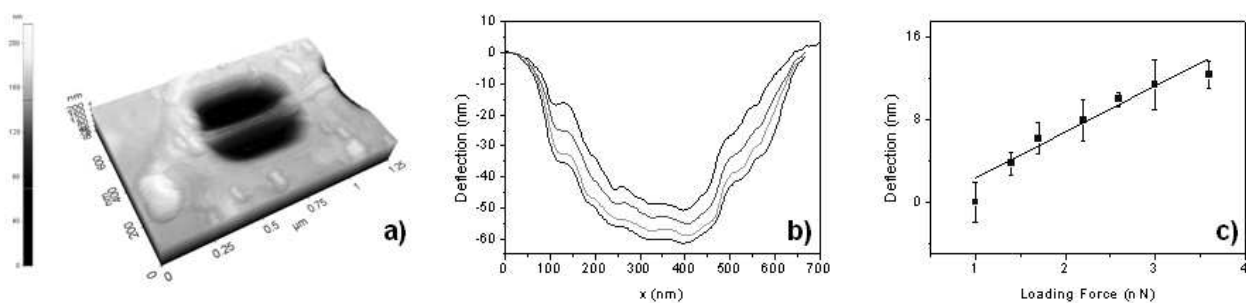


Table 1. Mean, maximum and minimum, bending modulus (mean, max. and min. E_b) of carbon nanotubes produced by the water assisted growth and the equimolar reaction.

	Mean E_b (GPa)	Max. E_b (GPa)	Min. E_b (GPa)
Water assisted grown carbon nanotubes	570	1,200	240
Equimolar grown carbon nanotubes	390	1,040	56

In Table 1 the mean, the maximum, and the minimum, bending modulus are summarized for carbon nanotubes grown via the water assisted synthesis and the equimolar C_2H_2 -CO₂ reaction. The latter CCVD route will be described in detail in the following Section 2.3.2. The main difference observed in the mechanical properties of the carbon nanotubes produced by the equimolar reaction process and by the water assisted method is the smaller range of bending modulus variation for carbon nanotubes produced by the water assisted growth process. This phenomenon is based on the fact that carbon nanotubes, produced by the water assisted growth process, exhibit a smaller average diameter with a narrower diameter distribution. In the case of the equimolar process, carbon nanotubes were produced using CaCO₃ nanoparticle support, generally leading to a larger carbon nanotube diameter and a broader diameter distribution compared to carbon nanotubes from the water assisted growth.

2.3.2. Equimolar C_2H_2 -CO₂ reaction

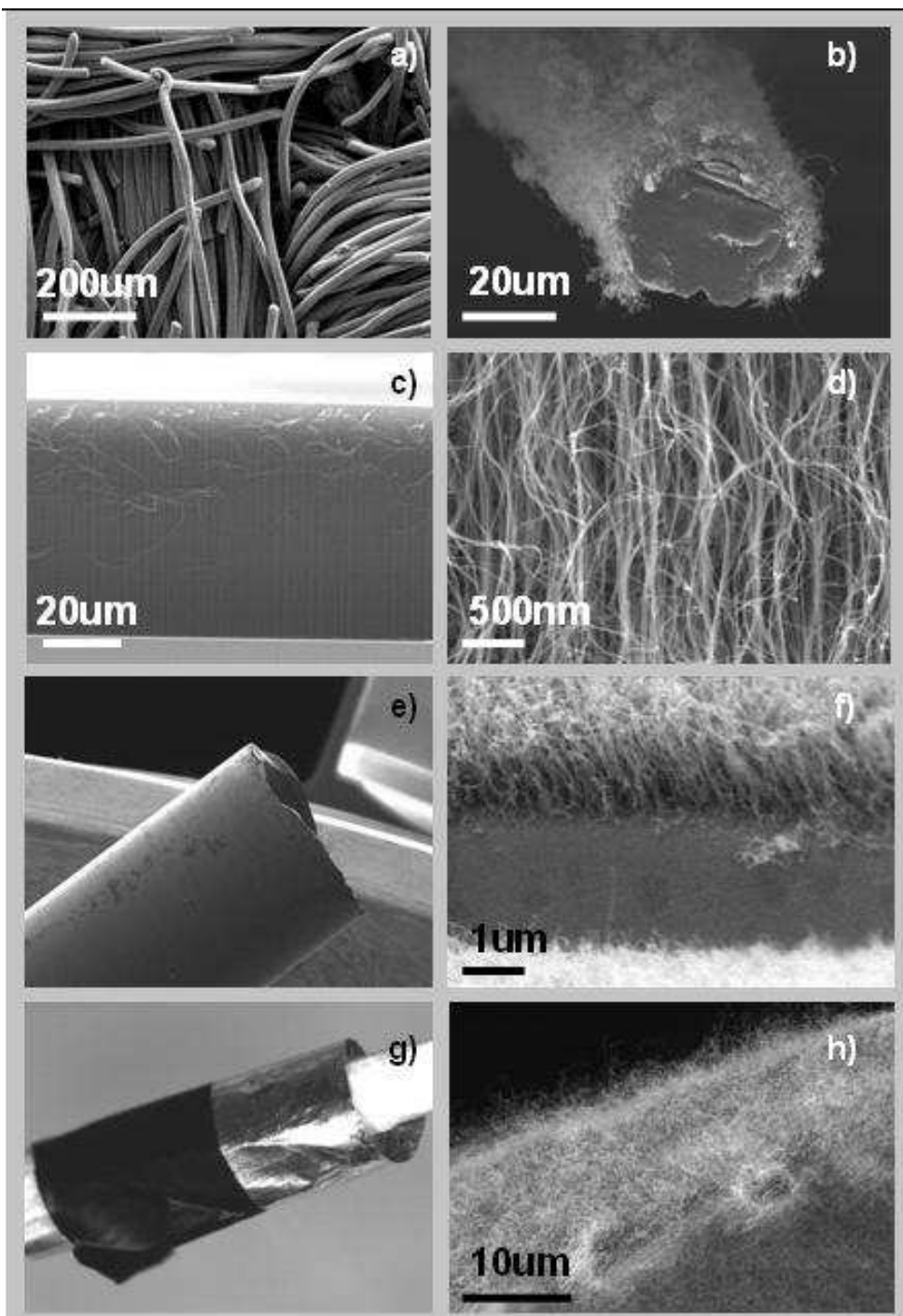
Inspired by the carbon nanotubes growth using CaCO₃ support that produces CO₂ by thermal decomposition, we studied the precise effect of CO₂ on the carbon nanotubes growth by adding CO₂ gas into the reactor. For these studies, MgO was selected as catalyst support because MgO does not form a carbonate at temperatures higher than 300 °C (see Section 2.2.1). Consequently, carbon nanotubes synthesis at temperatures higher than 300 °C excludes the CO₂ contribution from the support and enables monitoring of the carbon nanotubes growth with the precise control of the added amount of CO₂ gas. At 680 °C, the carbon nanotubes yield obtained as a function of the CO₂/C₂H₂ ratio reveals a maximum at CO₂/C₂H₂ = 1 [43,44]. Any deviation from this optimum gas-phase composition does not only decrease the carbon nanotubes yield but also leads to the production of amorphous carbon. In the absence of CO₂ no carbon nanotubes are produced. It has to be mentioned that carbon nanotubes growth using MgO typically requires high temperature (>750 °C). Thus, C₂H₂-CO₂ reaction enables synthesis of carbon nanotubes in conventionally unfavorable conditions.

We have very recently discovered that the equimolar C₂H₂-CO₂ reaction can be applied to many different support systems resulting in a flexible, highly reproducible and high yield synthesis of carbon nanotubes [24]. The C₂H₂-CO₂ reaction leads to oxidative dehydrogenation reaction of acetylene, which has been widely used in olefin industry for the production of unsaturated hydrocarbons [54]. However, to our knowledge this process has never been considered for the synthesis of carbon nanotubes.

Figure 6 demonstrates representative growth of carbon nanotubes produced by the oxidative dehydrogenation reaction of C₂H₂ with CO₂ on a broad range of support materials including carbon fibers, alumina, glass and aluminum foil. These materials are decorated prior to the growth with Fe

based-metallic nanoparticles (Fe_2Co or Fe) by a simple co-precipitation process (see Section 3 for details). For all support materials, the produced carbon phase entirely consists of carbon nanotubes, if the precise equimolar stoichiometry between C_2H_2 and CO_2 was applied. As observed by TEM, carbon nanotubes are multi-walled and of high crystallinity without any indication of amorphous carbon. Similar structural characteristics are observed for all samples independent of the support material applied [24, see also supporting information].

Figure 6. Carbon nanotubes grown by the equimolar reaction over (a,b) carbon fibers, (c,d) carbon nanotubes forest over Fe_2Co particles supported by an alumina thin film, (e) and (f) carbon nanotubes on glass, (g) and (h) carbon nanotubes on aluminum foil.



In Figure 7, the resulting carbon nanotubes yield is presented as the ratios C/support and C/metal obtained for various support materials including oxides, borides, nitrides and carbides. The numbers vary with the different support material. However, it has to be stated that on all these supports, the obtained carbon nanotubes yield is at least 10 times higher than without the oxidative dehydrogenation reaction.

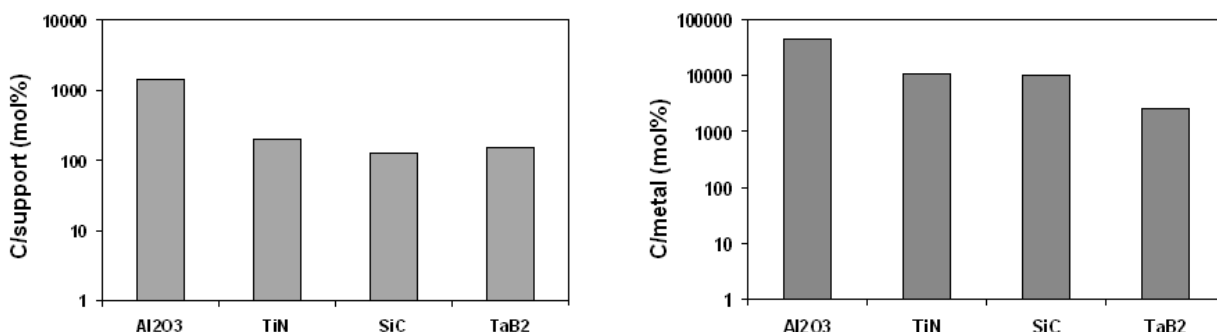
The oxidative dehydrogenation reaction can proceed along two overall chemical mechanisms as we proposed previously [24,42]:



Besides these two mechanisms, the thermal decomposition of acetylene can occur. However this process is kinetically limited at low temperatures, whereas the reactions (1) and (2) can spontaneously take place. In order to identify the precise chemical reaction involved, residual gas composition was analyzed in the exhaust during the synthesis. In particular, the partial pressures of the main reaction products (H_2O and CO) were monitored by means of quadrupolar mass spectroscopy (QMS).

Figure 8 shows the partial pressures measured during the synthesis of carbon nanotubes using Fe_2Co supported by Nb_2O_5 . The amount of water and CO produced clearly undergo temperature dependence. At 500 °C, a sudden change occurs where the water partial pressure, which was constantly increasing, abruptly decreases. Simultaneously the CO content increases. This significant change in the reaction gas composition at 500 °C can be explained by the change of reaction. Below 500 °C, a high amount of H_2O is produced, which is only present in the reaction path (1). In contrast, reaction (1) produces one molecule of CO per C_2H_2 molecule whereas reaction (2) yields twice the amount of CO molecules. Thus, the increase in the amount of CO in the exhaust is a clear indication for the transition from the reaction path (1) to path (2). These results clearly demonstrate that the oxidative dehydrogenation reaction of C_2H_2 with CO_2 proceeds along the reaction (1) below 500 °C, whereas the reaction (2) is kinetically preferential above 500 °C.

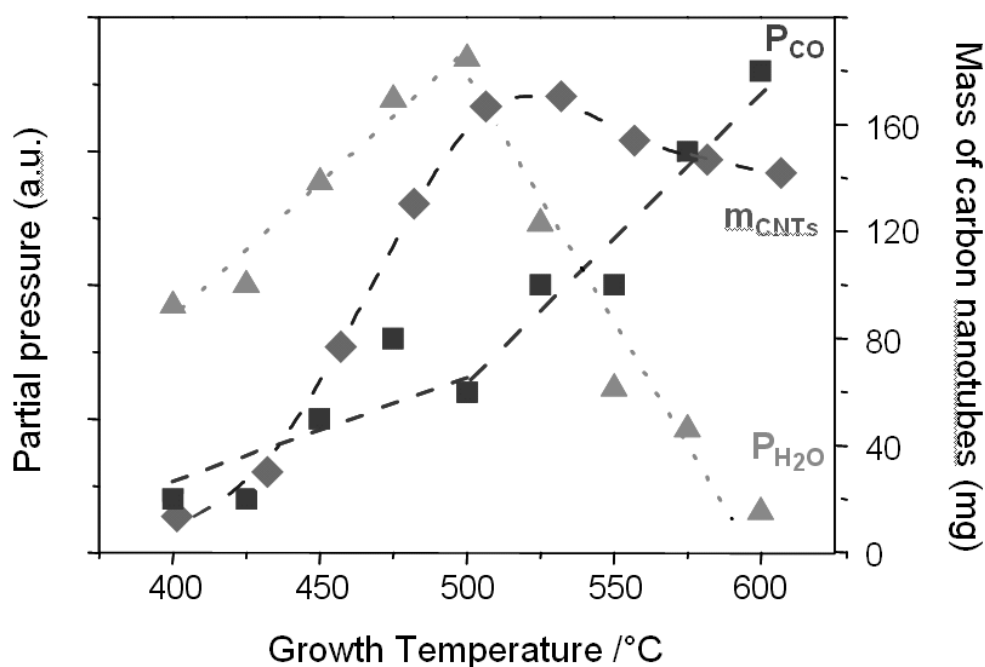
Figure 7. Efficiency of the carbon nanotubes produced by the equimolar reaction presented as (a) the ratio between the mass of carbon nanotubes obtained and the amount of support and (b) the ratio between the mass of carbon nanotubes obtained and Fe_2Co catalyst introduced into the reaction chamber.



As can be seen in Figure 8, the reaction path also affects the yield of carbon nanotubes produced. At temperatures below 500 °C, the oxidative dehydrogenation reaction follows the reaction (1). When the

temperature is increased from 400 to 500 °C, kinetics of the carbon nanotube synthesis thermally enhances, leading to a linear increase of the yield. A maximum is reached at 500 °C where the transition occurs. The slight decrease in the yield above 500 °C can be explained by the fact that twice less carbon atoms are produced along the reaction path (2) despite the thermal enhancement of the reaction kinetics. Consequently, the optimum temperature for the highest yield of carbon nanotubes is at the transition temperature where the reaction path changes from (1) to (2). The same phenomenon has been observed on the different support materials.

Figure 8. Evolution of the partial pressure of CO and H₂O, as well as the mass of carbon nanotubes produced as a function of growth temperature. Catalyst applied is Fe₂Co supported by Nb₂O₅. At 500 °C, a transition occurs for both parameters, as well as for the mass of the carbon nanotubes produced.



It has to be stated that the classical route of thermal decomposition of C₂H₂ is limited at low temperatures. Below 600 °C, we obtained only amorphous carbon instead of carbon nanotubes. However, the oxidative dehydrogenation reaction of C₂H₂ with CO₂ results in carbon nanotubes even at 400 °C. Hence, the oxidative dehydrogenation reaction significantly enhances the carbon nanotube growth kinetics and reduces the growth temperature. For different support materials, we observed different optimum temperatures [24]. For carbon fibers, the lowest optimum growth temperature of 400 °C was observed, whereas Al₂O₃ and SiC revealed a high optimum temperature of 650 °C. In Table 2 the highest yield growth temperature is listed for 10 different support materials. This variation is assumed to originate from the difference in adsorption strength and configurations of the gas molecules on the surface of the supported catalyst. C₂H₂ molecules adsorb most likely on the catalyst surface while CO₂ preferentially adsorbs on the support and forms a carbonate-like surface adsorbate. The oxidative dehydrogenation reaction could take place at the triple-joint junction, where the interface between the catalyst particle, support and the reaction gases, is located [43].

Table 2. The maximum yield temperature obtained for 10 different support materials when the oxidative dehydrogenation reaction is applied.

Support material	Maximum yield growth temperature / °C	Support material	Maximum yield growth temperature / °C
C	400	La ₂ O ₃	550
V ₂ O ₅	450	Bi ₂ O ₃	600
TaB ₂	500	TiO ₂	625
TiN	500	Al ₂ O ₃	650
Nb ₂ O ₅	500	SiC	650

The oxidative dehydrogenation reaction provides the possibility to grow carbon nanotubes in a broad range of temperatures by selecting the appropriate support material. Moreover, it has to be emphasized that, although the highest yields can be achieved at optimum temperature, the products obtained at lower temperatures also entirely consist of carbon nanotubes with structural characteristics comparable with those produced at the optimum condition. Hence, the oxidative dehydrogenation reaction enables the growth of carbon nanotubes in a broad range of growth temperatures from 300 to 750 °C. Other support materials may exist which have not been tested so far, with an optimum temperature far below the one obtained in this study.

3. Experimental Section

3.1. Catalyst Preparation

Stoichiometric amount of metal salts (cobalt (II) acetate tetrahydrate and iron (III) nitrate nonahydrate) corresponding to Fe₂Co composition was dissolved in distilled water. CaCO₃ particles were subsequently added. The total amount of metal corresponded to about 5wt%, relative to the catalyst support. The precipitation of Fe and Co salts onto the CaCO₃ particles was subsequently induced by adding a weak base to the solution. Commercially available CaCO₃ calcite powders were used (Fluka 21060 from Sigma-Aldrich Chemie GmbH and Calofort U from Speciality Minerals). In addition, two drying processes of the catalyst have been employed. At first, the suspension of CaCO₃ particles covered by Fe, Co salts was dried under vigorous stirring on a hot plate (hereafter called hot drying method). The second process is based on the sublimation of the solvent. The suspension was frozen by dropping into liquid nitrogen. Once collected, it was subsequently placed in a homemade freeze drying chamber. According to the phase diagram of water, sublimation of ice occurred by raising the temperature while the vapor pressure remained below 5 mbar.

3.2. Carbon Nanotubes Synthesis and Characterization

The growth of multi-walled carbon nanotubes was performed in our standard fixed bed reactor to accurately measure the acetylene conversion and the production yield. In these conditions, 100 mg of Fe₂Co supported by CaCO₃ were introduced in the reactor at 640 °C. Acetylene and argon were fluxed at 1.0 and 45 L/h respectively for 30 minutes. The reactor was subsequently cleaned by fluxing Ar for

10 minutes. It should be noted that the Fe₂Co catalyst nanoparticles are generated on the CaCO₃ support by reduction of the Fe and Co salts by the acetylene in situ.

For the water assisted growth, carbon nanotube forests were synthesized in a horizontally mounted quartz tube furnace by the water assisted CCVD process. Ethylene (50–400 sccm), as the carbon source, was diluted with argon (100–300 sccm) previously mixed with hydrogen (40–150 sccm). Water was continuously introduced in the reaction chamber by fluxing Ar (5–50 sccm) through a water bubbler. The water content was calibrated by quadrupolar mass spectrometry. Catalyst Fe (1 nm) was deposited on a silicon substrate with 500 nm oxide layer and additional Al₂O₃ (10 nm) as top layer. Furnace temperature was raised to 750 °C prior to the growth. One square centimeter pieces of substrate were used for the growth of carbon nanotubes carpets.

For the equimolar C₂H₂-CO₂ reaction, catalyst was prepared by dispersing the support particles in distilled water in which Fe and Co nitrate had previously been dissolved in 2:1 stoichiometry. After precipitation of the Fe₂Co salt upon drying or by addition of a weak base, the catalyst was collected and dried at 400 °C for 15min to ensure the decomposition of the Fe₂Co salts. The catalyst was subsequently introduced in the reactor at temperatures varying between 300 °C and 800 °C. An equimolar mixture of C₂H₂ and CO₂ (0.5L/h) was subsequently fluxed with Ar (20L/h) to produce carbon nanotubes.

Samples were characterized by scanning electron microscopy (SEM, Philips XL 30 FEG operated at 30 kV) and transmission electron microscopy (TEM, Philips CM20 and CM200 FEG, both operated at 200 kV).

4. Conclusions

Our recent results on the carbon nanotubes grown by CCVD process have been reviewed. We have demonstrated that in the family of Fe_{1-x}M_x alloys (with M = Co and Ni), the compounds Fe₂Co and Fe₂Ni are the most efficient catalysts. Besides the catalyst composition, the catalyst drying process significantly influences the catalyst particle size. The freeze drying process has been identified as favorable in order to avoid agglomeration of catalyst particles during the carbon nanotube synthesis. CaCO₃ has been found as a support material which actively influences the growth of carbon nanotubes by the CO₂ produced by its thermal decomposition. The positive effect of CO₂ has also been demonstrated by adding gaseous CO₂ into the reactor. The interaction between C₂H₂ and CO₂ significantly promotes carbon nanotube growth and allows the growth of carbon nanotubes on unfavorable substrate materials, as well as at much lower temperatures, rather than via traditional decomposition of C₂H₂.

Also the water assisted growth leads to enhanced catalytic efficiency yielding a dense mat of carbon nanotubes. Measurements of bending modulus of individual nanotubes show that the carbon nanotubes originating from the water assisted growth and the equimolar C₂H₂-CO₂ reaction are superior to conventional carbon nanotubes from decomposition of C₂H₂. Thus, we can conclude that higher catalytic efficiency results in reduced density of structural density, therefore in enhanced bending modulus. However, the water assisted growth leads to a narrower diameter distribution and consequently to a higher average bending modulus.

The growth of carbon nanotubes still remains complex. However, the recent outstanding results leading to remarkable improvement in the yield of the reaction, as well as in the improved structural and mechanical properties, demonstrate that also novel chemical routes could exist that involve unexplored mechanisms leading to significant improvements of the carbon nanotube growth.

Acknowledgements

We thank the Centre Interdisciplinaire de Microscopie Electronique (CIME) for access to electron microscopes and technical support. We also thank R. Gaál, B. Korbely, M. Duchamp, J.C. Andresen, S. Casimirius for fruitful discussions. This work was financially supported by the National Centre of Competence in Research (NCCR) “Nanoscale Science” of the Swiss National Science Foundation and by the CABTURES project funded by Nano-Tera.ch. M. Mionić thanks for the grant of the Swiss National Science Foundation (NSF 121814). R. Smajda was funded by the European project VIACARBON (ICT-2007.8.1). J.W. Seo thanks the Belgian Hercules Stichting for their support in HER/08/25 and the K.U. Leuven for the support in STRT1/08/025 and GOA/10/004.

References and Notes

1. Dai, H.J.; Kong, J.; Zhou, C.W.; Franklin, N.; Tombler, T.; Cassell, A.; Fan, S.S.; Chapline, M. Controlled chemical routes to nanotube architectures, physics, and devices. *J. Phys. Chem. B* **1999**, *103*, 11246-11255.
2. De Jong, K.P.; Geus, J.W. Carbon nanofibers: Catalytic synthesis and applications. *Catal. Rev. - Sci. Eng.* **2000**, *42*, 481-510.
3. Dai, H.J. Carbon nanotubes: Synthesis, integration, and properties. *Acc. Chem. Res.* **2002**, *35*, 1035-1044.
4. See, C.H.; Harris, A.T. A review of carbon nanotubes synthesis via fluidized-bed chemical vapor deposition. *Ind. Eng. Chem. Res.* **2007**, *46*, 997-1012.
5. Joselevich, E.; Dai, H.J.; Liu, J.; Hata, K.; Windle, A.H. Carbon nanotubes synthesis and organization. In *Carbon Nanotubes, Topics in Applied Physics*; Jorio, A., Dresselhaus, G., Dresselhaus, M.S., Eds.; Springer-Verlag: Berlin Heidelberg, Germany, 2008; Volume 111, pp. 101-164.
6. Liu, J.; Jiao, L.; Yao, Y.; Xian, X.; Zhang, J. Aligned, ultralong single-walled carbon nanotubes: From synthesis, sorting, to electronic devices. *Adv. Mater.* **2010**, *22*, 2285-2310.
7. Moisala, A.; Nasibulin, A.G.; Kauppinen, E.I. The role of metal nanoparticles in the catalytic production of single-walled carbon nanotubes - a review. *J. Phys.: Condens. Matter* **2003**, *14*, S3011-S3035.
8. Dupuis, A.C. The catalyst in the CCVD of carbon nanotubes - a review. *Prog. Mater. Sci.* **2005**, *50*, 929-961.
9. Harutyunyan, A.R. The catalyst for growing single-walled carbon nanotubes by catalytic chemical vapor deposition method. *J. Nanosci. Nanotech.* **2009**, *9*, 2480-2495.
10. Charlier, J.C.; Iijima, S. Growth mechanisms of carbon nanotubes. In *Carbon Nanotubes, Topics in Applied Physics*; Dresselhaus, M.S., Dresselhaus, G., Avouris, Ph., Eds.; Springer-Verlag: Berlin Heidelberg, Germany, 2008; Volume 80, pp. 55-80.

11. Bajwa, N.; Li, X.S.; Ajayan, P.M.; Vajtai, R. Mechanisms of catalytic CVD growth of multiwalled carbon nanotubes, *J. Nanosci. Nanotechnol.* **2008**, 8, 6054-6064.
12. Kumar, M.; Ando, Y. Chemical vapor deposition of carbon nanotubes: A review on growth mechanism and mass production. *J. Nanosci. Nanotechnol.* **2010**, 10, 3739-3758.
13. MacKenzie, K.J.; Dunens, O.M.; Harris, A.T. An updated review of synthesis parameters and growth mechanisms for carbon nanotubes in fluidized beds. *Ind. Eng. Chem. Res.* **2010**, 49, 5323-5338.
14. Nessim, G.D. Properties, synthesis, and growth mechanisms of carbon nanotubes with special focus on thermal chemical vapor deposition. *Nanoscale* **2010**, 2, 1306-1323.
15. Maruyama, S.; Kojima, R.; Miyauchi, Y.; Chiashi, S.; Kohno, M. Low-temperature synthesis of high-purity single-walled carbon nanotubes from alcohol. *Chem. Phys. Lett.* **2002**, 360, 229-234.
16. Seidel, R.; Duesberg, G.S.; Unger, E.; Graham, A.P.; Liebau, M.; Kreupl, F. Chemical vapor deposition growth of single-walled carbon nanotubes at 600 °C and a simple growth model. *J. Phys. Chem. B* **2004**, 108, 1888-1893.
17. Rümmeli, M.H.; Borowiak-Palen, E.; Gemming, T.; Pichler, T.; Knupfer, M.; Kalbac, M.; Dunsch, L.; Jost, O.; Silva, S.R.P.; Pompe, W.; Büchner, B. Novel catalysts, room temperature, and the importance of oxygen for the synthesis of single-walled carbon nanotubes. *Nano Lett.* **2005**, 5, 1209-1215.
18. Cantoro, M.; Hofmann, S.; Pisana, S.; Scardaci, V.; Parvez, A.; Ducati, C.; Ferrari, A.C.; Blackburn, A.M.; Wang, K.-Y.; Robertson, J. Catalytic chemical vapor deposition of single-wall carbon nanotubes at low temperature. *Nano Lett.* **2006**, 6, 1107-1112.
19. Meshot, E.R.; Plata, D.L.; Tawfick, S.; Zhang, Y.Y., Verploegen, E.A., Hart, A.J. Engineering vertically aligned carbon nanotube growth by decoupled thermal treatment of precursor and catalyst. *ACS Nano* **2009**, 3, 2477-2486.
20. Hata, K.; Futaba, D.N.; Mizuno, K.; Namai, T.; Yumura, M.; Iijima, S. Water-assisted highly efficient synthesis of impurity-free single-walled carbon nanotubes. *Science* **2004**, 306, 1362-1365.
21. Zhang, G.; Mann, D.; Zhang, L.; Javey, A.; Li, Y.; Yenilmez, E.; Wang, Q.; McVittie, J.P.; Nishi, Y.; Gibbons, J.; Dai, H.J. Ultra-high-yield growth of vertical single-walled carbon nanotubes: Hidden roles of hydrogen and oxygen. *Proc. Natl. Acad. Sci. U. S. A.* **2005**, 102, 16141-16145.
22. Futaba, D.N.; Hata, K.; Yamada, T.; Mizuno, K.; Yumura, M.; Iijima, S. Kinetics of water-assisted single-walled carbon nanotube synthesis revealed by a time-evolution analysis. *Phys. Rev. Lett.* **2005**, 95, 056104.
23. McNicholas, T.P.; Ding, L.; Yuan, D.N.; Liu, J. Density enhancement of aligned single-walled carbon nanotube thin films on quartz substrates by sulfur-assisted synthesis. *Nano Lett.* **2009**, 9, 3646-3650.
24. Magrez, A.; Seo, J.W.; Smajda, R.; Korbely, B.; Andresen, J.C.; Mionic, M.; Casimirius, S.; Forró, L. Low-temperature, highly efficient growth of carbon nanotubes on functional materials by an oxidative dehydrogenation reaction. *ACS Nano* **2010**, 4, 3702-3708.
25. Alvarez, W.E.; Kitayanan, B.; Borgna, A.; Resasco, D.E. Synergism of Co and Mo in the catalytic production of single-wall carbon nanotubes by decomposition of CO. *Carbon* **2001**, 39, 547-558.

26. Harutyunyan, A.R.; Pradhan, B.K.; Kim, U.J.; Chen, G.; Eklund, P.E. CVD synthesis of single wall carbon nanotubes under "soft" conditions. *Nano Lett.* **2002**, *2*, 525-530.
27. Flahaut, E.; Govindaraj, A.; Peigney, A.; Laurent, Ch.; Rousset, A.; Rao, C.N.R. Synthesis of single-walled carbon nanotubes using binary (Fe, Co, Ni) alloy nanoparticles prepared in situ by the reduction of oxide solid solutions. *Chem. Phys. Lett.* **1999**, *300*, 236-242.
28. Magrez, A.; Seo, J.W.; Mikó, Cs.; Hernadi, K.; Forró, L. Growth of carbon nanotubes with alkaline earth carbonate as support. *J. Phys. Chem. B* **2005**, *109*, 10087-10091.
29. Smajda, R.; Mionic, M.; Duchamp, M.; Andresen, J.C.; Forró, L.; Magrez, A. Production of high quality carbon nanotubes for less than \$1 per gram. *Phys. Status Solidi C* **2010**, *3*, 1236-1240.
30. Mionic, M.; Duncan, T.L.; Forró, L.; Magrez, A. Influence of the catalyst drying process and catalyst support particle size on the carbon nanotubes produced by CCVD. *Phys. Status Solidi B* **2008**, *10*, 1915-1918.
31. Chiang, W.H.; Sankaran, R.M. Linking catalyst composition to chirality distributions of as-grown single-walled carbon nanotubes by tuning $\text{Ni}_x\text{Fe}_{1-x}$ nanoparticles. *Nat. Mater.* **2009**, *8*, 882-886.
32. de los Arcos, T.; Vonau, F.; Garnier, M.G.; Thommen, V.; Boyen, H.-G.; Oelhafen, P.; Düggelin, M.; Mathis, D.; Guggenheim, R. Influence of iron–silicon interaction on the growth of carbon nanotubes produced by chemical vapor deposition. *Appl. Phys. Lett.* **2002**, *80*, 2383-2385.
33. Talapatra, S.; Kar, S.; Pal, S.K.; Vajtai, R.; Ci, L.; Victor, P.; Shaijumon, M.M.; Kaur, S.; Nalamasu, O.; Ajayan, P.M. Direct growth of aligned carbon nanotubes on bulk metals. *Nat. Nanotechnol.* **2006**, *1*, 112-116.
34. Nessim, G.D.; Seita, M.; O'Brien, K.P.; Hart, A.J.; Bonaparte, R.K.; Mitchell, R.R.; Thompson, C.V. Low temperature synthesis of vertically aligned carbon nanotubes with electrical contact to metallic substrates enabled by thermal decomposition of the carbon feedstock. *Nano Lett.* **2009**, *9*, 3398-3405.
35. de los Arcos, T.; Garnier, M.G.; Oelhafen, P.; Mathis, D.; Seo, J.W.; Domingo, C.; García-Ramos J.V.; Sánchez-Cortés S. Strong influence of buffer layer type on carbon nanotube characteristics. *Carbon* **2004**, *42*, 187-190.
36. de los Arcos, T.; Garnier, M.G.; Seo, J.W.; Oelhafen, P.; Thommen, V.; Mathis, D. The influence of catalyst chemical state and morphology on carbon nanotube growth. *J. Phys. Chem. B* **2004**, *108*, 7728-7734.
37. Nagaraju, N.; Fonseca, A.; Konya, Z.; Nagy, J.B. Alumina and silica supported metal catalysts for the production of carbon nanotubes. *J. Mol. Catal. A: Chem.* **2002**, *181*, 57-62.
38. Kathiyayini, H.; Nagaraju, N.; Fonseca, A.; Nagy, J.B. Catalytic activity of Fe, Co and Fe/Co supported on Ca and Mg oxides, hydroxides and carbonates in the synthesis of carbon nanotubes. *J. Mol. Catal. A: Chem.* **2004**, *223*, 129-136.
39. Kathiyayini, H.; Willems, I.; Fonseca, A.; Nagy, J.B.; Nagaraju, N. Catalytic materials based on aluminum hydroxide, for the large scale production of bundles of multi-walled carbon nanotubes. *Catal. Commun.* **2006**, *7*, 140-147.
40. Couteau, E.; Hernadi, K.; Seo, J.W.; Thien-Nga, L.; Mikó, Cs.; Gáál, R.; Forró, L. CVD synthesis of high-purity multiwalled carbon nanotubes using CaCO_3 catalyst support for large-scale production. *Chem. Phys. Lett.* **2003**, *378*, 9-17.

41. Schmitt, T.C.; Biris, A.C.; Miller, D.W.; Biris, A.R.; Lupu, D.; Trigwell, S.; Rahman, Z.U. Analysis of effluent gases during the CCVD growth of multi-wall carbon nanotubes from acetylene. *Carbon* **2006**, *44*, 2032-2038.
42. Seo, J.W.; Couteau, E.; Umek, P.; Hernadi, K.; Marcoux, P.; Lukic, B.; Mikó, Cs.; Milas, M.; Gáal, R.; Forró, L. Synthesis and manipulation of carbon nanotubes. *New J. Phys.* **2003**, *5*, 120:1-120:22.
43. Magrez, A.; Seo, J.W.; Kuznetsov, V.L.; Forró, L. Evidence of an equimolar C_2H_2 - CO_2 reaction in the synthesis of carbon nanotubes. *Angew. Chem., Int. Ed.* **2007**, *46*, 441-444.
44. Seo, J.W.; Magrez, A.; Milas, M.; Lee, K.; Lukovac, V.; Forró, L. Catalytically grown carbon nanotubes: from synthesis to toxicity. *J. Phys. D* **2007**, *40*, R109-R120.
45. Patil, K.C. Advanced ceramics - Combustion synthesis and properties. *Bull. Mater. Sci.* **1993**, *16*, 533-541.
46. Flahaut, E.; Peigney, A.; Laurent, C.; Rousset, A. Synthesis of single-walled carbon nanotube-Co-MgO composite powders and extraction of the nanotubes. *J. Mater. Chem.* **2000**, *10*, 249-252.
47. Futaba, D.N.; Hata, K.; Namai, T.; Yamada, T.; Mizumo, K.; Hayamizu, Y.; Yumura, M.; Iijima, S. Catalyst activity of water-assisted growth of single walled carbon nanotube forest characterization by a statistical and macroscopic approach. *J. Phys. Chem. B* **2006**, *110*, 8035-8038.
48. Yasuda, S.; Futaba D.N.; Yamada, T.; Satou, J.; Shibuya, A.; Takai, H.; Arakawa, K.; Yumura, M.; Hata, K. Improved and large area single-walled carbon nanotubes forest growth by controlling the gas flow direction. *ACS Nano* **2009**, *3*, 4164-4170.
49. Smajda, R.; Andresen, J.C.; Duchamp, M.; Meunier, R.; Casimirius, S.; Hernadi, K.; Forró, L.; Magrez, A. Synthesis and mechanical properties of carbon nanotubes produced by the water assisted CVD process. *Phys. Status Solidi B* **2009**, *246*, 2457-2460.
50. Yamada, T.; Namai, T.; Hata, K.; Futaba, D.N.; Mizumo, K.; Fan, J.; Yudasaka, M.; Yumura, M.; Iijima, S. Size-selective growth of double-walled carbon nanotube forests from engineered iron catalysts. *Nat. Nanotechnol.* **2006**, *1*, 131-136.
51. Lukic, B.; Seo, J.W.; Couteau, E.; Lee, K.; Gradecak, S.; Berkecz, R.; Hernadi, K.; Delpeux, S.; Cacciaguerra, T.; Beguin, F.; Fonseca, A.; Nagy, J.B.; Csanyi, G.; Kis, A.; Kulik, A.J.; Forró, L. Elastic modulus of multi-walled carbon nanotubes produced by catalytic chemical vapour deposition. *Appl. Phys. A: Mater. Sci. Process.* **2005**, *80*, 695-700.
52. Lee, K.; Lukić, B.; Magrez, A.; Seo, J.W.; Briggs, G.A.D.; Kulik, A.J.; Forró, L. Diameter-dependent elastic modulus supports the metastable-catalyst growth of carbon nanotubes. *Nano Lett.* **2007**, *7*, 1598-1602.
53. Wang, S.; Zhu, Z.H., Catalytic conversion of alkanes to olefins by carbon dioxide oxidative dehydrogenation - A review. *Energy Fuels* **2004**, *18*, 1126-1139.

Production of high quality carbon nanotubes for less than \$1 per gram

R. Smajda¹, M. Mionic¹, M. Duchamp¹, J. C. Andresen¹, L. Forró¹, and A. Magrez^{*1,2}

¹ Laboratoire de Nanostructures et Nouveaux Matériaux Electroniques, Ecole Polytechnique Fédérale de Lausanne (EPFL), Switzerland

² Center for Research on Electronically Advanced Materials, Ecole Polytechnique Fédérale de Lausanne (EPFL), Switzerland

Received 13 September 2009, revised 12 October 2009, accepted 12 October 2009

Published online 4 February 2010

PACS 81.05.Tp, 81.20.Ka, 89.20.Db

* Corresponding author: e-mail arnaud.magrez@epfl.ch, Phone: +41 21 693 7656, Fax: +41 21 693 4470

In this article, we report on the mass production of carbon nanotubes using a continuous production system based on a rotary tube furnace. At first, we have optimized the composition of the metallic nanoparticles. Bimetallic Fe₂Ni and Fe₂Co alloys exhibit higher catalytic activity than pure Fe, Co or Ni. Then, catalyst production process has been modified for the preparation of large quantity of catalyst with low aggregation suitable for large scale synthesis of CNTs. A production rate

of about 1.2 kg per day has been achieved. This is yielding to a cost production of less than \$1 per gram. Finally, we show that the CNTs growth can also be obtained on naturally occurring calcite support for further cost reduction of the synthesis. Quality of the CNTs produced has been established by measuring their mechanical properties using AFM. Young's modulus of the CNTs can be as high as the ideal value of 1 TPa.

© 2010 WILEY-VCH Verlag GmbH & Co. KGaA, Weinheim

1 Introduction Since their discovery [1], carbon nanotubes (CNTs) have been at the forefront of nanotechnology because of their remarkable electrical, optical, thermal and mechanical properties in combination with their extraordinary chemical stability. Developing applications for carbon nanotubes requires the production of pure materials in commercial quantities at affordable prices. Chemical Vapour Deposition (CVD) is considered by the industrialist to be the most suitable process to produce CNTs at low cost. Presently, the market price of pure carbon nanotubes is higher than \$10 per gram for a production capacity of few hundreds metric tonnes per year. They remain expensive compared to carbon black, with a price being of the order of \$1 per metric tonne. It is expected that the price of CNTs will fall as the demand increases and as the process improves in terms of production yield. However, it is important that the supply of carbon nanotubes remains of high quality.

In this paper, we demonstrate that with our continuous production system based on a rotary tube furnace a production rate of more than 1 kg/day can be achieved with a cost

of less than \$1 per gram. 75% of the nanotubes produced have a diameter smaller than 10 nm and a young modulus close to the ideal 1 TPa.

2 Experimental

2.1 Optimisation of the metal catalyst MWCNTs were synthesized by CVD of acetylene and carbon dioxide over supported Fe, Co, Ni catalysts alloys. In a typical catalyst preparation, a stoichiometric amount of metal salts (cobalt (II) nitrate hexahydrate-Sigma Aldrich 60832 ≥99%; and/or iron (III) nitrate nonahydrate-Sigma Aldrich 254223 ≥99.99% and/or nikel(II) nitrate hexahydrate-Sigma Aldrich 72252 ≥98.5%) are dissolved in distilled water. Support (CaCO₃- Fluka C4830 ≥99%) is subsequently dispersed into the solution. The resulting mixture (with Fe₂M/FeCO₃ = 5%; M= Ni or Co) was dried on a hot plate under continuous stirring. Large batches of as-prepared catalyst were produced as well and kept in boxes without special care. The syntheses of CNTs were carried out in a horizontally mounted quartz tube furnace (stationary conditions) in the temperature range of 350 and 850 °C.

For the CNTs synthesis, the as-prepared catalyst was placed on a quartz boat and was rapidly introduced into the reaction chamber. The furnace was flushed with Ar for 10 min and finally exposed to a mixture of C_2H_2 and CO_2 with a flux of 1 L/h. After 15 min growth time, the furnace was flushed again with Ar for 10 min.

2.2 Large scale synthesis of CNTs using the rotary tube furnace We elaborated a continuous production method based on a rotary tube furnace (Fig. 1) to overcome the limited capacity and scalability of the fixed bed reactor [2, 3]. The oven has an 80 mm diameter rotating quartz tube. The catalyst was continuously introduced into the reaction tube with an endless screw place at the end of the catalyst container. Acetylene and argon were fluxed at 10 L/h and 80 L/h respectively. After collecting, the material is purified. The catalyst and support are dissolved in a 1.5 M hydrochloric acid during the purification process. MWCNTs are subsequently filtered, washed with distilled water and dried at 120 °C overnight.



Figure 1 View of the rotary tube furnace used for large-scale synthesis of CVD. A: Catalyst stock continuously driven inside the 3 inch quartz tube. Raw materials (CNTs + Catalyst) are collected in B

2.2 CNTs preparation for mechanical properties characterisation Atomic Force Microscopy (AFM) samples are prepared by dispersing the CVD grown CNTs in ethanol and suspended by 10 minutes sonication using an ultrasonic finger. One droplet of CNT suspension is deposited on the micro-fabricated Si_3N_4 membrane. After one minute, the solution was dried off with a nitrogen flux. Individual CNTs were found to bridge holes of the Si_3N_4 membrane, with their entire length in contact with the membrane surface. AFM images are taken with contact mode and varying loads on each image. Bending modulus of the CNTs is extracted by measuring the vertical deflection at the middle of the suspended part of the nanotube.

3 Results and discussion

3.1 Optimisation of the catalyst composition The Chemical Vapor Deposition developed is based on the equimolar reaction between acetylene and CO_2 at the surface of a supported metal catalyst [4]. We have already shown that best supports for the growth of CNTs are alkaline earth carbonate [5]. Here we have focused our study

on the composition of the metallic nanoparticles of the catalyst. Beside pure Fe, Ni and Co metals, bimetallic alloys with Fe_2M ($M = Ni$ and Co) composition have been tested. We have shown that when catalyst is introduced inside the CVD reactor, an intermediate oxide (spinel with Fe_2NiO_4 , Fe_2CoO_4 composition) of metal transition is formed prior to the reduction into metal nanoparticles, proceeding when acetylene and CO_2 gases are introduced. This oxide is single phase when Fe_2M stoichiometry is applied (as well as for pure Fe, Ni and Co metals). Any deviation from this composition ($Fe/M=2$) induce the presence of a second phase with lower catalytic activity [5]. We clearly see in Table 1 that the mass of CNTs bimetallic alloys exhibits higher catalytic activity compared to pure Fe, Co, and Ni transition metals. The reaction yield, calculated as the ratio between the mass of nanotubes produced and the mass of carbon introduced (as acetylene) is dramatically enhanced by a factor of more than 4 for Fe_2Ni and Fe_2Co compared to Ni and Co respectively.

Catalyst composition	mg of CNTs produced per g of catalyst	Reaction yield (%)
Co	250	9
Fe	350	13
Ni	370	14
Fe_2Co	1310	49
Fe_2Ni	1670	62

Table 1 Maximum mass of CNTs produced for different supported metallic nanoparticles. Growth was performed at 650–700 °C.

Element	Content (wt%)
Co	0.15 ± 0.02
Fe	0.47 ± 0.03
Ca	0.21 ± 0.02
Total	0.83 ± 0.03

Table 2 Impurities content within the purified CNTs as a result of the ICP MS analysis.

3.2 Large scale production of CNTs For the mass production of CNTs, larger quantities of catalyst should be produced. Compared to previous report [5, 6], we developed a new process based on the co-precipitation of the transition metals on the surface of $CaCO_3$ by the addition of a weak base. In a typical catalyst preparation, $CaCO_3$ is dispersed in water by a strong stirring. Transition metal nitrates are added to the slurry. Triethylamine, ammoniac, or

urea is added while the pH raises 10. This induces the deposition of Fe, Co or Ni mixed hydroxides. The slurry (solid/liquid ratio is about 1/3) of CaCO_3 coated with metallic nanoparticles is consequently frozen by dropping in liquid nitrogen and dried afterwards by sublimation. With our equipment, about 3 kg of ice can be collected in 24 hours. It has been found that freeze drying process (also known as lyophilisation) produces less aggregated powder. Therefore, almost all catalytic particles are exposed [7]. This is suitable for mass production and for increasing the production yield compared to those reported in the Table 1. It has to be noticed that despite being widely used in food industry, lyophilisation remains

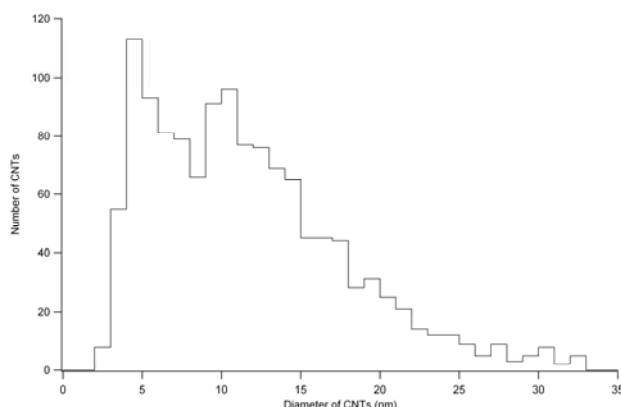


Figure 2 Diameter distribution of CNTs produced in the rotary tube furnace. Diameters of 1000 CNTs have been measured from TEM micrographs.

relatively expensive. Other drying processes like spray drying or roller drying processes, widely used in powder industry, can be used as well and are probably more suitable for large scale production of catalyst at low cost.

To evaluate the yield of the synthesis, we have introduced 2.1 g of catalyst in the quartz tube of our rotary tube furnace. The growth was performed in conditions described in the experimental part of the paper but in stationary conditions (quartz tube not rotating). The mass of CNTs produced is 13.1 g. This corresponds to about 4300 mg of CNTs per gram of catalyst and a reaction yield of about 85%. In contrast to the values reported in Table 1, no noticeable difference has been observed between Fe_2Co and Fe_2Ni transition metal alloys. However, the reaction yield is enhanced and the mass of CNTs produced per gram of catalyst dramatically increased.

Large quantities of catalyst have been produced and the furnace was run for couple of hours. Catalyst is introduced in the rotating quartz tube at a rate of about 10 g per hour. A production rate of about 1200 g of CNTs per day has been achieved.

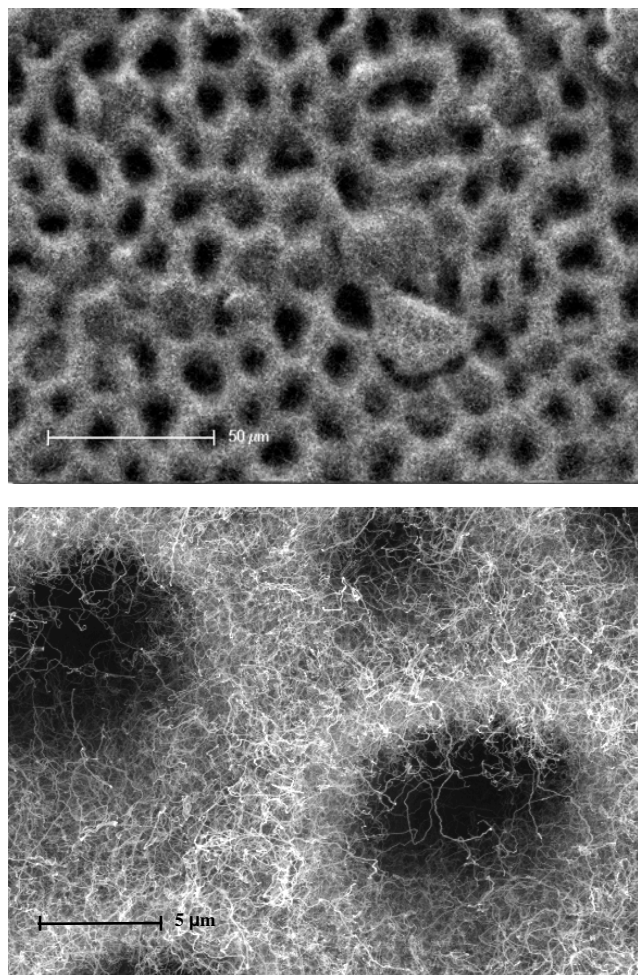


Figure 3 SEM micrographs of carbon nanotubes grown on a sea urchin shell. The growth was performed at 500°C to preserve the porous structure of the shell. Mass production experiments with the rotary tube furnace are performed at 640 °C.

The diameter distribution, Fig. 2, shows that CNTs have a mean diameter of about 11 nm. 75% of CNTs have a diameter below 15 nm (Fig. 2). After purification with HCl, most of the supported catalyst has been removed such as the C content is higher than 99 % (Table 2).

We calculated the cost of the CNTs production using our rotary tube furnace over one year. The cost of the chemicals (for catalyst preparation (support, precursor salts...)) and CNTs purification (distilled water, acids...)) is estimated from the price of the products provided by Sigma Aldrich. Acetylene and argon are purchased from Air liquid. The price of the furnace as well as the salary for one technician for one year is included in the calculations. The electricity required to run the rotary tube furnace is accounted as well. This leads to a production cost of \$0.5 per gram of purified CNTs. This represents a drastic cost reduction since only 1.2 kg per day can be produced in our reactor, as compared to a price of \$10 per gram achieved

for few hundreds metric tons production capacity of industrial reactors.

Beside the possibility of increasing the size of the reactor of our rotary tube furnace to process more catalyst simultaneously, production cost could be further reduced by using less expensive chemicals as compared to high grade materials used for the mass production of CNTs, previously reported in this paper. Hence, CaCO_3 is a sedimentary rock being the third most common constituent of the earth's crust. We have performed the growth of CNTs using the shell, made in calcite, of a sea urchin as support (Fig. 3). The sea urchin shell was collected in Bodrum (Mediterranean Sea, Turkey) and did not experience any surface treatment before or after the Fe film deposition. After exposing the Fe coated shell to acetylene at 600°C , the shell surface is entirely covered with CNTs while the production yield is preserved as compared to CNTs growth process performed over catalyst produced from high grade material. It shows that CNTs can be grown on naturally occurring minerals. This paves the way towards further cost reduction for CNTs production. On the other hand, purification of CNTs produced from natural calcite will be achieved with oxidizing acids (HNO_3 , H_2SO_4 ...) and/or basic solutions (NH_3 , NaOH ...) to ensure a complete dissolution of impurities present in natural calcite support. However, further study of the influence of the impurities on the CNTs quality will have to be carried out.

3.3 Mechanical properties of CNTs The mechanical properties of CNTs have been measured by the "swiss cheese" method [8, 9]. CNTs can be easily dispersed in a solvent. Once deposited on the alumina porous membrane, part of the CNTs can lie over a hole. The adhesion of a CNT on the flat parts of the substrate is usually much stronger than the normal force applicable by the AFM cantilever, so that we modelled the suspended nanotube as a doubly clamped beam (see Fig. 4). We also assumed

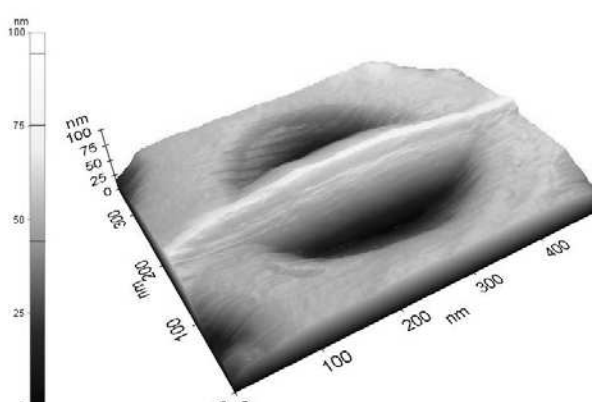


Figure 4 Typical AFM image of CNT bridging the hole of a Si_3N_4 membrane.

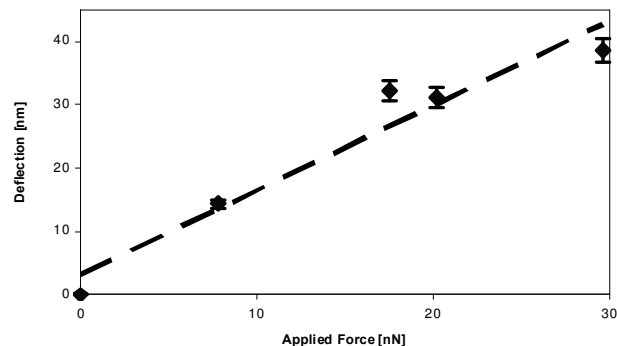


Figure 5 $F-\delta$ curve obtained for a CNTs of a diameter of $10(\pm 1)$ nm and of a suspended length of $500(\pm 10)$ nm. The calculated Young's modulus of the CNT is $1013 (\pm 354)$ GPa.

that the beam has a uniform and circular cross section. The midpoint of a doubly clamped beam deflects by δ when loaded with a force F , and the bending modulus E_b can be derived from the $F-\delta$ graph using the equation

$$E_b = \left(\frac{L^3}{192 I} \right) \left(\frac{dF}{d\delta} \right) \quad (1)$$

where L is the suspended length and I is the second moment of area of the beam, which for a filled cylinder is $\delta D^4/64$. D is the outer diameter of the nanotube. We consider shear to be negligible for the suspended CNTs, as in the case of long thin beams, and take the bending modulus to be the Young's modulus.

To measure the stiffness of a suspended nanotube, we applied a force at its midpoint with an AFM cantilever, acquiring force-displacement data. The $F-\delta$ curves were then obtained by subtracting a reference force-displacement curve taken on a flat substrate. Young's moduli are obtained by fitting lines through these curves (see Fig. 5). CNTs are known to exhibit exceptional mechanical properties. Very high Young's moduli of about 1TPa have been obtained for CNTs produced by high temperature process like arc discharge or laser ablation [8, 9]. On the other hand, the graphitic structure of CNTs produced by CVD, usually below 1000°C , contains a large defect density. Therefore, CVD grown CNTs are regarded as materials with very poor mechanical properties. However, we have recently shown that the Young's modulus of CNTs with diameter below 20 nm exhibit clear diameter dependence [10, 11]. CNTs with smaller diameter have better structure quality and consequently mechanical properties similar to high temperature grown CNTs.

In this study, we measured the mechanical properties of CNTs produced in the rotary tube furnace at 640°C . They exhibit exceptional mechanical properties. When CNTs diameter is lower than 10 nm, the Young's modulus can be as high as 1 TPa (Fig. 5). In the materials produced in mass, 53% of CNTs have a diameter lower than 10 nm and 75%

of CNTs have a diameter lower than 15 nm (Fig. 2) for which the Young's modulus is higher than 100 GPa [11].

4 Conclusion In this work, we have reported the mass production of high quality CNTs at low cost by Chemical Vapour Deposition Process. As a result of catalyst composition optimisation, we have shown that bimetallic alloys with Fe_2M ($\text{M}=\text{Ni}$ or Co) exhibits higher catalytic activity than pure Fe, Co or Ni. Using our rotary tube furnace, we have produced CNTs at a rate of 1.2 kg per day. 85% of acetylene is transformed into CNTs. They exhibit a mean diameter of XX nm and have good mechanical properties with Young's modulus close to 1 TPa. The cost for the production of such CNTs is about \$0.5 per gram. This can be further reduced by using natural calcite.

Acknowledgements We thank the Centre Interdisciplinaire de Microscopie Electronique (CIME) for access to electron microscopes and the technical support of A.J. Kulik for the AFM measurements is acknowledged. This work was partially funded by the European Framework "VIACARBON" as well as the Swiss National Foundation and its NCCR "Nanoscale Science".

References

- [1] M. Monthioux and V.L. Kuznetsov, Carbon **44**, 1621-1623 (2006).
- [2] E. Couteau, K. Hernadi, J.W. Seo, L. Thien-Nga, Cs. Mikó, R. Gaál, and L. Forró, Chem. Phys. Lett. **378**, 9-17 (2003).
- [3] J.W. Seo, E. Couteau, P. Umek, K. Hernádi, P. Marcoux, B. Lukic, Cs. Mikó, M. Milas, R. Gaál, and L. Forró, New J. Phys. **5**, 120.1-120.22 (2003).
- [4] A. Magrez, J.W. Seo, V.L. Kuznetsov, and L. Forró, Angew. Chem. Int. Ed. **46**, 441-444 (2007).
- [5] A. Magrez, J.W. Seo, Cs. Mikó, K. Hernádi, and L. Forró, J. Phys. Chem. B **109**, 10087-10091 (2005).
- [6] J.W. Seo, A. Magrez, M. Milas, K. Lee, V. Lukovac, and L. Forró, J. Phys. D: Appl. Phys. **40**, R109-R120 (2007).
- [7] M. Mionić, D.T.L. Alexander, L. Forró, and A. Magrez, Phys. Status Solidi B **245**, 1915-1918 (2008).
- [8] J.P. Salvetat, G.A.D. Briggs, J.M. Bonard, R. R. Bacsa, A.J. Kulik, T. Stoeckli, N.A. Burnham, and L. Forró, Phys. Rev. Lett. **82**, 944-947 (1999).
- [9] J.P. Salvetat, A.J. Kulik, J.M. Bonard, G.A.D. Briggs, T. Stoeckli, K. Méténier, S. Bonnamy, F. Béguin, N.A. Burnham, and L. Forró, Adv. Mater. **11**, 161-165 (1999).
- [10] B. Lukic, J.W. Seo, R.R. Bacsa, S. Delpoux, F. Béguin, G. Bister, A. Fonseca, J.B. Nagy, A. Kis, S. Jeney, J.A. Kulik, and L. Forró, Nano Lett. **5**, 2074-2077 (2005).
- [11] K. Lee, B. Lukic, A. Magrez, J.W. Seo, G.A.D. Briggs, A.J. Kulik, and L. Forró, Nano Lett. **7**, 1598-1602 (2007).

SCIENTIFIC REPORTS



OPEN

Influence of synthesis parameters on CCVD growth of vertically aligned carbon nanotubes over aluminum substrate

Received: 2 June 2017

Accepted: 1 August 2017

Published online: 25 August 2017

Anna Szabó¹, Egon Kecsenovity^{1,2}, Zsuzsanna Pápa³, Tamás Gyulavári¹, Krisztián Németh¹, Endre Horvath⁴ & Klara Hernadi¹ 

In the past two decades, important results have been achieved in the field of carbon nanotube (CNT) research, which revealed that carbon nanotubes have extremely good electrical and mechanical properties. The range of applications widens more, if CNTs form a forest-like, vertically aligned structure (VACNT). Although, VACNT-conductive substrate structure could be very advantageous for various applications, to produce proper system without barrier films i.e. with good electrical contact is still a challenge. The aim of the current work is to develop a cheap and easy method for growing carbon nanotubes forests on conductive substrate with the CCVD (Catalytic Chemical Vapor Deposition) technique at 640 °C. The applied catalyst contained Fe and Co and was deposited via dip coating onto an aluminum substrate. In order to control the height of CNT forest several parameters were varied during the both catalyst layer fabrication (e.g. ink concentration, ink composition, dipping speed) and the CCVD synthesis (e.g. gas feeds, reaction time). As-prepared CNT forests were investigated with various methods such as scanning electron microscopy, Raman spectroscopy, and cyclic voltammetry. With such an easy process it was possible to tune both the height and the quality of carbon nanotube forests.

Vertically aligned carbon nanotubes (VACNTs) henceforth denoted also as carbon nanotube forests (CNT forest) were first synthesized in 1996¹, and subsequently they got into the focus of research in nanotechnology. Catalytic chemical vapor deposition (CCVD) proved to be the most efficient way for the production of vertically aligned CNTs. The most common and efficient catalysts are the mono- or bimetallic transition metals (Fe, Co, Ni), while Al₂O₃, SiO₂ or MgO are generally applied as supports^{2–6}. Breakthrough in development occurred in 2004 when Hata *et al.*⁷ modified the CNT growth and introduced a small amount of water into the CVD chamber together with the carbon source. Lot of studies have been published so far related successful CNT growth⁸, however, the properties of both the support and the catalytic layer considerably affect the properties of CNT forests, i. e. density, orientation, length, thickness and graphitization of the product, and therefore further investigations are necessary in this field.

In 2001, it was shown by Mauron *et al.* that carbon nanotubes can be oriented perpendicularly to the substrate surface with high densities of nucleation centers, moreover, high CNT density can be achieved by using high quantity of iron oxide clusters which facilitated the growth in the desired orientation⁹.

The CVD parameters (such as carbon source, gas feed, reaction time, reaction temperature, etc.) also have significant role in the formation of VACNTs. Iijima *et al.* have investigated the kinetics of water-assisted CVD by a quantitative time-evolution analysis and concluded that the complex behavior of the time evolution of supergrowth can be easily explained by analyzing the two fitting parameters of the simple growth model, i.e. initial growth rate and the characteristic catalyst lifetime¹⁰. Since then only a few papers were published which

¹Department of Applied and Environmental Chemistry, University of Szeged, Szeged, 6720, Rerrich B. ter 1, Hungary.

²MTA-SZTE "Lendület" Photoelectrochemistry Research Group, University of Szeged, Szeged, 6720, Rerrich B. ter 1, Hungary. ³Department of Optics and Quantum Electronics, University of Szeged, Szeged, 6720, Dom ter 9, Hungary.

⁴Laboratory of Physics of Complex Matter (LPMC), Ecole Polytechnique Federale de Lausanne, Centre Est, Station 3, CH-1015, Lausanne, Switzerland. Correspondence and requests for materials should be addressed to K.H. (email: hernadi@chem.u-szeged.hu)

attempted to find correlation between gas feed (mostly acetylene as carbon source, argon as carrier and hydrogen as reducing agent) and the characteristics of vertically aligned carbon nanotubes^{11–14}.

From the perspective of the catalyst, the thickness, composition, density and adherence of the transition metal layer are crucial parameters and have major effect on the properties of CNT growth. The applied techniques so far are very effective but rather expensive such as magnetron sputtering^{15, 16}, radio frequency sputtering^{17, 18}, electron beam evaporation^{19–21} and physical vapor deposition^{22, 23}, therefore developing a cheap, easy-to-handle method would be desirable. In 2003 it was already pointed out that high-quality but not aligned SWNTs can be synthesized directly onto silicon and quartz substrates using the easy and costless dip-coating approach for the deposition of catalytic metals²⁴.

Nyikos *et al.* reported that by using an efficient dip coating process, a metal substrate and an optimized Fe:Mo (47:3) catalyst system, the CNT diameter, specific surface area and gravimetric capacity of the forest could be controlled²⁵. Vertically aligned CNTs were reproducibly synthesized also onto a metal surface (bulk Cu) by Shanov *et al.* and the effects of Ti, Ni, and Ni–Cr intermediate layers were found to play an important role in achieving vertical alignment of CNTs²⁶.

While the results about precise growth mechanism of carbon nanotubes are still rather contradictory, there are a couple of points during CVD growth wherein researchers agree^{27–32}, namely, i) the process starts with the formation and then the reduction of the nanoparticles from the initially homogeneous catalyst layer (even in the absence of carbon source) ii) and continues with the nucleation and the growth of carbon nanotubes. The importance of a (native) oxide layer on the substrates is also well known since it promotes the transformation of metal films, such as Fe, Co, Ni and their alloys, into catalyst insulated nanoparticles^{33, 34} which can facilitate the growth of CNTs. Although, VACNT-conductive substrate structure could be very advantageous for various applications, to produce proper system without barrier films i.e. with good electrical contact is still a challenge.

The aim of this work was to investigate the controlled growth of vertically aligned carbon nanotubes over a simple aluminum plate. The effect of synthesis parameters was followed by scanning and transmission electron microscopies as well as Raman spectroscopy.

Experimental

Materials. As for substrate aluminum plate produced by WRS Materials Company was used in every experiment. For building catalyst layer cobalt (cobalt(II)-nitrate hexahydrate, 99% (Sigma-Aldrich)) and iron (iron(I-II)-nitrate nonahydrate, 99.9% (Sigma-Aldrich)) precursors were dissolved in absolute ethanol (VWR). During the CVD synthesis the gas feed contained ethylene, hydrogen and nitrogen (all supplied by Messer Hungary).

Catalyst preparation. First the ethanolic solution of catalyst metals was prepared using $Fe(NO_3)_3 \times 9H_2O$ and $Co(NO_3)_2 \times 6H_2O$ salts. The ratios of catalyst metals varied was as follows: Fe:Co = 0:1, 1:3, 2:3, 1:1, 3:2, 3:1, and 1:0, respectively. The concentrations of the ink (iron and cobalt containing ethanolic solution) were 0.022 M, 0.044 M, 0.066 M, 0.11 M, 0.22 M, 0.44 M and 0.66 M, respectively. In most cases the following catalyst solution was used: 0.11 M with the Fe:Co ratio of 2:3 for which 0.888 g $Fe(NO_3)_3 \times 9H_2O$ and 0.855 g $Co(NO_3)_2 \times 6H_2O$ were homogenized in ethanol in a volumetric flask of 50 cm³. In order to prevent the effect of aging which might modify the properties of the solution³⁵ catalyst inks were always prepared freshly before dip coating.

In the second step the support (aluminum sheet) was pretreated before catalyst deposition. In order to remove any contamination (motes, grease spots, etc.) from its surface the aluminum sheet was placed into an ultrasound bath containing distilled water then it was washed with ethanol and acetone sequentially. After that the decontaminated support was heat treated at 400 °C in a static oven for 1 h which resulted in a native oxide layer of higher thickness. This alumina layer is fairly advantageous for two reasons, it serves an effective catalyst support in CVD, and also provides better wetting of the surface by the ink. For dip coating and CVD 3 × 2.5 cm sized support sheets were prepared.

Dip coating is a flexible method to build thin layers onto the surface of catalyst support under controlled conditions. Before dip coating aluminum sheets were flattened for better equipartition. For the catalyst preparation a KSV dip coater LM (KSV Instruments Ltd.) was used. Dipping speed was set to 200 mm × min⁻¹ in every experiment, and the speed of withdrawal varied between 50–200 mm × min⁻¹. Aluminum plates were kept in the ink for 5 seconds. In order to stabilize the metal nitrate layer in oxide state the dip coated samples were heated again at 400 °C (with a heating rate of 30 °C × min⁻¹) in a static oven for 1 h.

CCVD synthesis. For the synthesis of CNT forests the common CCVD method was applied. Before synthesis, the size of the catalyst samples on aluminum plate were further reduced to 3 × 0.4 cm to fit the quartz boat since the diameter of quartz tube was 20 mm. As the melting point of aluminum is 660 °C all CCVD syntheses were carried out at 640 °C. The gas feed contained ethylene as carbon source (70–120 cm³ × min⁻¹), nitrogen as carrier (50–75 cm³ × min⁻¹), hydrogen as reductive agent (100–130 cm³ × min⁻¹), and – in certain experiments – water vapor (32–42 cm³ × min⁻¹).

The schematics of the CCVD reactor is shown in Fig. 1. In a typical synthesis first the reactor was rinsed by nitrogen to remove oxygen traces from the system. Then the catalyst sample in a quartz boat was placed into the reactor tube under continuous nitrogen flow. When the system reached the reaction temperature hydrogen was added to the gas feed for 5 mins in order to reduce the catalyst sample. The CCVD reaction was initiated with the addition of ethylene (and water vapor) flow. Reaction time varied from 2 to 30 mins, however, most frequently 15 min run was applied. After the synthesis all gas feed turned off except nitrogen. Then the system was rinsed for 2 min after that the quartz tube was removed from the oven and was cooled down to room temperature under continuous nitrogen flow.

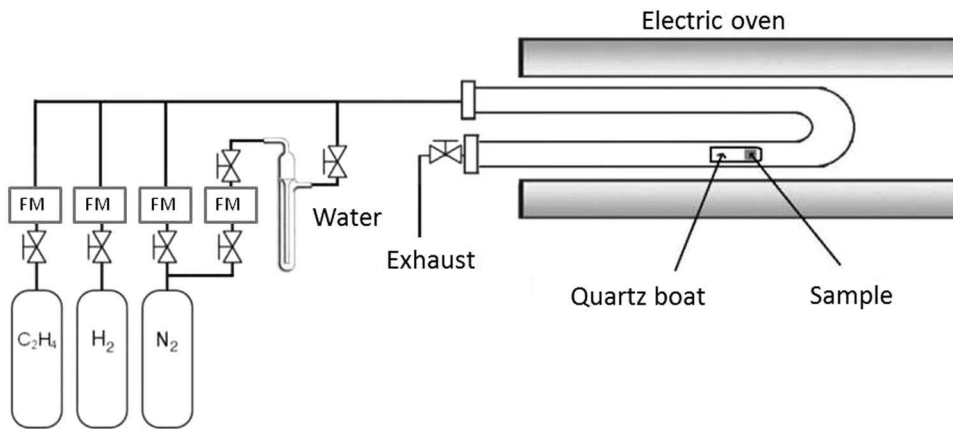


Figure 1. Schematic image of CCVD reactor.

Characterization of CNT samples. To investigate the morphology of CNT forests Scanning Electron Microscopy (SEM) analysis was carried out with a Hitachi S-4700 Type II FE-SEM (5–15 keV) instrument. In order to take images of the forests from side, the sample holder was turned at an angle of 35° during the measurements. Heights of the forests were calculated regarding this value. SEM results were evaluated by using ImageJ software.

The quality of carbon nanotubes was examined via (high resolution) Transmission Electron Microscopy (TEM) using a Philips CM 10 (100 keV) type instrument. During sample preparation CNT bunches were collected from the surface of Al substrate which were suspended in 1.25 cm³ absolute ethanol. From this suspension 2–3 droplets were deposited onto the surface of a holey carbon grid (Lacey, CF 200). Images were analyzed by using Soft Imaging Viewer software.

The quality and graphitic properties of carbon nanotube forests were investigated by Raman spectroscopy. The measurements were carried out with Thermo Scientific DXR Raman microscope with 532 nm excitation wavelength.

Results and Discussion

Catalyst preparation. Since the properties of catalyst layer are crucial regarding the CNT forest growth during CCVD synthesis, parameters affecting catalyst deposition were examined first. The effect of dip coating speed and the concentration/ratio of catalyst ink on the features of CNT forest growth were investigated in detail.

The effect of dip coating. In this series the speed of withdrawal varied in the range of 50–200 mm × min⁻¹ but the concentration and the metal ratio of catalyst ink were fixed at values of 0.11 M and 2:3, respectively. CCVD parameters were the following: the flow rates for ethylene, hydrogen, nitrogen and water vapor were 70, 100, 50 and 30 cm³ × min⁻¹, respectively, while the reaction time was 15 minutes in each run. Our former result revealed that the influence of aging in case of ethanolic solution of Fe(NO₃)₃ × 9H₂O is a significant issue. The color changes to dark reddish brown in a few hours which is also an important sign of oligomer formations³⁵. This phenomenon is disadvantageous during dip coating therefore always freshly prepared ink was used for layer preparation. From the SEM analysis of grown CNT forests a qualitative conclusion was drawn. Both the height and quality of CNT forest are rather poor when the lowest dip coating speed was applied. A tendency was observed that increasing the speed of withdrawal results in higher forests with progressively better orientation.

The effect of catalyst ratio. In these experiments the effect of Fe:Co ratio of catalyst ink on the properties of CNT forests was investigated. While CCVD parameters and ink concentration were the same as mentioned in the previous paragraph, the ratio of two catalyst metals varied as follows: Fe:Co = 0:1, 1:3, 2:3, 1:1, 3:2, 3:1, and 1:0, respectively. Monometallic catalyst layers are of great importance since both iron and cobalt were reported to be active in normal CCVD carbon nanotube synthesis, moreover Fe alone proved to be suitable for growing CNT forest³⁶. However, in our system no carbon deposit could be observed in case of using pure metal salt as ink. It can be concluded that for CNT forest synthesis bimetallic catalyst layer is required on the surface of Al support. It is known from the literature that the role of alumina is advantageous since suppresses the diffusion and aggregation of catalyst nanoparticles by forming metal-dissolved alumina after catalyst metals diffuse into alumina and precipitate as nanoparticles³⁷. In our case native oxide layer was developed by heat treatment in order to avoid dissolution of catalysts in metallic substrate. Alumina is considered as a key material to initiate catalysis of carbon nanotube growth. The effect of Fe:Co ratio on CNT forest was investigated via SEM (Fig. 2a).

It was revealed that all bimetallic layers were active in CCVD synthesis. Although in the literature other research groups used the 1:1 ratio most often in our system this 1:1 ratio resulted in the lowest carbon nanotube forest. SEM images pointed that there is only a slight difference in the quality and orientation of CNT forests, presumably only a slight preference can be concluded for samples of higher cobalt content. Plotting the height of CNT forest as a function of catalyst composition (see Fig. 2b) it was found that Fe:Co ratio has a strong influence on the growth. While the lowest value, approx. 20 µm was obtained when the Fe:Co ratio was 1:1, the highest

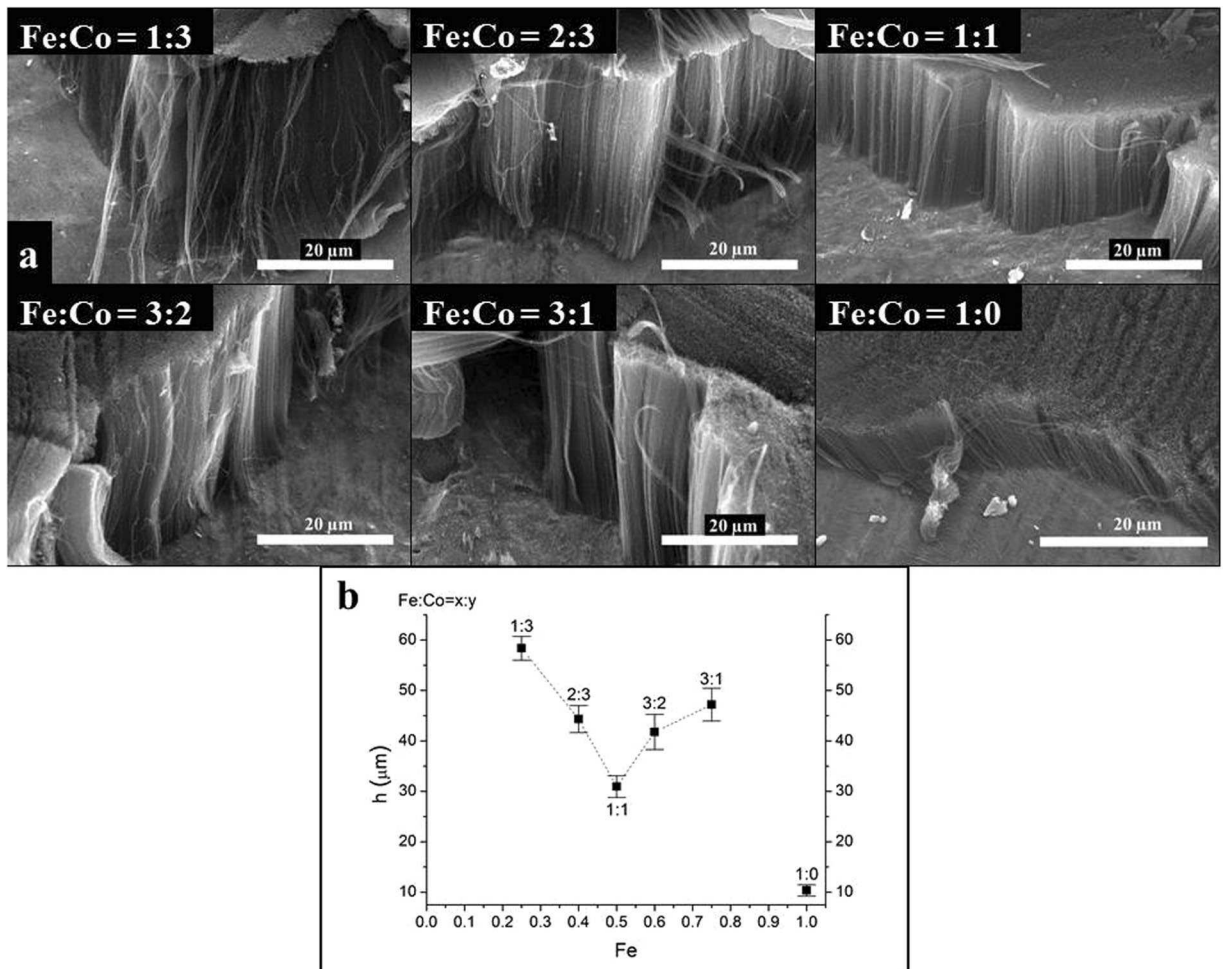


Figure 2. SEM images of CNT forests synthetized at various catalyst ratios (a) and heights of CNT forests (b).

(almost 3 times higher) CNT forest of almost 60 μm grew on the layer in case of 1:3 ratio. In spite of the fact that Magrez *et al.* have already proved the positive role of $\text{Fe}_2\text{Co}^{38}$, catalyst layers of other composition resulted in CNT forests of 40–50 μm height.

The effect of ink concentration. Thereinafter the effect of ink concentration on CCVD growth was studied. While CCVD parameters and Fe:Co ratio were the same as mentioned before, the concentrations of the catalyst ink varied as follows: 0.022 M, 0.044 M, 0.066 M, 0.11 M, 0.22 M, 0.44 M and 0.66 M, respectively. During the investigation of CNT forests grown over layers using various catalyst ink concentrations, it was demonstrated, that ink with the lowest concentration cannot be used for layer formation since no significant carbon deposit was observed on the surface of Al substrate. As it can be seen in Fig. 3a, applying catalyst ink of 0.044 M carbonaceous material has deposited onto the surface during CCVD synthesis, nevertheless, only disordered carbon nanotubes can be observed. By applying higher ink concentrations well-aligned carbon nanotubes were formed, however, even from SEM analysis it can be seen that both their orientation and density changed with concentration (Fig. 3a). Diagram in Fig. 3b illustrates the height of CNT forests as a function of ink concentration.

It can be deduced that ink concentrations lower than 0.11 M result in proportionally lower CNT forest, nevertheless this tendency does not continue above 0.11 M. Instead, the heights of CNT forests varied in the range of 12–18 μm, consequently increasing ink concentration has no significant influence on the height. According to our results in the range of low ink concentrations, the carbon nanotube forests' height is affected dramatically by the ink concentration, the height varied between 0.87–6.66 μm. The growth of the highest carbon nanotube forests can be observed in the case of the reference ink concentration (0.11 M), meaning it is the optimum concentration for the synthesis of carbon nanotube forests with relatively increased height. In the section “Further analysis of carbon nanotubes composing forests” it is discussed that the diameter of the carbon nanotubes is not influenced by the ink concentration, supported also by the TEM images.

Catalyst morphology was further investigated since it might have significant role on the future properties of both individual carbon nanotubes and CNT forests. To characterize the catalyst layer blank CCVD experiments were carried out: every step was identical, only the carbon source (ethylene) was omitted from the system. In the absence of hydrocarbon obtaining catalyst layer close to pre-synthetic form was assumed. SEM images taken after blank experiments can be seen in Fig. 4a. Aluminum substrate is homogeneously covered by catalyst of various

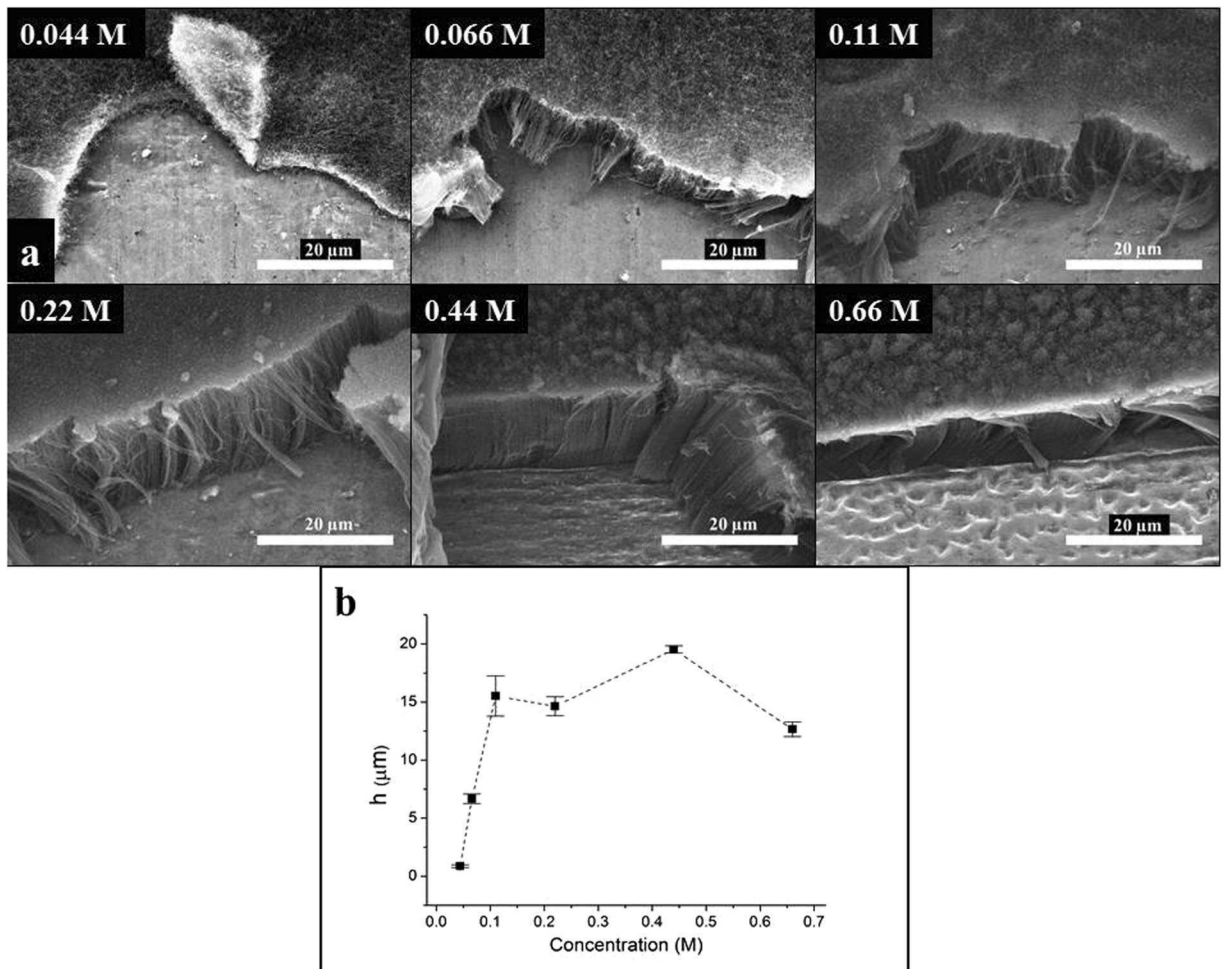


Figure 3. SEM images of CNT forests synthesized by varying the catalyst ink concentration (a) and heights of CNT forests (b).

particle sizes in case of different ink concentrations, however, due to sintering their size cannot be determined precisely. While the depth of native oxide layer (after the treatment described in the previous section) was 10 nm, the average thickness of catalyst layer was found to be 20 nm.

From SEM analysis of both CNT forests and catalyst particles, it can be presumed that the density of CNT forest depends on the quality of catalyst layer deposited onto the surface of Al substrate. As it was already mentioned before (Fig. 3a) the density of CNT forest might depend on the ink concentration. To prove this assumption we attempted to measure the “concentration” of CNT forests. As a preliminary approach samples before and after CCVD synthesis (e.g. initial aluminum substrate with catalyst layer and the same with carbon deposit) were weighed. Since CNT forest contains more than 90% air, the accuracy of this method is only approximate. Nevertheless, from the increase in mass and from the height and area of CNT forest, density can be calculated. These approximate data can be found in Fig. 4b, and it can be concluded that the highest CNT forest can be obtained by applying catalyst ink of 0.11 M concentration.

In order to verify this result an independent technique, namely cyclic voltammetry was carried out on CNT forests prepared using different ink concentrations (Fig. 4c). From these results not only the density of the samples but the existence of electric contact between CNTs and Al support was also proved. From cyclic voltammograms charge capacity can be calculated directly, thus the electrochemically accessible surface can be determined. This parameter is in strong correlation with CNT forest density (assuming constant CNT diameter) since the sample contains more carbon nanotubes, which leads to higher surface area and higher density. This fact is of great importance because many potential applications (e.g. batteries, sensors, catalyst supports) are based on the available surface together with unique electric conductance of CNTs as well. Results confirmed the estimation of density obtained by the mass measurements.

Changes of different parameters during CCVD synthesis. Adjusting the parameters of CCVD synthesis properly is very important for fine-tuning the structure of vertically aligned carbon nanotube arrays. In this section the effect of gas feed and reaction time will be discussed. In each case SEM analysis of carbon deposit was performed from which the height of CNT forests were determined.

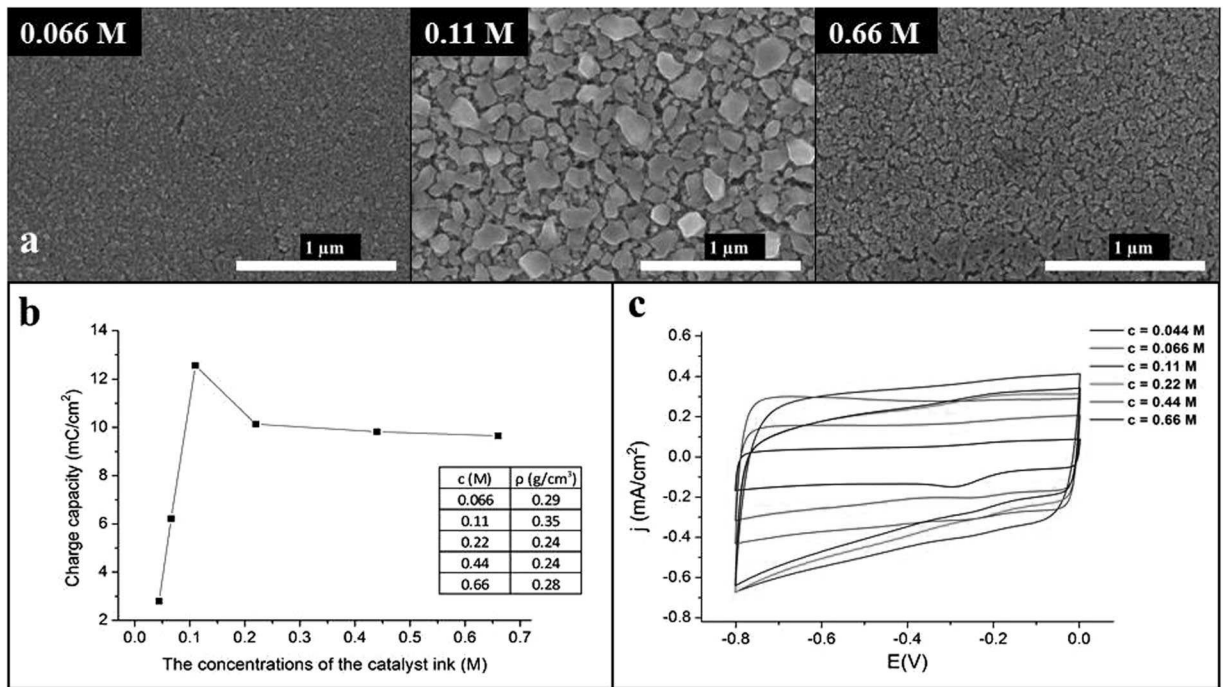


Figure 4. SEM images of CNT forests pre-synthesized (a), charge capacity diagram of CNT forests by varying the ink concentration (b) and cyclic voltammograms of CNT forests by varying the ink concentration (c).

nitrogen	ethylene	hydrogen	water vapor
50			32
60	70	100	37
75			42
	70		32
50	95	100	37
	120		42
	70	100	32
50	70	110	37
		130	42
	70	100	20
50			30
			40
			50
			60

Table 1. The composition of gas feed for different syntheses.

The effect of gas feed. Firstly the effect of nitrogen, hydrogen and ethylene feed was investigated. While reaction time was fixed (15 mins), two parallel series were carried out: with and without water vapor. In order to investigate how nitrogen flow affects the synthesis, the gas feed was varied as follows: $50\text{ cm}^3 \times \text{min}^{-1}$, $60\text{ cm}^3 \times \text{min}^{-1}$, and $75\text{ cm}^3 \times \text{min}^{-1}$, respectively (increasing always by 20%), together with $70\text{ cm}^3 \times \text{min}^{-1}$ of ethylene and $100\text{ cm}^3 \times \text{min}^{-1}$ of hydrogen. Measurements were carried out either with or without water vapor. The composition of gas feed for different syntheses are summarized in Table 1.

From SEM analysis both the height and alignment of CNT forests were determined. Figure 5 shows SEM images of carbon nanotube forests synthesized by different nitrogen flow either in the presence ((d)-(f)) or the absence ((a)-(c)) of water vapor. It can be seen that the quality, the orientation of the samples are always better if the gas feed contained water. This feature can be attributed to the fact that without water vapor the system contains more defects, resulting in chaotic like orientation of the carbon nanotube. In the case when water vapor is present in the system it facilitates the inhibition of defects, also it can oxidize the present amorphous carbon in the system, supporting the desired orientation of the carbon nanotube forests. Concerning the quality similar observations were made when the flow of ethylene or hydrogen were altered.

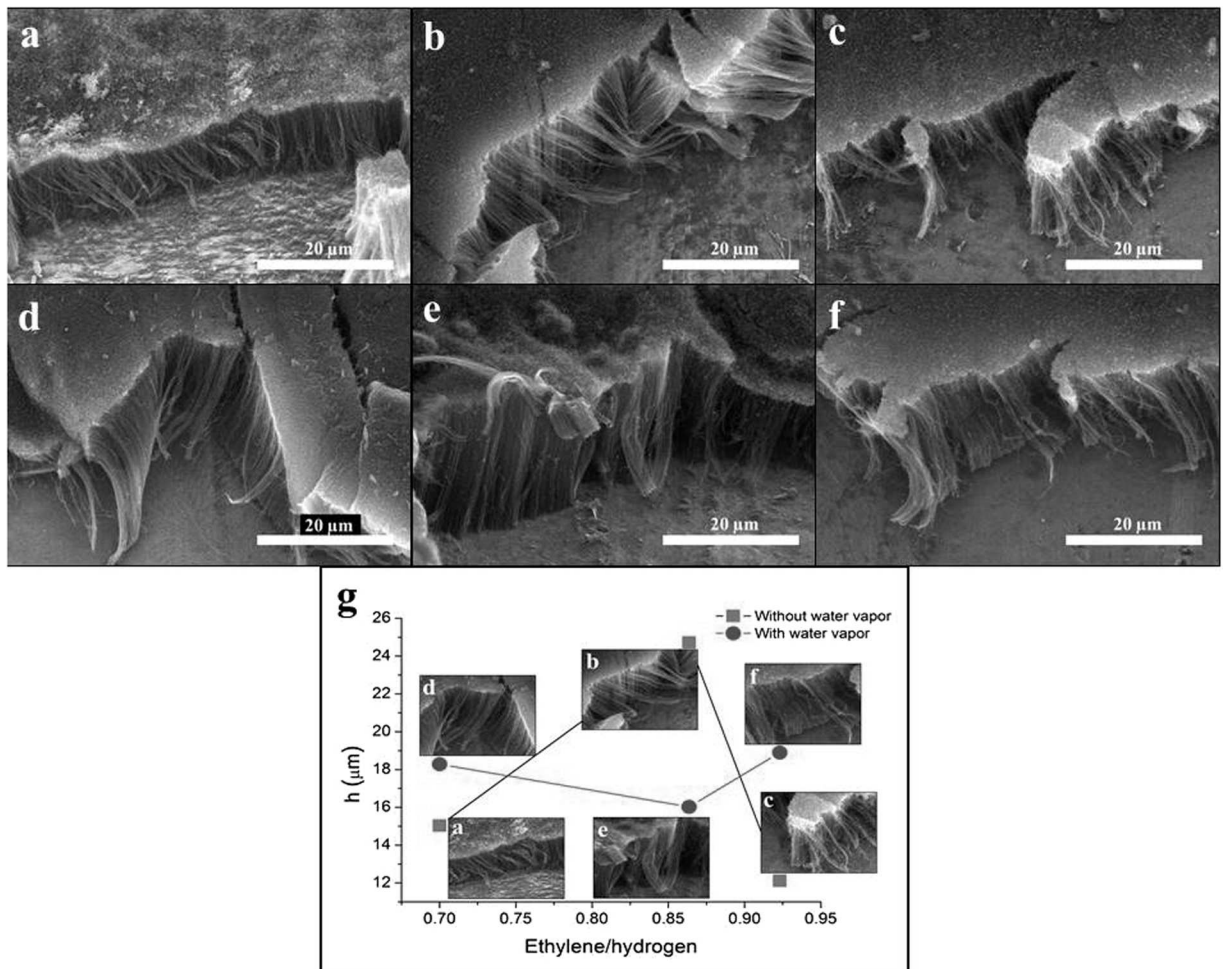


Figure 5. SEM images of CNT forests synthesized by varying the nitrogen gas feed without water vapor $50\text{ cm}^3 \times \text{min}^{-1}$ (**a**), $60\text{ cm}^3 \times \text{min}^{-1}$ (**b**), and $75\text{ cm}^3 \times \text{min}^{-1}$ (**c**), SEM images of CNT forests synthesized by varying the nitrogen gas feed with water vapor $50\text{ cm}^3 \times \text{min}^{-1}$ (**d**), $60\text{ cm}^3 \times \text{min}^{-1}$ (**e**), and $75\text{ cm}^3 \times \text{min}^{-1}$ (**f**), and heights of CNT forests (**g**).

Plotted heights of CNT forests fabricated under various conditions are summarized in Fig. 5g. From these data it can be concluded that water vapor has significant influence not only on the alignment of the samples but on their height too. While the highest CNT forest obtained was 24.7 μm using the lowest gas feed without water vapor (Fig. 5b), the lowest one was 12.1 μm using the highest gas feed without water vapor (Fig. 5c). It can be deduced that CNT forest's height is decreasing with increasing gas feed, however, this tendency cannot be applied in the presence of water vapor.

The effect of water vapor feed. Since the effect of water on the CNT growth is indisputable its influence was investigated more thoroughly. Results pointed out that water assisted CCVD synthesis provides CNT forest of better quality, moreover, the presence of water affects the height as well. These two effects are probably due to the oxidizing feature of water vapor which facilitates the removal of less graphitized carbon nanotubes (thus providing better orientation) on one hand and controls/reduces its height on the other¹⁰. Therefore, the optimization of water vapor content in the gas feed is crucial. In these experiments the flow rate of nitrogen, ethylene and hydrogen was constant, $50\text{ cm}^3 \times \text{min}^{-1}$, $70\text{ cm}^3 \times \text{min}^{-1}$, and $100\text{ cm}^3 \times \text{min}^{-1}$, respectively, and the water vapor feed was varied in the range of 20 to $60\text{ cm}^3 \times \text{min}^{-1}$.

SEM investigation (Fig. 6a) revealed that the highest CNT forest (21.9 μm) was obtained in case of $30\text{ cm}^3 \times \text{min}^{-1}$ water vapor flow. If lower value is applied, the CNT forest is consisted of sinuous carbon nanotubes with the smallest observed height (7 μm). Although when the concentration of water vapor was increased it had a negative effect on the heights of the graphitic carbon nanotube forests (their height was reduced), which was discussed above. Increasing the water vapor feed (see Fig. 6b) resulted in the decrease of height of CNT forest which can be explained by the reaction of carbon nanotubes with water vapor. E.g. the rate of CNT growth becomes lower than the rate of decomposition (discussed before).

The effect of reaction time. The effect of reaction time was investigated in the next series in which all gas flows were kept constant. In these experiments nitrogen was used to purge the system for 1.5 min then to reduce

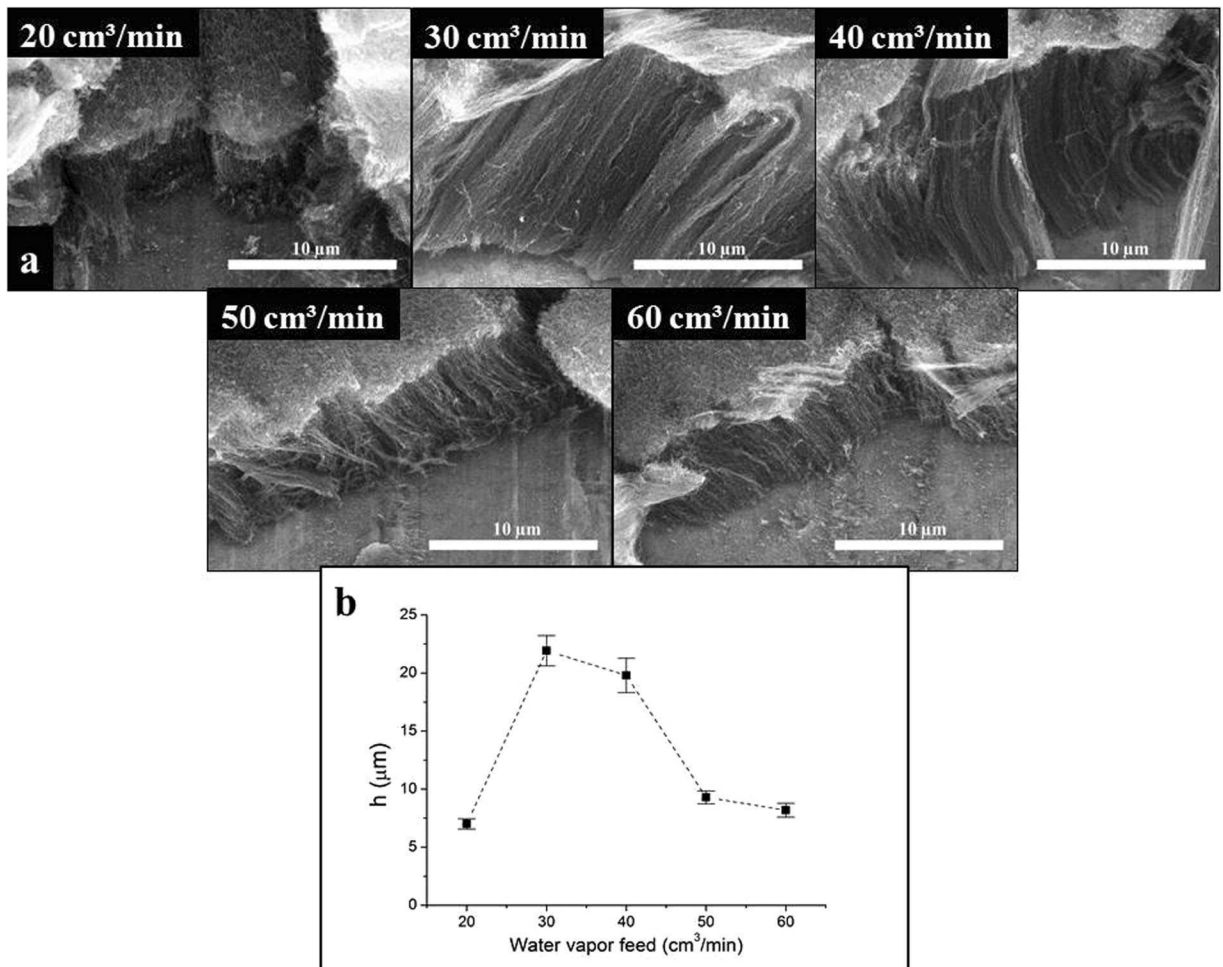


Figure 6. SEM images of CNT forests synthesized by varying the water vapor feed (a) and heights of CNT forests (b).

the catalyst hydrogen was added to the gas flow for 5 min. CVD reaction was started with launching the flow of both ethylene and water vapor. Considering the optimum water vapor feed described in the previous section it was worth to study at which reaction time the presence of water starts to hinder the growth of CNTs. Therefore the effect of reaction time was investigated in the range of 5 to 60 minutes.

It is well known from the literature that the alignment of CNT forests is mainly due to van der Waals interactions between growing nanotubes, and the steric hindrance between neighboring CNTs³⁹. From SEM images (Fig. 7) it can be concluded that after 5 min the system reaches the stage when alignment has just started, and CNT forest of moderate height (6.7 μm) was observed. At the very beginning of the CVD synthesis CNTs are growing inordinately non-perpendicular to the substrate surface. At a certain length of the tubes – due to the above-mentioned interactions – their orientation is initiated resulting in “forest formation”. Reaction time longer than only 5 mins provided a much higher orderliness of the product, both the quality and the length of carbon nanotubes improved significantly (Fig. 7b). From Fig. 7i it can be seen that under these conditions the highest carbon nanotube forest of 28 μm can be obtained after 15 min. After that, probably due to the gradual inactivation of catalyst particles the growth of carbon nanotubes stalls, and the synthesis as well as the degradation by continuous water vapor feed becomes competitive resulting in the stagnation of height of the forest. With further deactivation of the catalyst, reaction with water vapor starts to dominate and in approximately 60 min the complete disappearance of the carbon deposit occurs.

It was already observed in the literature that internal constraints might cause vertical orientation during CVD that can be facilitated by increasing the catalyst layer on the surface of the substrate, resulting in a so-called “crowding effect”⁴⁰. In order to determine if the synthesis time can be further reduced, catalyst ink of the highest concentration (0.66 M) was investigated at different reaction times in the range of 2 to 15 minutes. SEM measurements (Fig. 7) revealed the properties of carbon deposit after various CVD synthesis periods. Experiments at 2–4–6 minutes (Fig. 7e–g, respectively) thoroughly demonstrated the evolution of CNT forest. After 2 minutes carbon deposit appeared, however, neither carbon nanotubes nor orderliness of forming fibers could be recognized. During the synthesis of 4 minutes the quality of carbon deposit has changed significantly, but no characteristic alignment could be observed. 6 minutes of reaction time was the shortest period when well-oriented CNT forest of 12.5 μm could be observed. In case of 15 min reaction time the height of CNT forest became 18.5 μm

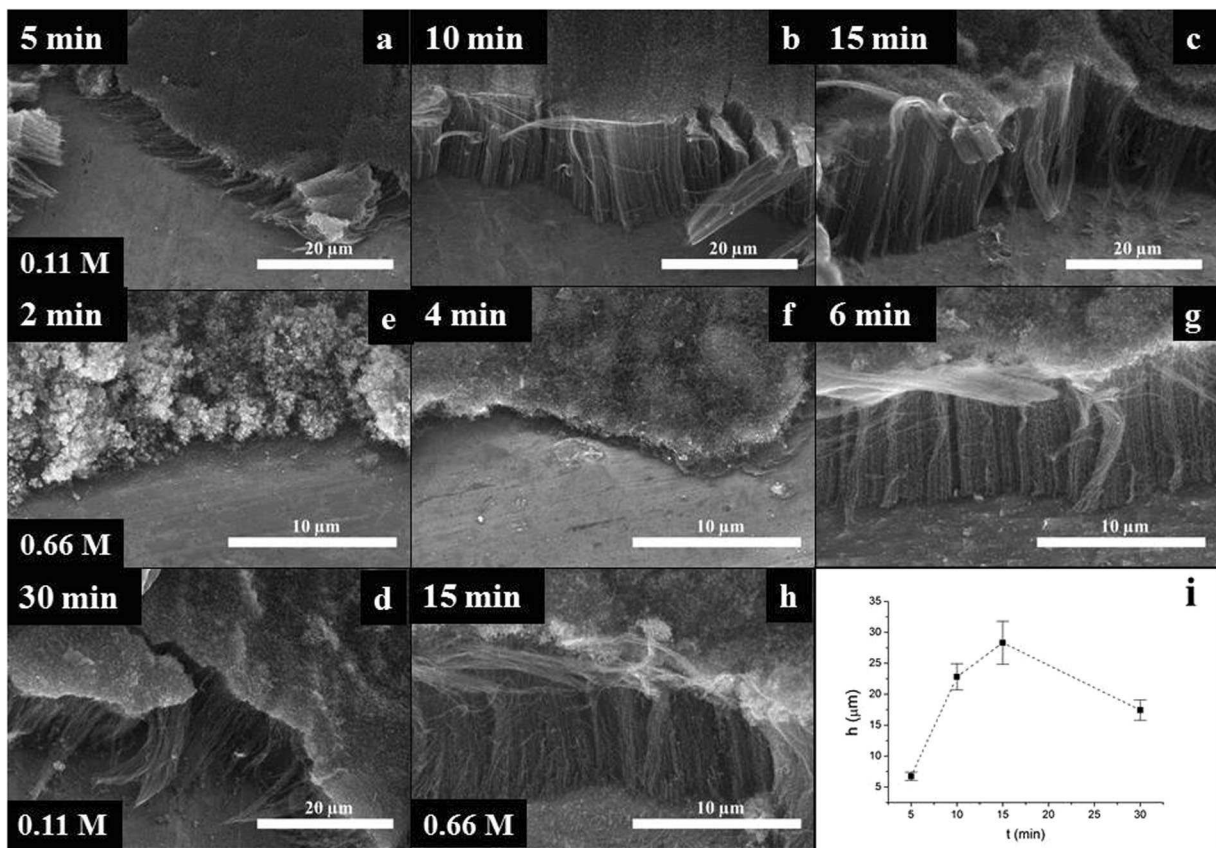


Figure 7. SEM images of CNT forests synthesized by varying the reaction time with 0.11 M ink concentration (a–d), SEM images of CNT forests synthesized by varying the reaction time with 0.66 M ink concentration (e–h) and heights of CNT forests with 0.11 M ink concentration (i).

(Fig. 7h.) From this series it can be concluded that increasing the concentration of the catalyst ink the necessary reaction time can be somewhat reduced.

Further analysis of carbon nanotubes composing forests. TEM. To determine the quality of carbon nanotubes composing the forest TEM analysis was also carried out (Fig. 8a). HR images verified the high-level graphitization of their walls which consist of 3 to 6 walls in average (Fig. 8b). These investigations also proved that these forests are grown by the root mechanism^{41,42}. However, in certain regions separated catalyst particles covered by thick graphite layer could be observed (Fig. 8c). As an illustration, carbon nanotubes prepared with catalyst ink concentration of 0.066 M, 0.11 M and 0.66 M, respectively, are shown in Fig. 8d. The outer diameter of the CNTs is in the range of 6 to 10 nm, and there is only an insignificant difference in these values as a function of concentration. From TEM images it can be also observed that the surfaces of CNTs are rather clean, i.e. outer surfaces contains almost no amorphous layers of carbon.

Raman spectroscopy. Figure 8e shows representative Raman spectra of CNT forest samples prepared by catalyst ink concentration of 0.066 M, 0.11 M and 0.66 M, respectively. Practically these spectra are identical which means that there is no significant difference between the qualities of carbon nanotubes. Their I_G/I_D ratios are 1.07 ± 0.04 . This result is in accordance with the observations from TEM investigations. From literature data it can be supposed that increasing CVD temperatures result in an even higher level of graphitization⁴³, however, in our case aluminum substrate of relatively low melting point demands a temperature limit for the synthesis.

Conclusion

In this study, a cheap and easy method was presented for the production of VACNTs onto conductive substrate. It was shown that CNT forest height grown onto an Al plate during CCVD synthesis can be controlled by numerous parameters. When varying catalyst ink concentration during the formation of catalyst layer via dip coating, the highest forest was obtained at Fe:Co = 1:3 ratio. Increasing the catalyst ink concentration, it was found that approximately above 0.11 M the height of the forest did not change significantly. The components of gas feed during CCVD also affected the parameters of forming CNT forests, however, water vapor has the most determinate role on their height. In accordance with former literature observations it was established that no considerable alignment occurs when CNTs are shorter than 10 μm. Above this value the orderliness of CNT forests becomes conspicuous more or less independently of either reaction time or catalyst ink concentration. However, the water vapor and reaction time influence both the carbon nanotube forests height and orientation. From the analysis

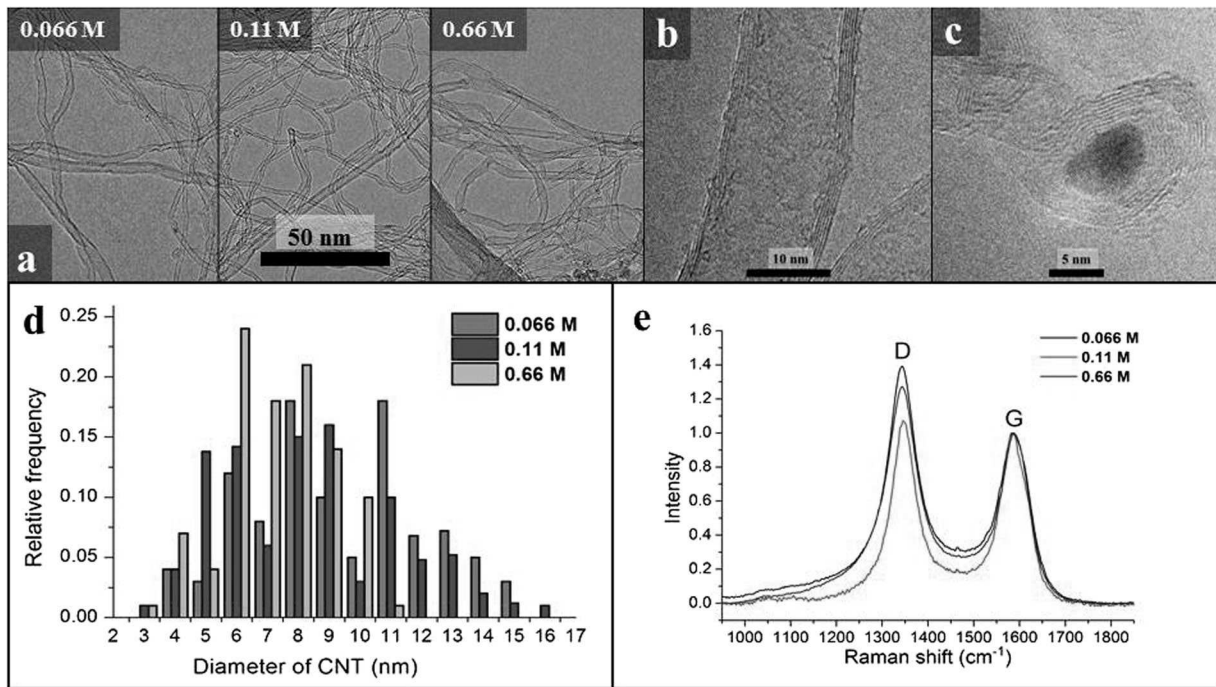


Figure 8. TEM images of CNT forests synthesized by varying the ink concentration (**a**), TEM images of the CNT walls (**b**), TEM images of the catalyst particle (**c**), the diameter distribution of CNT (**d**) and Raman spectra of the CNT forests of different ink concentration (**e**).

of CNT diameter it was concluded that the catalyst ink concentration does not affect the diameter of catalyst particles significantly. It is presumed that both the quality of the ink and CCVD conditions control the diameter of CNT. Authors expect that this simple and cheap method will open up novel applications in nanotechnology devices.

References

1. Li, W. Z. *et al.* Large-scale synthesis of aligned carbon nanotubes. *Sci.* **274**, 1701–1703 (1996).
2. Noda, S. *et al.* Millimeter-thick single-walled carbon nanotube forests: Hidden role of catalyst support. *Jpn. J. Appl. Physics, Part 2: Lett.* **46**, 0–3 (2007).
3. Mattevi, C. *et al.* In-situ X-ray photoelectron spectroscopy study of catalyst- support interactions and growth of carbon nanotube forests. *The J. Phys. Chem. C* **112**, 12207–12213 (2008).
4. Sakurai, S. *et al.* Role of subsurface diffusion and ostwald ripening in catalyst formation for SWNT forest growth. *J Am Chem Soc* **134**, 2148–2153 (2011).
5. Robertson, J. *et al.* Applications of carbon nanotubes grown by chemical vapor deposition. *Jpn. J. Appl. Phys.* **51**, 1–8 (2012).
6. Halonen, N. *et al.* Controlled CCVD synthesis of robust multiwalled carbon nanotube films. *J. Phys. Chem. C* **112**, 6723–6728 (2008).
7. Hata, K. *et al.* Water-assisted highly efficient synthesis of impurity-free single-walled carbon nanotubes. *Sci.* **306**, 1362–1364 (2004).
8. Jiang, C., Liang, Y., Yang, J. & Zhao, B. Influence of total gas flow on carbon nanotube forests synthesised by water-assisted chemical vapour deposition. *Micro & Nano Lett.* **8**, 779–782 (2013).
9. Mauron, P., Emmenegger, C., Zuttel, A., Nutzenadel, C. & Schlapbach, L. Synthesis of oriented nanotube films by chemical vapor deposition. *Carbon Nanotub.* **40**, 1339–1344 (2002).
10. Futaba, D. N. *et al.* Kinetics of water-assisted single-walled carbon nanotube synthesis revealed by a time-evolution analysis. *Phys. Rev. Lett.* **95**, 1–4 (2005).
11. Tripathi, N., Mishra, P., Harsh, H. & Islam, S. S. Fine-tuning control on CNT diameter distribution, length and density using thermal CVD growth at atmospheric pressure: an in-depth analysis on the role of flow rate and flow duration of acetylene (C₂H₂) gas. *Appl. Nanosci.* **5**, 19–28 (2014).
12. Patole, S., Alegaonkar, P., Lee, H.-C. & Yoo, J.-B. Optimization of water assisted chemical vapor deposition parameters for super growth of carbon nanotubes. *Carbon* **46**, 1987–1993 (2008).
13. Tripathi, N., Mishra, P., Joshi, B. & Islam, S. Precise control over physical characteristics of carbon nanotubes by differential variation of argon flow rate during Chemical Vapor Deposition processing: A systematic study on growth kinetics. *Mater. Sci. Semicond. Process.* **35**, 207–215 (2015).
14. Ma, Y., Dichiara, A. B., He, D., Zimmer, L. & Bai, J. Control of product nature and morphology by adjusting the hydrogen content in a continuous chemical vapor deposition process for carbon nanotube synthesis. *Carbon* **107**, 171–179 (2016).
15. D L Arcos, T., Oelhafen, P., Thommen, V. & Mathys, D. The influence of catalyst's oxidation degree on carbon nanotube growth as a substrate-independent parameter. *J. Phys. Chem. C* **111**, 16392–16396 (2007).
16. Burt, D. P. *et al.* Effects of metal underlayer grain size on carbon nanotube growth. *J. Phys. Chem. C* **113**, 15133–15139 (2009).
17. Lacerda, R. G. *et al.* Thin-film metal catalyst for the production of multi-wall and single-wall carbon nanotubes. *J. Appl. Phys.* **96**, 4456–4462 (2004).
18. Ren, A. Z. F. *et al.* Synthesis of large arrays of well-aligned carbon nanotubes on glass. *Sci.* **282**, 1105–1107 (1998).
19. Yao, Y., Falk, L. K. L., Morjan, R. E., Nerushhev, O. A. & Campbell, E. E. B. Synthesis of carbon nanotube films by thermal CVD in the presence of supported catalyst particles. Part II: The nanotube film. *J. Mater. Sci. Mater. Electron.* **15**, 533–543 (2004).

20. Eres, G., Puretzky, A. A., Geohegan, D. B. & Cui, H. *In situ* control of the catalyst efficiency in chemical vapor deposition of vertically aligned carbon nanotubes on predeposited metal catalyst films. *Appl. Phys. Lett.* **84**, 1759–1761 (2004).
21. Teblum, E., Gofer, Y., Pint, C. L. & Nessim, G. D. Role of catalyst oxidation state in the growth of vertically aligned carbon nanotubes. *J Phys Chem C* **116**, 24522–24528 (2012).
22. Dubosc, M. *et al.* Impact of the Cu-based substrates and catalyst deposition techniques on carbon nanotube growth at low temperature by PECVD. *Microelectron. Eng.* **84**, 2501–2505 (2007).
23. Fejes, D. *et al.* Super growth of vertically aligned carbon nanotubes on pulsed laser deposited catalytic thin films. *Appl. Phys. A: Mater. Sci. Process.* **118**, 855–861 (2015).
24. Murakami, Y., Miyauchi, Y., Chiashi, S. & Maruyama, S. Direct synthesis of high-quality single-walled carbon nanotubes on silicon and quartz substrates. *Chem. Phys. Lett.* **377**, 49–54 (2003).
25. Dürfler, S. *et al.* Tailoring structural and electrochemical properties of vertical aligned carbon nanotubes on metal foil using scalable wet-chemical catalyst deposition. *J. Power Sources* **208**, 426–433 (2012).
26. Li, G., Chakrabarti, S., Schulz, M. & Shanov, V. Growth of aligned multiwalled carbon nanotubes on bulk copper substrates by chemical vapor deposition. *J. Mater. Res.* **24**, 2813–2820 (2009).
27. Magrez, A., Seo, J. W., Smajda, R., Mionić, M. & Forró, L. Catalytic CVD synthesis of carbon nanotubes: Towards high yield and low temperature growth. *Mater.* **3**, 4871–4891 (2010).
28. D S Meneses, D., Malki, M. & Echegut, P. Structure and lattice dynamics of binary lead silicate glasses investigated by infrared spectroscopy. *J. Non-Crystalline Solids* **352**, 769–776 (2006).
29. Johnson, P. B. & Christy, R. W. Optical constants of copper and nickel as a function of temperature. *Phys. Rev. B* **11**, 1315–1323 (1975).
30. Lichtenstein, T. Handbook of Thin Film Materials. *Coll. Eng. Appl. Sci. Univ. Rochester* (1979).
31. Dijon, J. *et al.* How to switch from a tip to base growth mechanism in carbon nanotube growth by catalytic chemical vapour deposition. *Carbon* **48**, 3953–3963 (2010).
32. Mata, D. *et al.* Upscaling potential of the CVD stacking growth method to produce dimensionally-controlled and catalyst-free multi-walled carbon nanotubes. *Carbon* **50**, 3585–3606 (2012).
33. Dresselhaus, M. S., Dresselhaus, G., Saito, R. & Jorio, A. Raman spectroscopy of carbon nanotubes. *Phys. Reports* **409**, 47–99 (2005).
34. Antunes, E. F. *et al.* Comparative study of first- and second-order Raman spectra of MWCNT at visible and infrared laser excitation. *Carbon* **44**, 2202–2211 (2006).
35. Kind, H. *et al.* Printing gel-like catalysts for the directed growth of multiwall carbon nanotubes. *Langmuir* **16**, 6877–6883 (2000).
36. Smajda, R. *et al.* Synthesis and mechanical properties of carbon nanotubes produced by the water assisted CVD process. *Phys. Status Solidi (B) Basic Res.* **246**, 2457–2460 (2009).
37. Kaneko, A., Yamada, K., Kumahara, R., Kato, H. & Homma, Y. Comparative Study of Catalytic Activity of Iron and Cobalt for Growing Carbon Nanotubes on Alumina and Silicon Oxide. *The J. Phys. Chem.* **116**, 26060–26065 (2012).
38. Magrez, A. *et al.* Striking influence of the catalyst support and its acid-base properties: New insight into the growth mechanism of carbon nanotubes. *ACS Nano* **5**, 3428–3437 (2011).
39. Bower, C., Zhu, W., Jin, S. & Zhou, O. Plasma-induced alignment of carbon nanotubes. *Appl. Phys. Lett.* **77**, 830–832 (2000).
40. Nozaki, T., Ohnishi, K., Okazaki, K. & Kortshagen, U. Fabrication of vertically aligned single-walled carbon nanotubes in atmospheric pressure non-thermal plasma CVD. *Carbon* **45**, 364–374 (2007).
41. Yang, J. *et al.* Growth of high-density carbon nanotube forests on conductive TiSiN supports. *The J. Phys. Chem.* **106**, 5 (2015).
42. Sugime, H. *et al.* Low temperature growth of ultra-high mass density carbon nanotube forests on conductive supports. *Appl. Phys. Lett.* **103**, 5 (2013).
43. Andrews, R., Jacques, D., Qian, D. & Rantell, T. Multiwall Carbon Nanotubes: Synthesis and Application. *Acc. Chem. Res.* **35**, 1008–1017 (2002).

Acknowledgements

The authors are very grateful to the financial support provided by the OTKA NN114463. A.Sz. acknowledges the financial support of GINOP-2.3.2- 15-2016- 00013 project. This work was also supported by the Swiss National Science Foundation (No. 513733).

Author Contributions

All the Authors contributed to the discussion of the results and writing the manuscript. A.Sz. conceived and designed experiments. E.K. contributed by taking the TEM images of CNT forests and contributed by cyclic voltammetry measurements of CNT forests. T.Gy. contributed by taking SEM images of CNT forests. K.N. contributed by Raman measurements of CNT forests. Zs.P. contributed by ellipsometry measurements of CNT forests. K.H. conceived and designed the experiments.

Additional Information

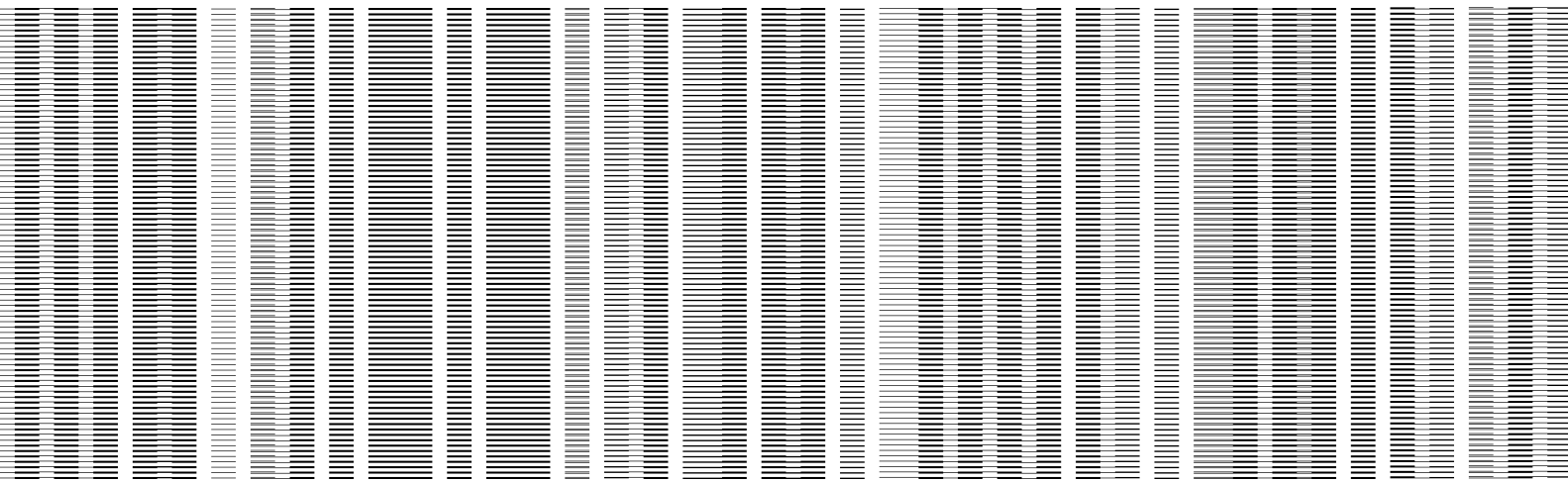
Competing Interests: The authors declare that they have no competing interests.

Publisher's note: Springer Nature remains neutral with regard to jurisdictional claims in published maps and institutional affiliations.



Open Access This article is licensed under a Creative Commons Attribution 4.0 International License, which permits use, sharing, adaptation, distribution and reproduction in any medium or format, as long as you give appropriate credit to the original author(s) and the source, provide a link to the Creative Commons license, and indicate if changes were made. The images or other third party material in this article are included in the article's Creative Commons license, unless indicated otherwise in a credit line to the material. If material is not included in the article's Creative Commons license and your intended use is not permitted by statutory regulation or exceeds the permitted use, you will need to obtain permission directly from the copyright holder. To view a copy of this license, visit <http://creativecommons.org/licenses/by/4.0/>.

© The Author(s) 2017



12007 125524 R1

12007 125524 R1

12007 125524 R1

524 100 7 125
2 100

100% Natural

100% Natural

100% Natural

100% Natural

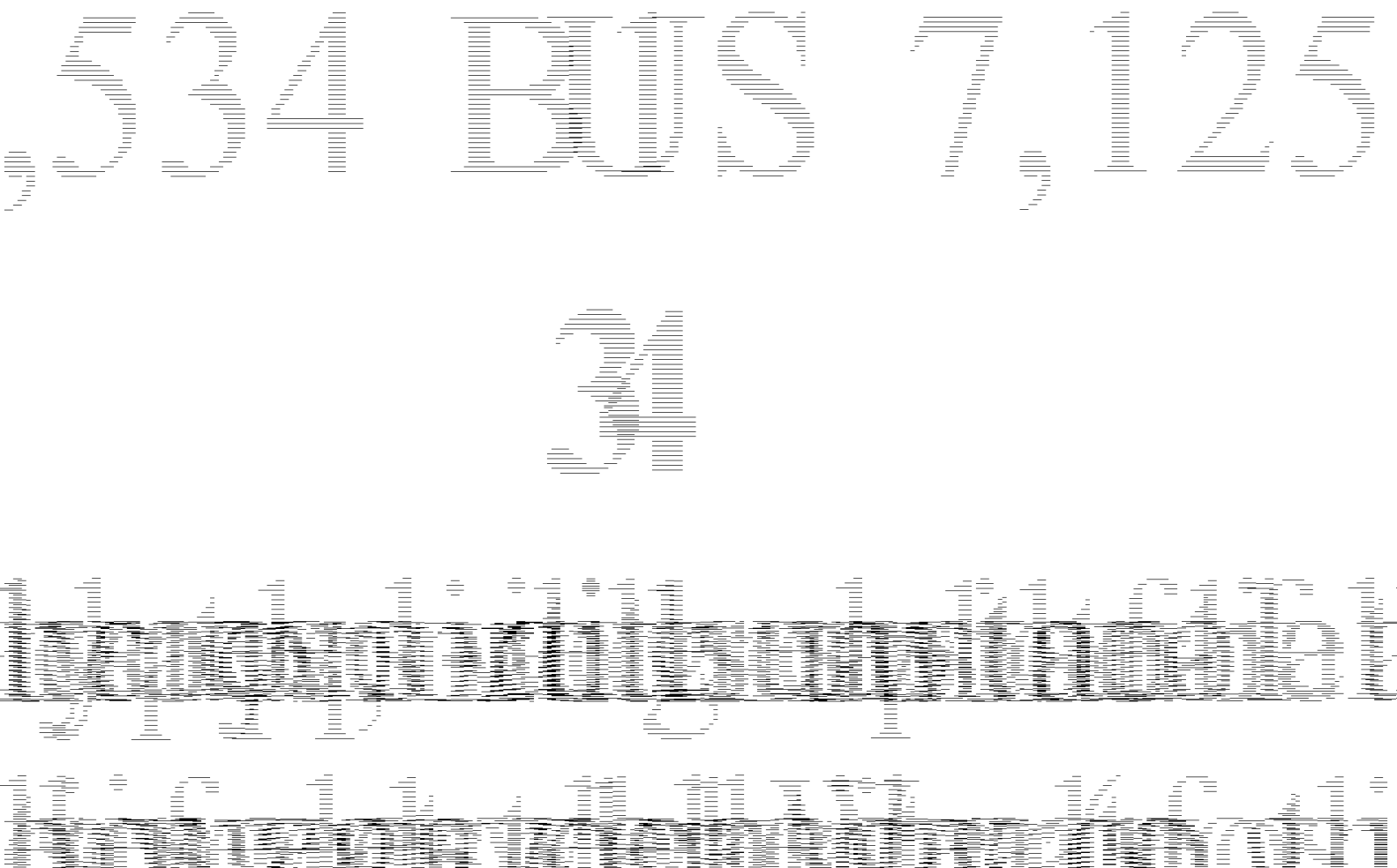
100% Natural

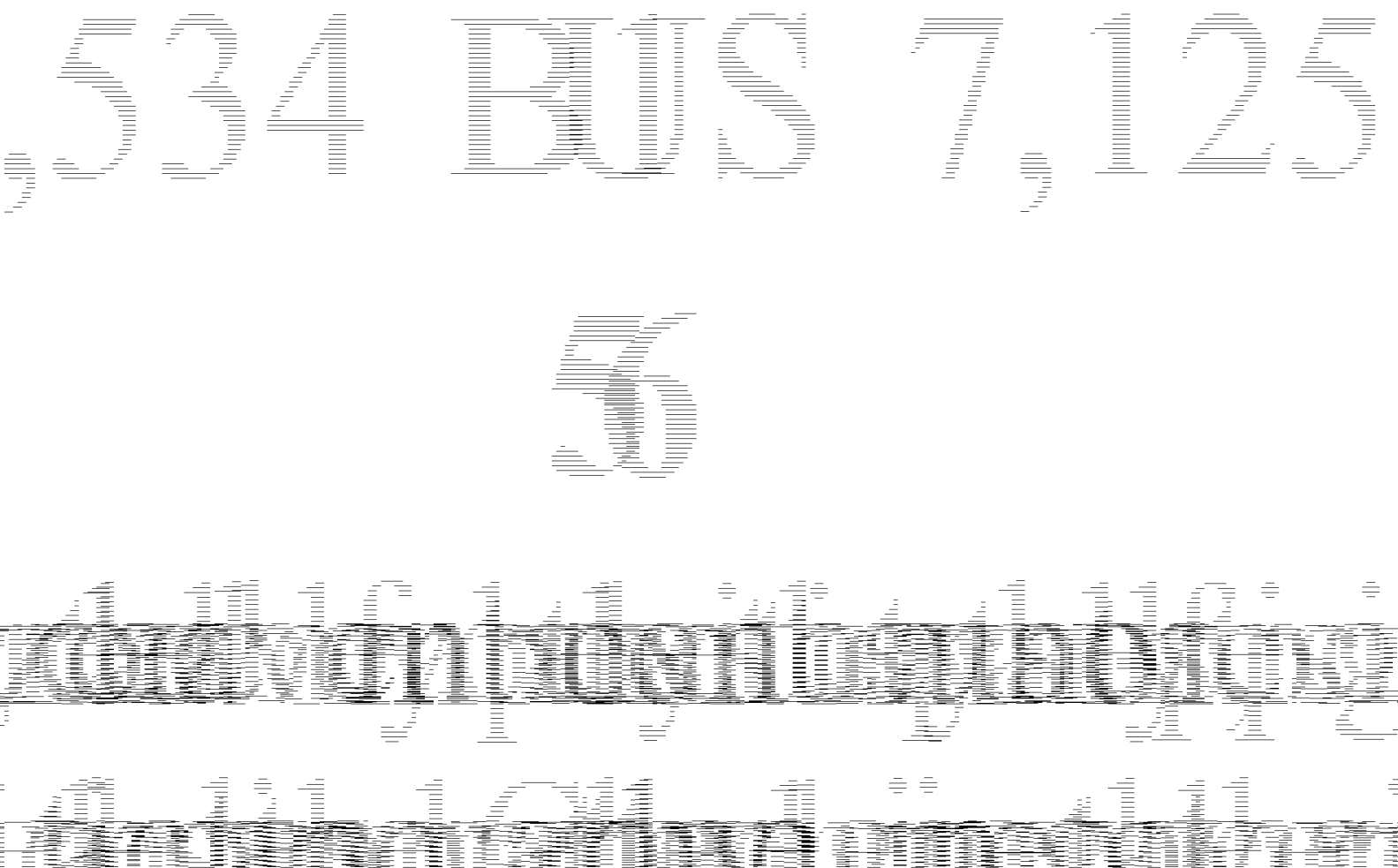
100% Natural

A decorative vertical border element consisting of a series of parallel horizontal lines at the top and bottom, with a central column of vertical lines.

12

THESE ARE THE WORDS OF GOD WHICH HE GAVE ME, THAT I MIGHT TELL YOU, AND THAT YE MIGHT BELIEVE THAT I COME FROM GOD.





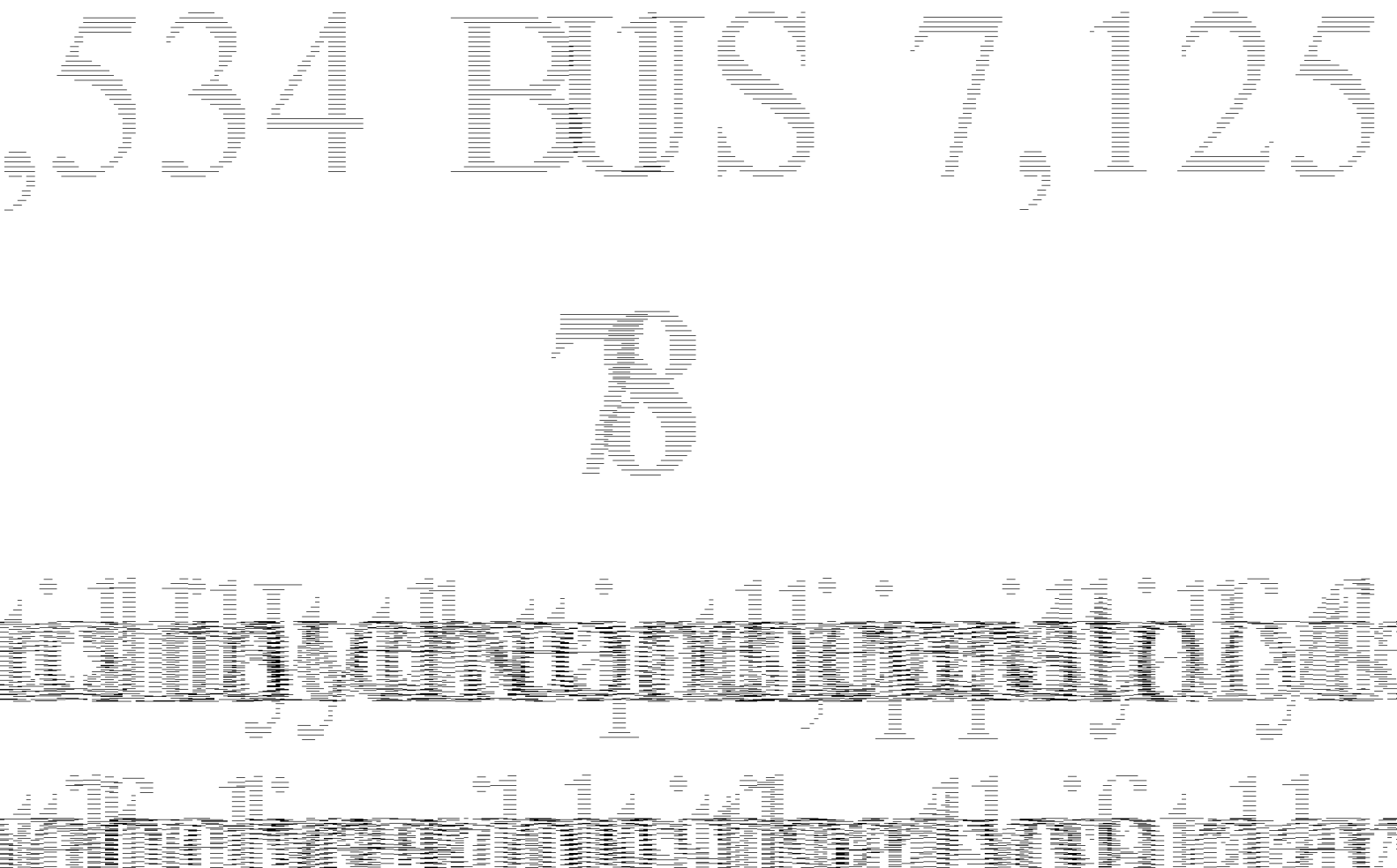
524

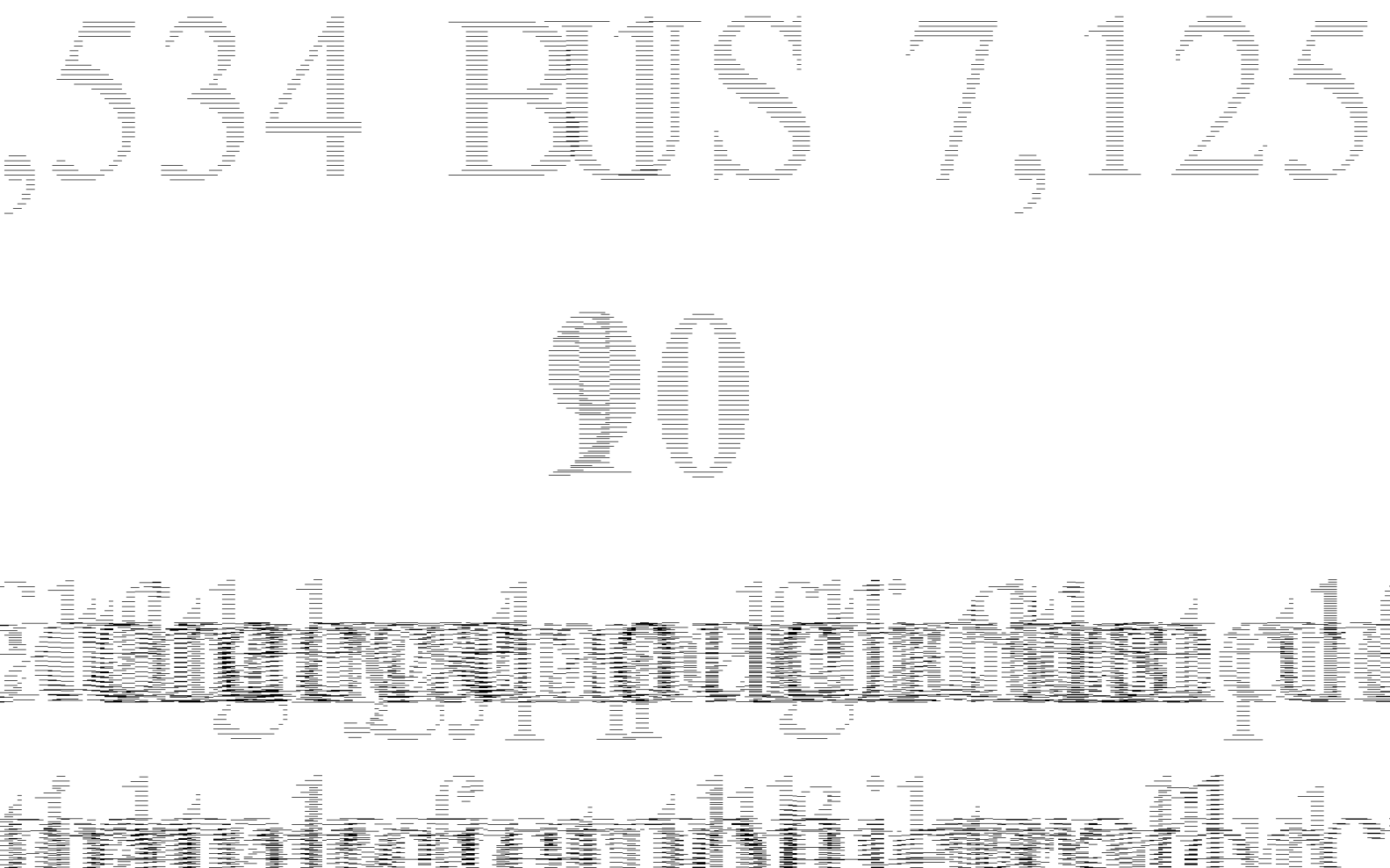
EDC

7

25

30





A horizontal strip consisting of 100 vertical black bars of varying heights, arranged in a grid-like pattern. The bars represent a sequence of binary digits (bits) from left to right. The sequence starts with a short bar, followed by a tall bar, then a short bar, and so on, creating a repeating pattern of two short bars and one tall bar.

The image shows the number 112 composed of numerous horizontal black lines of varying lengths. The digits are formed by groups of lines: '11' has two vertical columns of lines, and '2' has a single column that tapers to the right.

A spectrogram illustrating the frequency spectrum of a signal over time. The vertical axis represents frequency, ranging from 0 to 1000 Hz. The horizontal axis represents time, ranging from 0 to 10 seconds. The plot displays a dense, multi-layered pattern of vertical lines, indicating the presence of numerous frequency components at different times. The overall envelope of the signal shows a slight downward trend in frequency over the duration of the recording.

